AD NUMBER

AD-374 839

CLASSIFICATION CHANGES

TO **UNCLASSIFIED**

FROM **CONFIDENTIAL**

AUTHORITY

OCA per Gp-4 mrkngs on doc and ADTC, USAF ltr; 21 Sep 77

19990226086

AD NUMBER

AD-374 839

NEW LIMITATION CHANGE

TO **DISTRIBUTION STATEMENT - A**

Approved for public release;
distribution is unlimited.

LIMITATION CODE: 1

FROM **No Prior DoD Distr Scty Cntrl St'mt Assgn'd**

AUTHORITY

ADTC, USAF ltr; 21 Sep 77

AFATL-TR-66-64

Marking and Detection (U)
(Laser Technique)

by

Robert Goldstein
Beatrice Hammond
Jay L. Richman
et al
ISOMET CORPORATION

JULY 1966

AIR FORCE ARMAMENT LABORATORY
RESEARCH AND TECHNOLOGY DIVISION
AIR FORCE SYSTEMS COMMAND
EGLIN AIR FORCE BASE, FLORIDA

DAD 66-4980

SECURITY MARKING

The classified or limited status of this report applies to each page, unless otherwise marked.
Separate page printouts MUST be marked accordingly.

THIS DOCUMENT CONTAINS INFORMATION AFFECTING THE NATIONAL DEFENSE OF THE UNITED STATES WITHIN THE MEANING OF THE ESPIONAGE LAWS, TITLE 18, U.S.C., SECTIONS 793 AND 794. THE TRANSMISSION OR THE REVELATION OF ITS CONTENTS IN ANY MANNER TO AN UNAUTHORIZED PERSON IS PROHIBITED BY LAW.

NOTICE: When government or other drawings, specifications or other data are used for any purpose other than in connection with a definitely related government procurement operation, the U. S. Government thereby incurs no responsibility, nor any obligation whatsoever; and the fact that the Government may have formulated, furnished, or in any way supplied the said drawings, specifications, or other data is not to be regarded by implication or otherwise as in any manner licensing the holder or any other person or corporation, or conveying any rights or permission to manufacture, use or sell any patented invention that may in any way be related thereto.

REPRODUCTION QUALITY NOTICE

This document is the best quality available. The copy furnished to DTIC contained pages that may have the following quality problems:

- Pages smaller or larger than normal.
- Pages with background color or light colored printing.
- Pages with small type or poor printing; and or
- Pages with continuous tone material or color photographs.

Due to various output media available these conditions may or may not cause poor legibility in the microfiche or hardcopy output you receive.

☐ If this block is checked, the copy furnished to DTIC contained pages with color printing, that when reproduced in Black and White, may change detail of the original copy.

[redacted]

MARKING AND DETECTION (U)
(Laser Technique)

by

Robert Goldstein
Beatrice Hammond
Jay L. Richman, et al

[redacted]

(This page is Unclassified)

[redacted]

FOREWORD

This is the final report of a program conducted under Contract No. AF 08(635)-4299, "Laser Technique for Marking and Detection." Program Manager at Isomet Corporation was Mr. Robert Goldstein. Lt James Clary of the Air Force Armament Laboratory, Eglin Air Force Base, Florida was the Project Manager. This work was performed from May 26, 1964 through March 31, 1966.

We gratefully acknowledge the assistance of the following Air Force personnel during the Eglin Air Force Base field measurements program: Major G. Carter, 1st Lt G. McCollum, 1st Lt J. Clary, 1st Lt R. Strobel, Col J. Waterman.

This technical report has been marked in accordance with the DoD Industrial Security Manual by the contractor.

Publication of this report does not constitute Air Force approval of the report's findings or conclusions. It is published only for the exchange and stimulation of ideas.

[redacted]

[redacted]

[redacted]

1. SECRET ABSTRACT

Further experimental studies and field measurements confirmed the feasibility of the Isomet laser concept for marking and detection of individuals. In this concept a phosphor agent is disseminated from an aircraft on military targets, which are later interrogated by a laser transmitter. The phosphor return, as well as the laser pulse, are in the infrared spectrum and hence are completely covert.

No basic system limitations were uncovered by the tests or studies. A ground based test set was designed, built and used in field measurements at Eglin Air Force Base. Background radiation from sunlight, terrain and foliage did not materially degrade the system performance. System operation was demonstrated in the field over an unobstructed path as well as through foliage. Phosphors with improved characteristics were developed.

It is recommended that the development of the Isomet laser concept be continued in three areas:

1. Design, construction and testing of a flyable prototype based on present state-of-the-art system components.

2. Further development of phosphor agents and dissemination techniques.

3. Field testing of a marking and detection system in which a phosphor agent is disseminated from aircraft, and interrogation is conducted with a portable ground-based laser transmitter. Data gained in this last set-up can be directly applied to the flight program.

[redacted]

(The reverse side of this page is blank)

[redacted]

[redacted]

[redacted] CONTENTS

[redacted]

[redacted]

[redacted]

2. INTRODUCTION

2.1 Isomet Laser - M & D System

This is the final report of the second, in a series of two contracts, conducted to evaluate the feasibility of the Isomet Laser M & D concept. The primary goal is a feasible concept for covert airborne delivery and subsequent detection of marking chemicals for identifying and locating enemy personnel.

The laser M & D concept involves the use of an infrared emitting phosphor as the marking agent and an infrared laser transceiver as the detection system. The detection of phosphor marked personnel is achieved by simultaneously illuminating an area with a laser beam and photometrically sensing the characteristic phosphor emission from this area. Since both spectral regions are not visible, the interrogation is covert.

The laser output wavelength was chosen on the basis of availability of laser materials and the requirement for covert operation. The most promising materials were $CaWO_4(Nd^{3+})$ and Nd doped glass, which emit in the infrared at 1.06 microns. Phosphors were selected and developed to have stimulated emission at somewhat longer wavelengths; in the region of 1.8 to 2.1 microns where atmospheric transmission windows exist. The photometer was designed to detect phosphor wavelengths and reject laser wavelengths.

2.2 Program

This program, performed at Isomet Corporation under Contract No. AF08(635)-4299, was a continuation of work done under Contract No. AF08(635)-3784. During the initial program, techniques, components, and system variables for covert marking and detection were studied and established. The system feasibility was shown both analytically and through laboratory experiments.

The purpose of the second program, carried out under Contract AF08(635)-4299, was to investigate environmental effects on system performance, conduct further studies on suitable phosphors and to experimentally verify the feasibility of the system by ground field tests using a test set.

Specifically, the following areas were investigated:

a. Experimental verification of the derived range equation.

b. The effects on system performance of various backgrounds.

c. The characterization, improvement and development of phosphors.

d. The effect of target geometry on system response.

e. The effect of target obscuration by various amounts of vegetative cover.

f. The effect of operating along a slant range from a tower to simulate an airborne environment.

The results of both laboratory and field testing show that the system provides a practical means for covert detection of marked personnel, equipment, and areas. The experimental and test programs did not uncover any basic system limitations, and we continue to believe that the laser technique for marking and detection offers great promise.

3. EXPERIMENTAL PROGRAM

The experimental program was divided into five major parts:

1. Phosphor research
2. Laser optimization and adaptation
3. Detector Evaluation
4. Development of test set
5. Field Measurements

3.1 Phosphor Research

The objective of the phosphor research program was the development of an infrared excited, infrared emitting material which would have the following additional characteristics:

A. Low toxicity
B. Innocuous appearance
C. Wavelength difference between excitation and emission spectra sufficient to afford complete separation at the detector
D. High radiant efficiency

To meet these requirements many phosphors were prepared and evaluated. In addition, a search of the literature was continued in an effort to find new phosphor systems. Although organic phosphors might be desirable from the viewpoint of dissemination and innocuous appearance, no likely formulations were discovered in the technical publications which were searched. After extensive screening, a group of promising materials were selected for further testing and development. The concentration of doping agents and the heat treatment of each phosphor were varied to optimize the desirable characteristics. The measurements and procedures utilized in evaluating the various phosphor compositions are described below.

3.1.1 Emission Spectra and Relative Efficiency

All phosphors made during the previous contract as well as all new formulations were evaluated for relative efficiency and fluorescent spectral characteristics with 1.06 micron excitation.

Relative efficiency was measured using a Beckman DK2A

spectrometer with a fluorescent attachment. The excitation source was a tungsten filament lamp filtered by means of a 5 cm long water filter and 1.06 micron spike transmission filter. The transmission curve for the filter is shown in Figure 1. The transmission peaks at 1.06 microns with a half-width of 0.3 millimicrons, where half-width is defined as the wavelength difference between two 50% transmission points.

The system was aligned by placing a white card in the fluorescent attachment, and adjustments made until the reflected signal at 1.06 microns was maximized. The white card was then replaced by phosphor cards and the spectrum was scanned from 1.2 - 3.5 microns for phosphor emission. The phosphor cards were made by sprinkling phosphor powder on cards covered with double coated pressure sensitive tape. Both the white card and the phosphor cards were approximately 1/2" x 1", which is the size of the opening in the Beckman DK2A fluorescent attachment holder. This technique leads to some differences in phosphor density on the cards because of differences in the particle size of the phosphors.

In order to eliminate the effects of differences in alignment or variations in lamp output in the Beckman light source, each time the relative efficiencies of new phosphors were measured, one of the "old" phosphor cards from previous measurements was also recorded. In the first half of the program, the phosphor card used to normalize the new data was V-5A. Later, V-21 was used since there was more of this composition available. Periodically, both V-5A and V-21 were measured, in addition to the new phosphors, to be sure that the ratio of the relative efficiencies stayed the same.

To insure that there was no deterioration of the "standard" phosphor cards due to aging or a decrease in phosphor coverage of the card due to handling, new phosphor cards were periodically made up using the original V-21 phosphor powder.

Fluctuations of about $\pm$ 10% were noticed in the ratio of relative efficiency of V-21 and V-5A for a series of different runs made over a period of months. This was attributed to differences in the positioning of the phosphor cards in the holder and illuminating different areas of the cards where the phosphor densities were slightly different. This was more than adequate reproducibility for a test designed to semi-quantitatively evaluate new phosphor preparations.

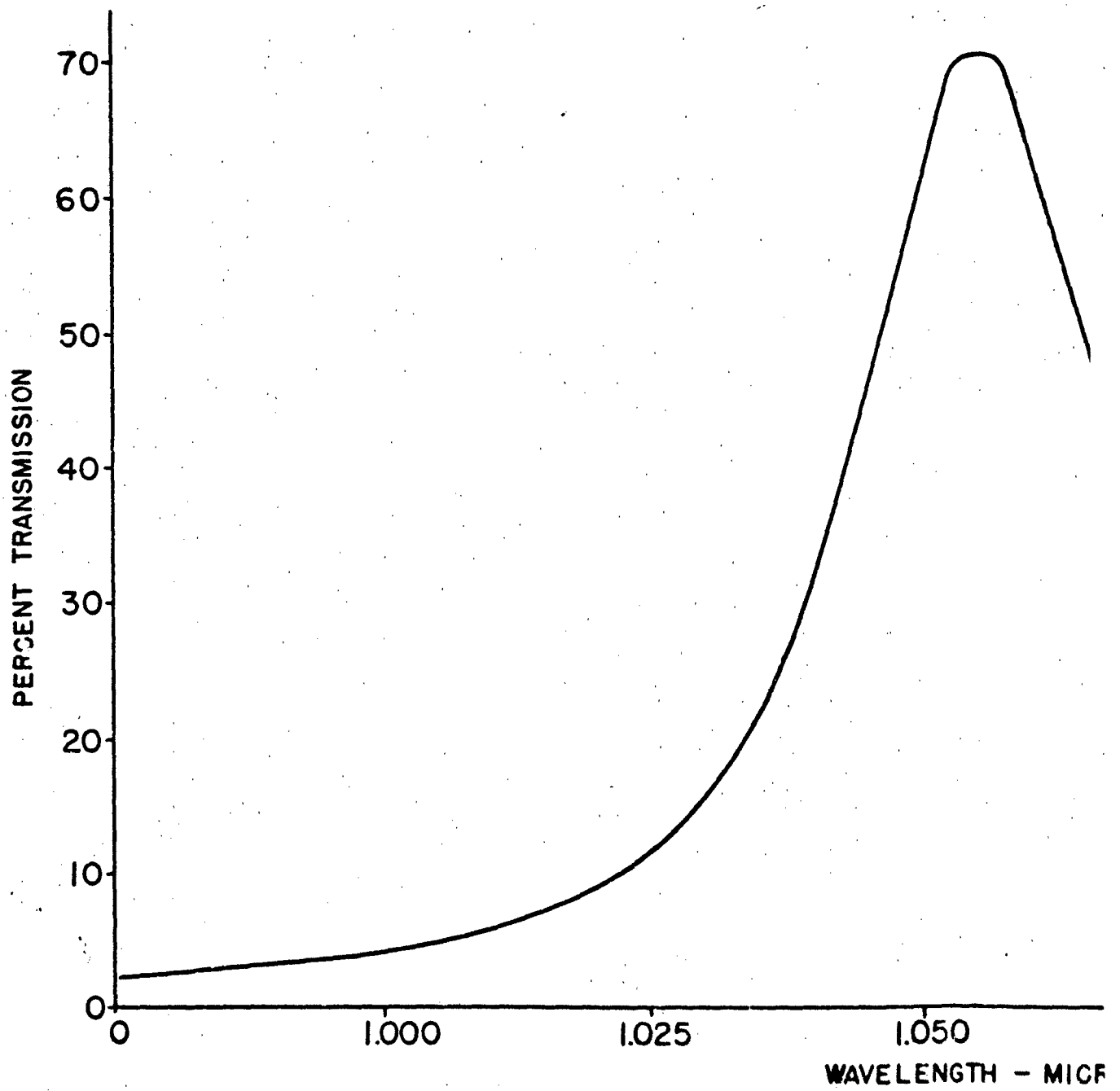

1 | 1.06 MICRON SPIKE TRANSMI

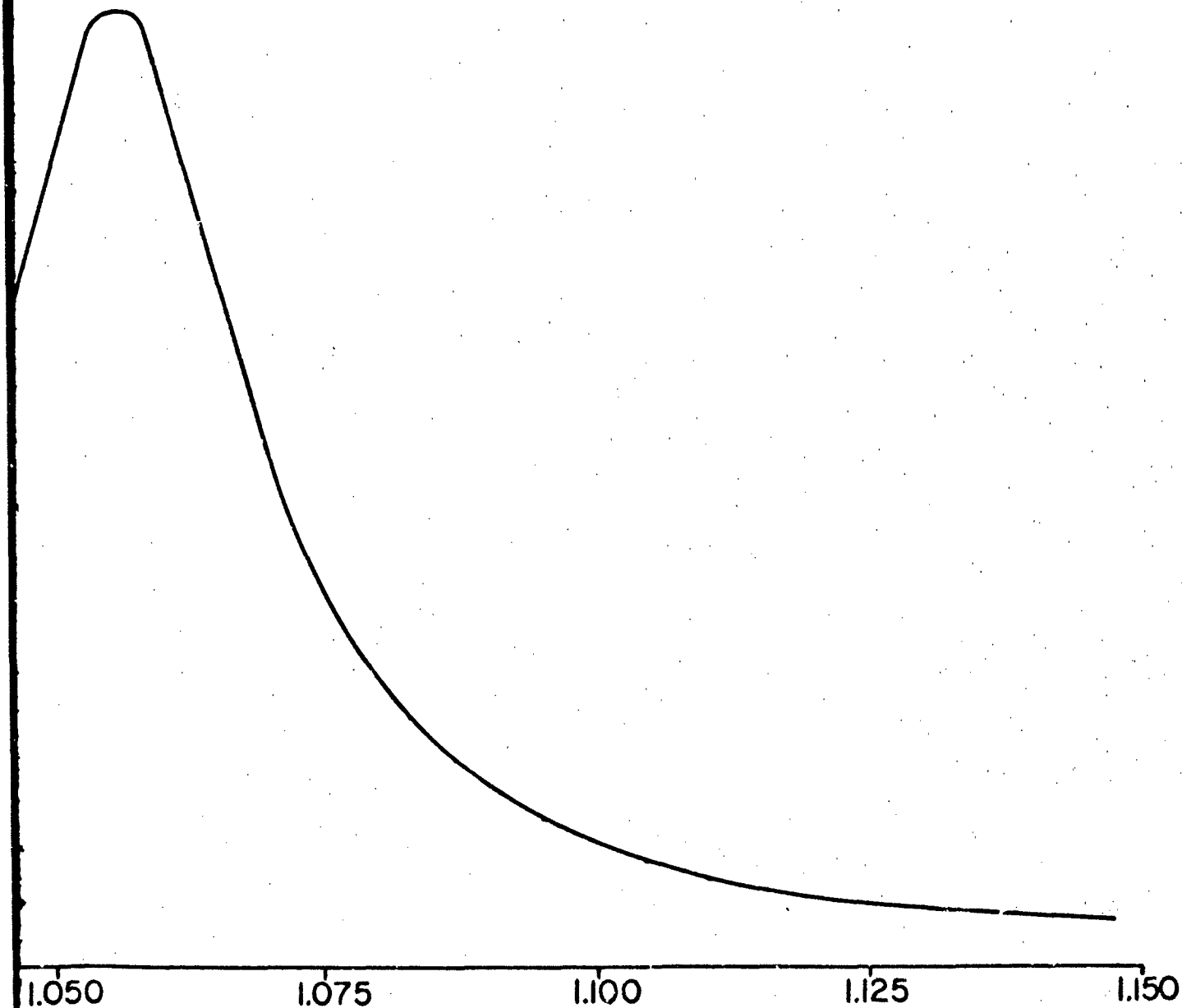

E TRANSMISSION FILTER

FIGURE 1

Tables 1 and 2 present the results of these phosphor measurements. The values of the phosphor efficiency cited in these Tables are taken relative to the radiant efficiency of standard phosphor V-21, which was determined to be 1.82%. For example, if a phosphor was measured to have only half the peak signal of V-21, its efficiency was tabulated at 0.91%.

3.1.2 Decay Time Measurements

The decay times of the phosphors were measured using a $CaWO_4(Nd^{3+})$ laser pumped to approximately 25 joules. This low input was used in order to provide a pump pulse with a decay time much shorter than the expected phosphor decay time. The phosphor return was detected by use of a photometer with a negligible time constant compared to the phosphor time constants. This was checked by monitoring the laser pulse with a photometer and comparing a reflected signal from a white card with the signal from a phosphor card. Decay time was measured for signals which occurred after the laser was known to be off.

Later measurements were made with a gold doped germanium detector of the type used in the field test system, filtered to reject the laser light and pass any signal beyond 1.3 microns. These measurements are reproducible to $\pm$ 20 microseconds. The variation is due to two factors. The first results simply from the inability to measure the oscilloscope photographs to better than 10%. The second factor is due to the characteristics of the phosphors themselves. The decay of zinc or cadmium sulfide phosphors is not the simple exponential decay which would indicate a "monomolecular" process, but is composed of two components. One is a simple exponential decay. Superimposed on this is a hyperbolic decay or "bimolecular process" where the decay is dependent on the number of available recombination centers(1). This portion of the decay curve is dependent on the excitation intensity; thus, although the decay is approximately exponential, the actual value of the decay time depends on the position on the decay curve at which the measurement is made, and can vary up to about 20 microseconds. Although this effect was apparent over the range of intensity used both in the laboratory and in the final test set, there was no detectable difference in decay time for the final large batch phosphor.

3.1.3 ZnS(Cu,V) Phosphors

Of all the phosphors prepared, those of the ZnS or

(1) D. Curie, Luminescence in Crystals (John Wiley and Sons, Inc. New York, 1963), p. 148.

TABLE 1

Phosphors Which Did Not Exhibit Fluorescence Between 1.3 and 3 Microns With 1.06 Micron Excitation

Sample No.	Composition
--	$CaSiO_3$–CdSe (Cu,In)
20	Cd (Se,S) (Cu,Mn)
--	CdSe–CdS (Cu,In)
--	HgS–ZnS
A1-2	ZnS (Cu,Al)
--	CdS (Cu,In)
--	$CaSiO_3$ (Cu,In)
--	$CaSiO_3$ (Sn,In) (NaCl)
--	$CaSiO_3$ (U,Sn,In)
C	ZnS (Cu,Al)
A-2	ZnS (Cu,Al)
A1-3	ZnS (Cu,Al)
A1-6a	ZnS (Cu,Al)
A1-6b	ZnS (Cu,Al)
A1-7	CdS (Cu,Al)
--	HgS
--	CdS (Cu)
--	CdSe (Cu,In)
--	CdSe–H_2Se
5	CdS (Cu_2,Tl) (NaCl)
7c	CdS (Cu,Pb) (NaCl)
8b	CdS (Cu,Ni) (NaCl)
8c	CdS (Cu,Tb) (NaCl)
11	ZnS (Cu,Al) (NaCl)
11a	ZnS (Cu,Co) (NaCl)
15	Al_2O_3 (Dy)
15a	Al_2O_3 (Cu,Dy)
16	CdS (Cu,In)
18a	CdSe,CdS (In,Cu,Dy) (NaCl)
Type 145	ZnS (Cu)
--	SmHAPI
A1-5(1)	ZnS (Cu,Al)
7b	CdS (Cu,Tl) (NaCl)
8	CdS (Cu,Sn) (NaCl)
8a	CdS (Cu,Co) (NaCl)
9	PbS (Ag,Tb) (NaCl)
9a	PbS (Cu,Tb) (NaCl)

TABLE 1

(Continued)

Sample No.	Composition
10	CdS (Ag) (NaCl)
10a	CdS (Ag,Tb) (NaCl)
11b	CdS-ZnS (Cu,Tb) (NaCl)
12	Cu_2S (Tb) (NaCl)
12a	Cu_2S (Ag) (NaCl)
12b	Cu_2S (Co) (NaCl)
14	CdSe (Cu) (NaCl)
14a	CdSe (Cu,Dy) (NaCl)
14b	CdSe (Mn) (NaCl)
14c	CdSe (Ag) (NaCl)
17	CdSe (Cu,In) (NaCl)
17a	CdSe (Mn) (NaCl)
17b	CdSe (Mn,Dy) (NaCl)
17c	CdSe (Mn,In) (NaCl)
18	CdSe-CdS (In,Cu) (NaCl)
18b	CdSe (In,Cu) (NaCl)
19b	CdSe (Cu,Cl,In,Dy)
HC-1A	70CdS-30HgS (Cu)
HC-2	ZnS (Cu)
HC-3	70CdS-30 purified HgS (Cu)
HC-5	CdS (Au,Al)
HC-4	70CdS-30HgS (Au,Al)
HC-6	HgS (Cu 2×10^{-4})

TABLE 2

Vanadium Series Phosphors

Expt. No.	Dopant V*	Dopant X**	Host ZnS	Temp. °C	Firing Atmosphere	Time, Hours	Fluorescence Peak, Microns	Relative Efficiency	Decay Time Microseconds
V-1	2	2Cu	1	950	S-vacuum	2	1.8	0.57	150
V-2	2	2Cu	1	1120	H_2S	2	2.0	0.54	90
V-3	2	2Cu	CdS-1	950	H_2S		2.1	0.8	30
V-4	2	2Ag	CdS-1	950	H_2S	2	2.1	0.54	120
V-5a	2	2Cu	1	950	H_2S	2	1.8	0.8	130, 140
V-5b	2	2Cu	1	950	H_2S	2	2.0	0.8	80
				+1120	H_2S	2			
V-5c	2	2Cu	1	950	H_2S	2	1.8	0.63	115
V-5d	2	2Cu	1	950	H_2S	4	1.8	0.55	140
V-5e	2	2Cu	1	950	H_2S	2	1.8	0.75	110
				+950	$H_2S + H_2O$	2			
V-5f	2	2Cu	1	950	H_2S	4	None		
				+950	Air	2			
V-6a	2	2Cu	1	950	H_2S	2	1.8	0.16	140
V-6b	2	2Cu	1	750	H_2S	4	1.8	0.28	175
V-7a	2		1	850	H_2S	2	1.8	0.51	155
V-7b	2	2Cu	1	850	H_2S	4	1.8	0.35	115
V-8a	2	2Cu	1	1000	H_2S	2	1.8	0.45	140
V-8b	2	2Cu	1	1000	H_2S	4	1.8	0.46	150
V-9a	2	2Cu	1	1100	H_2S	2	2.0	0.54	115
V-9b	2	2Cu	1	1100	H_2S	4	2.0	0.47	110
V-9c	2	2Cu	1	1100	H_2S	4	2.0	0.44	100
				+1100	$H_2S + H_2O$	2			
V-10a	2	2Cu	1	950	Air	2	None		
V-10b	2	2Cu	1	950	Air	4	None		

* Concentration x 10^{-4} (molar) of dopant

** x is additional activator (S) and concentration x10^{-4} (molar)

TABLE 2
(Continued)

Expt. No.	Dopant V*	Dopant X**	Host ZnS	Temp. °C	Firing Atmosphere	Time, Hours	Fluorescence Peak, Microns	Relative Efficiency	Decay Time Microseconds
ZnS			RCA 33-219						
V-11a	10	10Cu	1	950	H_2S	2	1.8	0.56	140
V-11b	10	10Cu	1	950	H_2S	2	1.8	0.75	155
V-12a	5	5Cu	1	950	H_2S	2	1.8	0.29	140
V-13a	1	1Cu	1	950	H_2S	2	1.8	1.35	145
V-14a	0.5	0.5Cu	1	950	H_2S	2	1.8	1.82	160
V-14b	0.5	0.5Cu	1	1100	H_2S	2	2.0		110
				+950	H_2S	2			
V-15a	2		1	950	H_2S	2	None		
V-16a	2	0.5Cu	1	950	H_2S	2	1.8	1.03	165
V-17a	2	5Cu	1	950	H_2S	2	1.8	0.18	160
V-18a	2	2Cu	1	1100	H_2S	2	1.8	0.81	110
V-19a	0.5	0.5	1	950	H_2S	2			
V-19a	0.5	0.5Cu	1	1100	H_2S	2	1.8	1.12	130
				+950	H_2S	2			
V-20	0.25	0.25Cu	1	950	H_2S	2	1.8	1.33	150
V-21#	0.5	0.5Cu	1	950	H_2S	2	1.8	1.82	165
V-22	0.5	0.5Cu	1	950	H_2S	6	1.8	2.06	150
V-23	0.5	0.5Ag	1	950	H_2S	2	1.8	0.47	
V-24	2	2Ag	1	950	H_2S	2	1.8	4.85	190
V-25	2	2Ag	1	1100	H_2S	2	1.8	6.25	
V-26	0.5	0.5Au	1	950	H_2S	2	None		
V-27	2	2Au	1	950	H_2S	2	1.8	0.28	
V-28	2	2Au	1	1100	H_2S	2	1.8	1.21	
V-29	0.5	0.5Pb	1	950	H_2S	2	None		
V-30	2	2Pb	1	950	H_2S	2	None		
V-31	2	2Pb	1	950	H_2S	2	None		

#Large batch phosphor used for Field Test Target #1

CONFIDENTIAL

TABLE 2
(Continued)

Expt. No.	Dopant V*	Dopant X**	Host ZnS	Temp. °C	Firing Atmosphere	Time, Hours	Fluorescence Peak, Microns	Relative Efficiency	Decay Time Microseconds
V-32	V-21			950	H_2S	24	1.8	4.39	200
V-33	V-21			950	H_2S	60	1.8	3.79	160
V-34	V-21			1100	H_2S	104	2.0	1.82	120
V-34	V-21			980	Vacuum	168	1.8	1.52	160
V-36	1	1Cu	1	1100	H_2S		2.0	1.52	160
Q-21	V-21			980	Vacuum	104	None		
				+1060	Vacuum	138			
Q-11	2	2Cu	1	1000	Vacuum	120	1.8	1.21	200
Q-18	2	2Cu	1	980	Vacuum	336	1.8	0.15	160
Q-3	V-13a + Superbrite (1-5) 380-5005						1.8		
Q-6	0.01M + Borate Glass			900	H_2S	2	None		
R-1		32Eu	1	950	H_2S	2	None		
R-2		32Eu	1	1100	H_2S	1	None		
R-2a		32Eu	1	1100	H_2S + HCl	1	None		
R-3		32Eu					None		
		50Na	1	1100	H_2S	2	None		
R-4	R-3			950	H_2S	1 1/2	None		
R-5	2Er	2Cu	1	950	H_2S	2	None		
R-6	2Er	2Ag	1	950	H_2S	2	None		
R-7	0.5	2Cu 1.6Er	1	900	H_2S	2	1.8	0.56	
R-8	0.5	2Ag 1.6Er	1	950	H_2S	2	1.8	6.35	220

CONFIDENTIAL

CdS type doped with vanadium and a second coactivator showed the most promise for a high efficiency phosphor. The data and composition of these phosphors are shown in Table 2. As the data indicate, the most important variables are the heat treating temperature and the concentration and type of coactivator.

3.1.4 Effect of Heat Treatment

For the ZnS(Cu,V) phosphors, V-1 to V-19a, treatment below 1,000°C has no significant effect on the decay time of the phosphor, but there is some increase in efficiency with increasing temperature or with time at constant temperature. This is probably due to an increase in the uniformity of coactivator distribution in the zinc sulfide.

Heat treatment above 1,000°C produces two significant changes; the decay time is shortened from about 160 microseconds to 100 microseconds and the peak of the emission spectra shifts further into the infrared from 1.8 to 2.0 microns. This is due to a change in crystal structure from cubic to hexagonal, which zinc sulfide undergoes at about 1060°C. This hexagonal phase is also stable at room temperature. It would be expected that such a lattice would provide some different recombination sites for the coactivators, which would produce the difference in decay time and emission peak. Although this effect was quite pronounced in the (Cu,V) samples, it did not show up where the Cu was replaced by Au or Ag.

3.1.5 Effect of Coactivators

In the zinc sulfide (Cu,V) phosphors there is a very sensitive dependence of output efficiency on the concentration of Cu and V. This is plotted in Figure 2. Replacing Cu by Au or Ag produced two quite different effects. First, greater output efficiency is obtained with high concentrations of Au or Ag; and second, the efficiency is higher when the phosphors are heat treated above the transition temperature. There is no significant effect on the peak emission wavelength. The most efficient of all the phosphors prepared during this program is R-8 which in addition to Cu and V also contained erbium. The increase in efficiency is probably due to an increase in lattice absorption at 1 micron due to Er. There is also a slight increase in decay time. Unfortunately, this phosphor was formulated in a small batch at the end of the contract period, after the large batch phosphors and paints had been made, precluding its use in the field tests.

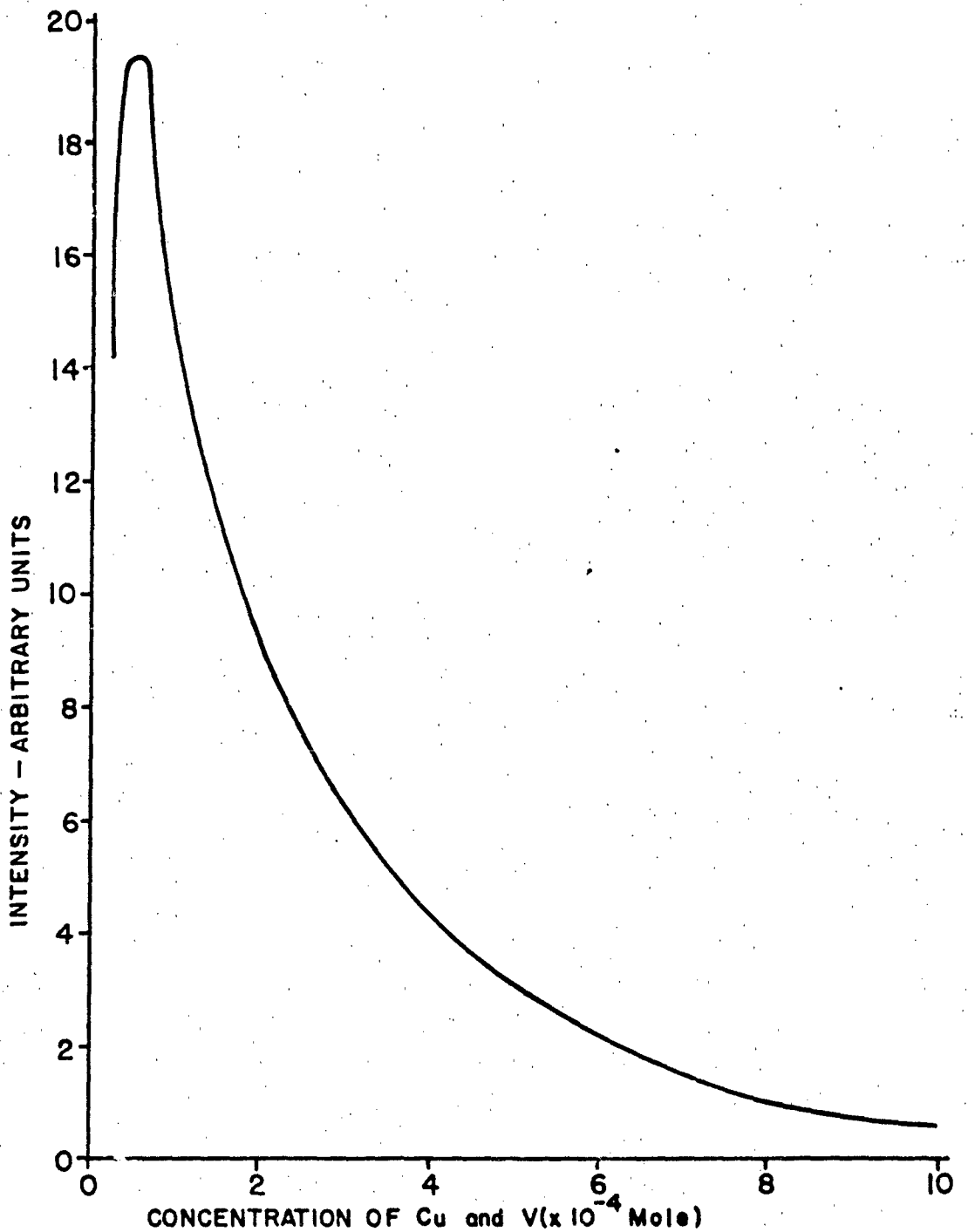

RELATIVE PHOSPHOR OUTPUT AS A FUNCTION OF DOPANT CONCENTRATION

FIGURE 2

3.1.6 Other Phosphor Formulations

Exclusive of the ZnS(Cu,V) phosphors, the other formulations which fluoresced under laser excitation were V-3 and V-4 and CdSe (Cu,In). The data for V-3 and V-4 are given in Table 2. It was not possible to measure the emission of the CdSe(Cu,In) phosphor with a 1.06 micron filter in the Beckman, since the emission is close to 1 micron. However, it was measured with a red filter and found to peak at 1.2 microns. When the phosphor was irradiated with a laser, there was a detectable phosphor return. Since the signal level was considerably lower than the vanadium series phosphors and the material is quite toxic, no further work was done on this series of phosphors with the exception of some investigation done under red excitation.

Many of the phosphors which were prepared are listed in the literature as being infrared emissive. Since they are not excited by 1.06 micron radiation, many of the old phosphors and all of the HC series were checked in the Beckman as described above, using a He-Ne laser which emits at 6328A. The emission peaks are given in Table 3.

3.1.7 New Phosphor Systems

Other systems which were investigated, but which did not fluoresce under 1.06 micron excitation, were the HC series containing CdS and CdS-HgS with different activators. CdS phosphors normally fluoresce in the red. With the addition of HgS, their emission shifts into the infrared. For example, CdS activated with Cu emits at 0.72 microns[2]. The addition of 30% HgS to CdS-Cu shifts the emission to 1.3 microns. Further additions to 75% shifts the emission to 1.75 microns.

Several phosphors containing 70% CdS, 30% HgS (C8) were prepared and tested as described above. They did not fluoresce with red or infrared excitation. Another set of phosphors containing CdS-HgS were activated with gold and aluminum in an attempt to shift the excitation and emission spectra further into the infrared. These compositions did not fluoresce with either 1.06 micron or 6328A excitation. In addition, the toxicity of this combination made it impractical for further investigation.

3.1.8 Phosphor Efficiency and Linearity

In order to determine the efficiency of the phosphor

(2) G.F.J. Garlick, M.J. Dumpleton; Phosphors Emitting Infrared Radiation, Proc. Phys. Soc., B., (London), 67,442-3 (1954).

TABLE 3

Red Excited Phosphors

No.	Composition	Peak Emission (Microns)
--	CdSe-CdS (Cu,In)	1.05
16	CdS (Cu,In)	1.05
--	CdS-80	1.0
A1-7	CdS (Cu,Al)	0.95
PC-100	CdS (Cu)	1.0
8c	CdS (Cu,Tb) NaCl	1.05
7c	CdS (Cu,Pb)	1.0
8	CdS (Cu,Sn) NaCl	1.1
7a	Cd (Cu,Tl 0.1) NaCl	1.0
7b	CdS (Cu,Tl 1.0) NaCl	0.95
11b	CdS ZnS (Cu,Tb) NaCl	1.05
17c	CdSe (Mn,In)	1.15
17a	CdSe (Mn)	1.15
14b	CdSe (Mn) NaCl	1.15
--	CdSe (Cu,In)	1.2
--	CdS (Cu,In)	1.1
HC-5	CdS (Au,Al)	1.05

both as a function of rate of excitation and pump intensity, the efficiency was measured with a CW lamp source with appropriate filters, as well as with a laser beam.

3.1.8.1 CW Efficiency

One method for determining the efficiency of a phosphor was the use of a tungsten iodide, high intensity light source filtered with a 1.06 micron spike transmission filter as well as a water filter (to remove the light from 1.06 to 2 microns). The experimental procedure was as follows: 1) the phosphor card, Batch 2 control card with V-21 phosphor, was placed on a V block 45° to the incident beam; 2) a Ge photometer with a series of 1.06 micron reject, 1.5 micron pass filters, was also aligned 45° to the phosphor card. The phosphor signal from the phosphor card was displayed on a Tektronix scope and the amplitude of the signal was recorded; 3) the phosphor card was replaced by a white card of the same dimensions with the filters removed and the signal amplitude was measured. The efficiency K_e, was then calculated using the following formula:

$$K_e = E = \frac{V_{phos} \times R_{1.06}}{V_{white\ card} \times R_{1.75} \times T_f} \times 100 \qquad (1)$$

where V = voltage recorded

$R_{1.06}$ = relative response of Ge at 1.06 microns = 0.71

$R_{1.75}$ = relative response of Ge at center pass band of the filters = 0.6

T_f = transmission of filter set at 1.7 microns = 72.5%

The efficiencies obtained for V-21 (batch 2 control card) were 0.54% and 0.43%. Since the detector responsivity falls off rapidly at longer wavelengths (beyond 1.75 microns) where the phosphor is also emitting, it was necessary to measure the relative response of the photometer over the full band of phosphor emission wavelengths.

This was done by using the Beckman DK-2A as a monochromator. The variation in intensity of the Beckman light source over the wavelengths of interest was checked by first operating the Beckman in the normal mode for measuring transmission. In this mode, the Beckman is designed to monitor the

signal on the Beckman PbS detector and automatically adjust the width of the monochromator slit so that the signal out of the detector is constant. When the Beckman was scanned over this range of wavelengths, the slit width remained constant. Since the relative response of PbS is flat over this spectral region, and the slit width remained constant, the lamp intensity is also constant.

The Beckman was then adjusted to operate as a monochromator and the slit set at an opening of 2 mm. The beam from the monochromator was then diverted into the Ge photometer by means of a right angle prism. The output of the photometer was applied to an RMS reading voltmeter. The range of phosphor wavelengths was scanned on the Beckman and the peak voltage, as well as the 1/2 and 1/4 power points were recorded. These values were then superimposed on the emission curve of the large batch phosphor and a weighted curve was drawn as shown in Figure 3. The emission curve (curve 1) was traced from a phosphor output curve recorded on the Beckman using its own PbS detector, as described in Section 3.1.1. The values of relative output do not represent relative signals from PbS and Ge photometers with the same filtering. The weighted curve (curve 2) indicates what fraction of the phosphor output the Ge photometer filter combination would detect. The resultant areas of phosphor output and the corrected curve indicating the effect of the detector-filter responsivity, were measured using a planimeter. The ratio of the areas was 4:1. This means that although the average value of the efficiency of the phosphor was 1.9%, the final system efficiency is only 1/4 of that value.

3.1.8.2 Phosphor Efficiency with Laser Excitation

Both the laser and the phosphor photometer used in these measurements were calibrated using a black body source at 1,000°C. The phosphor photometer was calibrated with the filters in place.

A. Phosphor Photometer Calibration

The responsivity of the phosphor photometer, R_p, was calculated from the following conditions:

Black Body Temperature	1,000°C
Range, r	900 cm
Aperture Area of Black Body, Aa	5.06×10^{-2} cm^2
Signal Voltage, V	4.4×10^{-1} volts
Filter 50% transmission points	1.5 and 1.7 microns

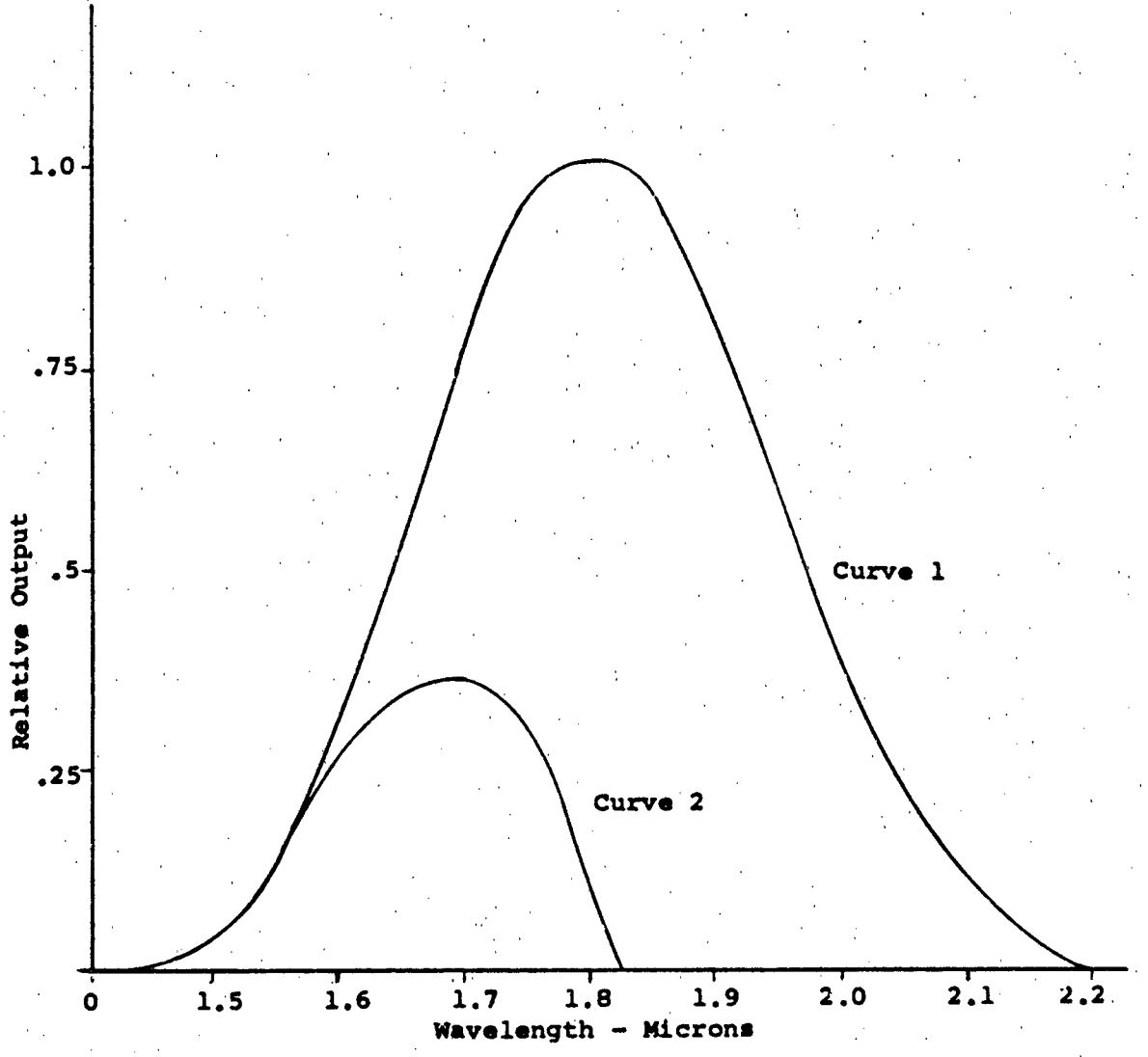

Curbe 1 - V-21 Phosphor Output
Curve 2 - Relative output corrected for Photometer Response.

EFFECTIVE PHOTOMETER SPECTRAL RESPONSE

FIGURE 3

From the black body temperature used, the source intensity in the spectral bandwidth of the filter set is found by use of the Radiation Slide Rule. The source intensity, N_o, was found to be:

$$N_o = 0.705 \text{ watts/cm}^2$$

The responsivity of the photometer is calculated using the following equation:

$$R = \frac{\pi r^2 V}{N_o A_a} \qquad (2)$$

$$= \frac{3.14 \times (9 \times 10^2)^2 \times 4.4 \times 10^{-1}}{7.05 \times 10^{-1} \times 5.06 \times 10^{-2}}$$

$$= 3.17 \times 10^7 \text{ volt-cm}^2/\text{watt}$$

B. Laser Photometer Calibration

The laser photometer was calibrated, without filters, using a black body source. The experimental conditions are as follows:

Black Body Temperature	1,000°C
Range, r	241 cm
Aperture Area of Black Boyd, A_a	2.02×10^{-1} cm^2
Signal Voltage, V	5×10^{-3} volts
Sensitive Spectral Range of the Photometer	0.7 to 1.18 microns

From the black body temperature used, the source intensity in the sensitive spectral region of the silicon detector photometer is found by use of a Radiation slide rule. This source intensity, N_o, was found by multiplying the fraction of power from the 1000°C black body in a 0.2 micron increment by the relative response of the detector in that same 0.2 micron increment. The sum of the products of these increments is thus the total source intensity normalized over the detector response. The source intensity was found to be:

$$N_o = 9.1 \times 10^{-2} \text{ watts/cm}^2$$

The responsivity of the laser photometer, R_L, is calculated using the following equation:

$$R_L = \frac{\pi r^2 V \rho}{N_o A_a} \qquad (3)$$

where ρ is the relative response of the photometer at 1.06 microns

$$= \frac{3.14 \times (2.41 \times 10^{2})^{2} \times 5 \times 10^{-3} \times 5 \times 10^{-1}}{9.1 \times 10^{-2} \times 2.02 \times 10^{-1}}$$

$$= 2.5 \times 10^{4} \text{ v-cm}^{2}/\text{watt}$$

3.1.9 Phosphor Efficiency Measurement

The phosphor efficiency was measured in the laboratory by aligning the phosphor and laser photometers so that their narrow angular fields coincided on the phosphor target at the point where the laser beam impinged. Initially the location of the laser beam on the target area was determined. A small light source was then placed at the beam location and both photometers were aligned until the output signals were maximized. The phosphor card was then put in the same position as the light source and the laser was fired. The output of the phosphor photometer was displayed on a scope and photographed. This measurement was made several times to assure reproducibility. The phosphor card was then replaced by a white card and a similar series of measurements were made for the laser photometer.

For the laser measurements, some additional filtering was necessary. The transmission of the filters was measured in the Beckman Scanning Spectrometer (Model DK-2A).

For this experiment, in order to insure that both photometers saw the entire output, the laser was physically masked down to approximately a 1/2" diameter point at the position of the phosphor card. The calculation of the energy efficiency is as follows:

$$E_L = \frac{2\pi r^2 V_L T_L}{T_f R_L} \qquad (4)$$

where E_L = energy out of laser
R_L = responsivity of laser photometer = 2.5×10^{4} V/w/cm^2
r = range of both photometers to target = 241 cm
T_f = filter transmission = 4.44×10^{-1}
V_L = peak signal voltage out of laser photometer = 0.4 volts average
T_L = 1/2 width of laser pulse = 2.5×10^{-5} sec.

Substituting into equation 4 yields E_L

$$E_L = \frac{(2)(3.14)(241)^2(0.4)(2.5)(10)^{-5}}{(4.44)(10)^{-1}(2.5)(10)^4}$$

$$E_L = 3.3 \times 10^{-4} \text{ joules}$$

We now calculate the energy from the phosphor, E_p using the relationship:

$$E_p = \frac{2\pi r^2 V_p T_p}{R_p} \qquad (5)$$

where V_p = peak voltage out of phosphor photometer = 0.36 volts average
T_p = 1/2 width of phosphor pulse = 330 microseconds
R^p = responsivity of phosphor photometer = 3.17×10^7 V/w/cm^2
r^p = 241 cm

Substituting these values into equation (5) yields the measured value, E_p:

$$E_p = \frac{(2)(3.14)(241)^2(0.36)(0.33)(10)^{-3}}{(3.17)(10)^7}$$

$$E_p = 1.37 \times 10^{-6} \text{ joules}$$

The energy efficiency of the phosphor K_e, is then

$$K_e = \frac{E_p \times 100}{E_L} \quad \text{or} \qquad (6)$$

$$K_e = \frac{1.37 \times 10^{-6}}{3.3 \times 10^{-4}} \times 100 = 0.4\%$$

This is a typical value of the energy efficiency for the phosphors measured in this program.

3.1.10 Phosphor Linearity

In order to determine the presence of saturation effects, if any, the phosphor emission was monitored as a function of laser input energy. Since the laser output is linear with flash lamp input, as shown in Figure 4, only relative values of the phosphor emission were measured. The measurements were made with input

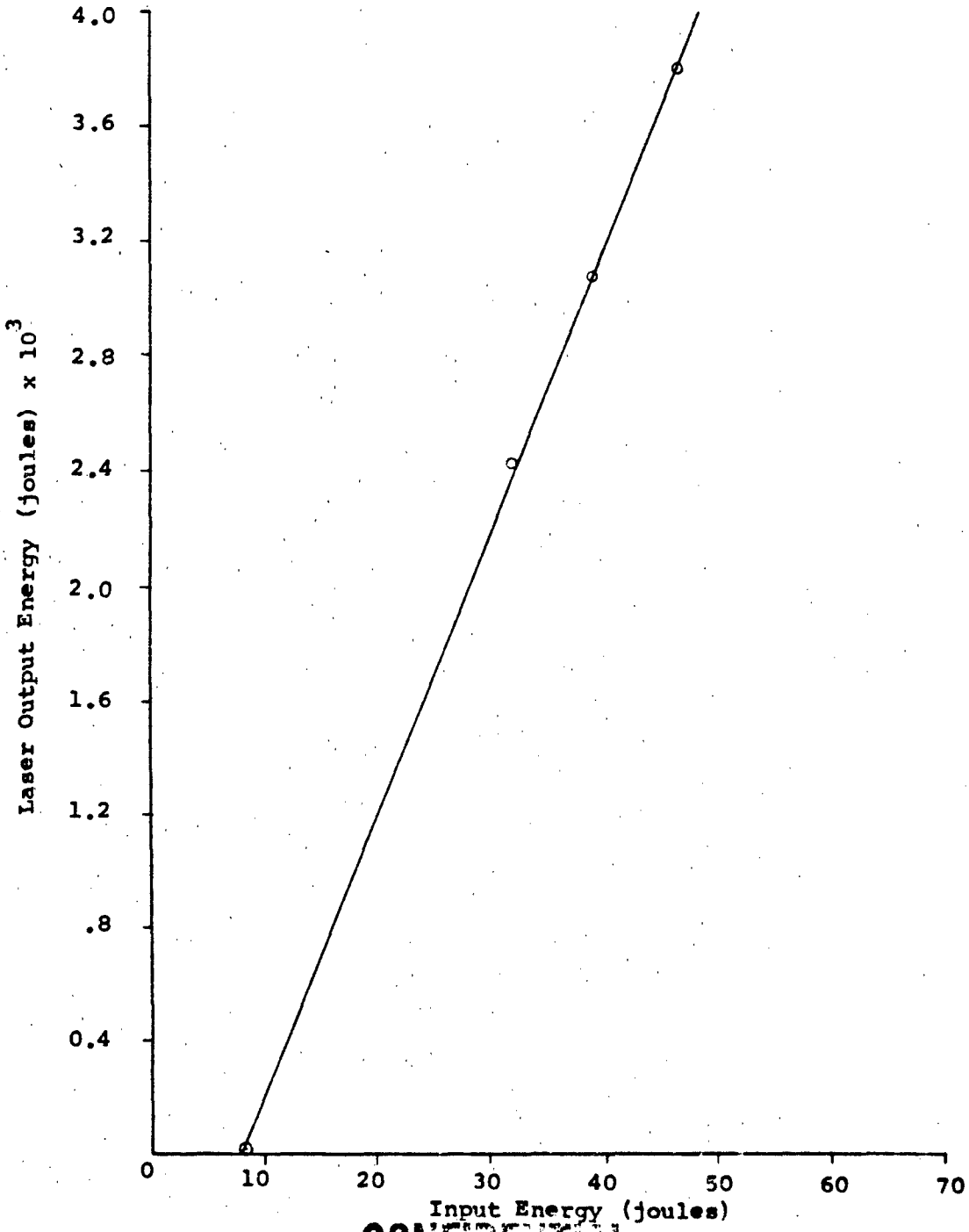

Laser Output Energy As A Function of Input Energy

FIGURE 4

energies up to 70 joules. The pulse duration was approximately 40 microseconds. The plot of phosphor output as a function of flash lamp input is shown in Figure 5.

When the laser power density of the test set was measured, subsequent experiments were run to be sure there were no saturation effects at this power level. The experimental procedure was as follows. A laser was aligned with external mirrors, with a 4% transmitting mirror as the output reflector. The laser pulse duration was approximately 60 microseconds. The laser output was monitored using a calibrated laser photometer and the flash lamp energy was increased until the laser output was 2.46 watts/cm^2.

A phosphor card, ZP-7B-2, was positioned in the path of the beam and the phosphor output was monitored with a phosphor photometer with 1.06 micron reject filters to eliminate the laser output. Filters with different transmissions were placed between the phosphor card and the laser to vary the incident power density on the phosphor card. The results are plotted in Figure 6. As this figure shows, there is no saturation of the phosphor with increasing laser energy or power density.

3.1.11 Phosphor Radiant Efficiency as a Function of Pump Time

The phosphor radiant efficiency can be defined in two ways. The first defines the radiant efficiency as the ratio of power out to power in for the phosphor in question. Power out is defined as the power [illegible]itted from the phosphor surface in the spectral emission ba[illegible]er in is defined as the pumping power impinging on the ph[illegible]urface at the wavelengths of phosphor absorption.

The second definition of radiant efficiency is the ratio of emitted energy to input energy. The emitted and input spectra are the same for either definition of efficiency.

Both the power and energy ratios were measured as a function of pump time with the total pulse energy held constant. The power ratio was predicted to vary with input time by the following relationship.

Assuming a phosphor which is linear with constant input pulse width as shown in Section 3.1.10, the power emitted at any time P_o (t) can be determined by,

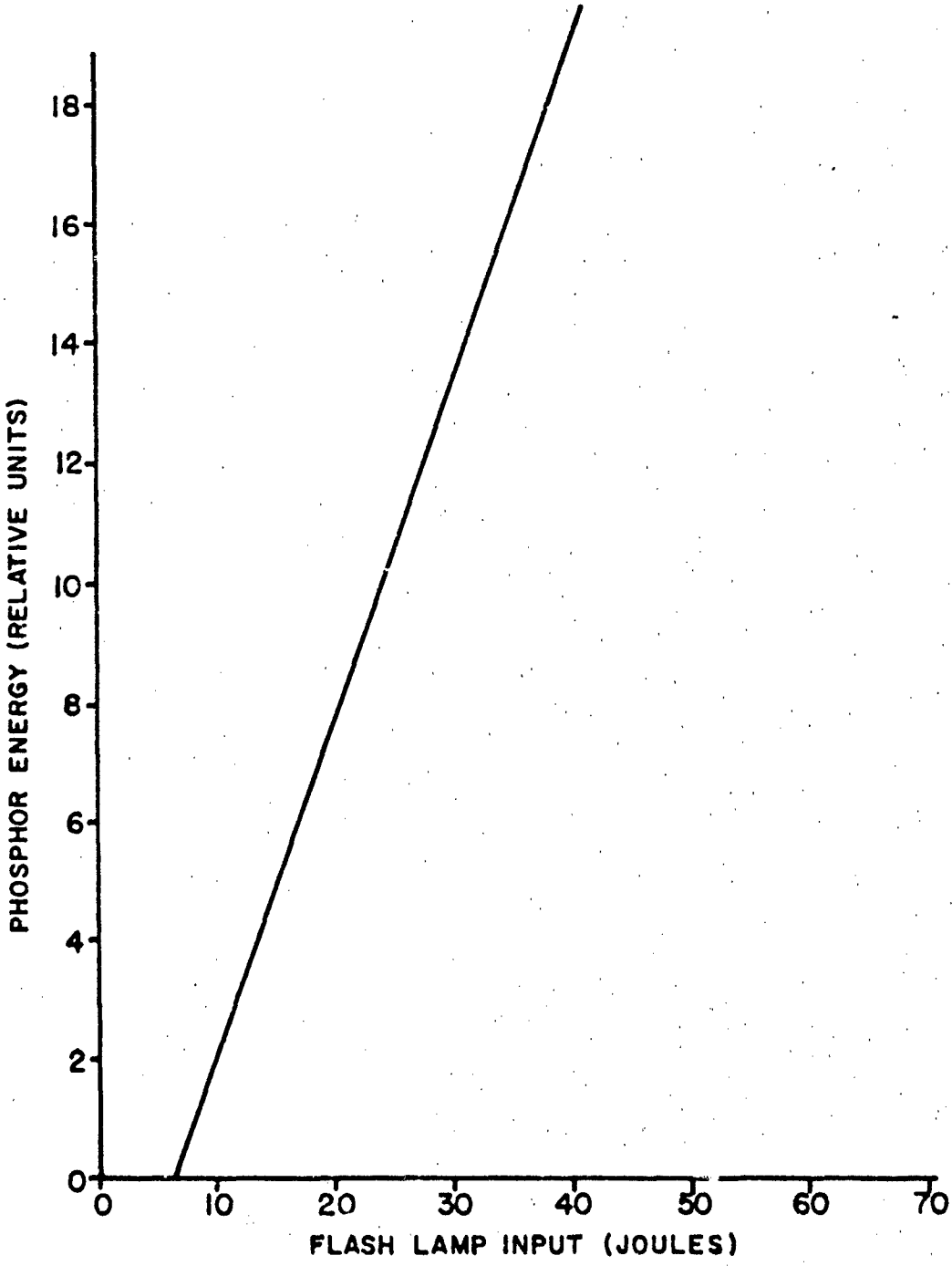

PHOSPHOR ENERGY AS A FUNCTION OF FLASH LAMP INPUT

FIGURE 5

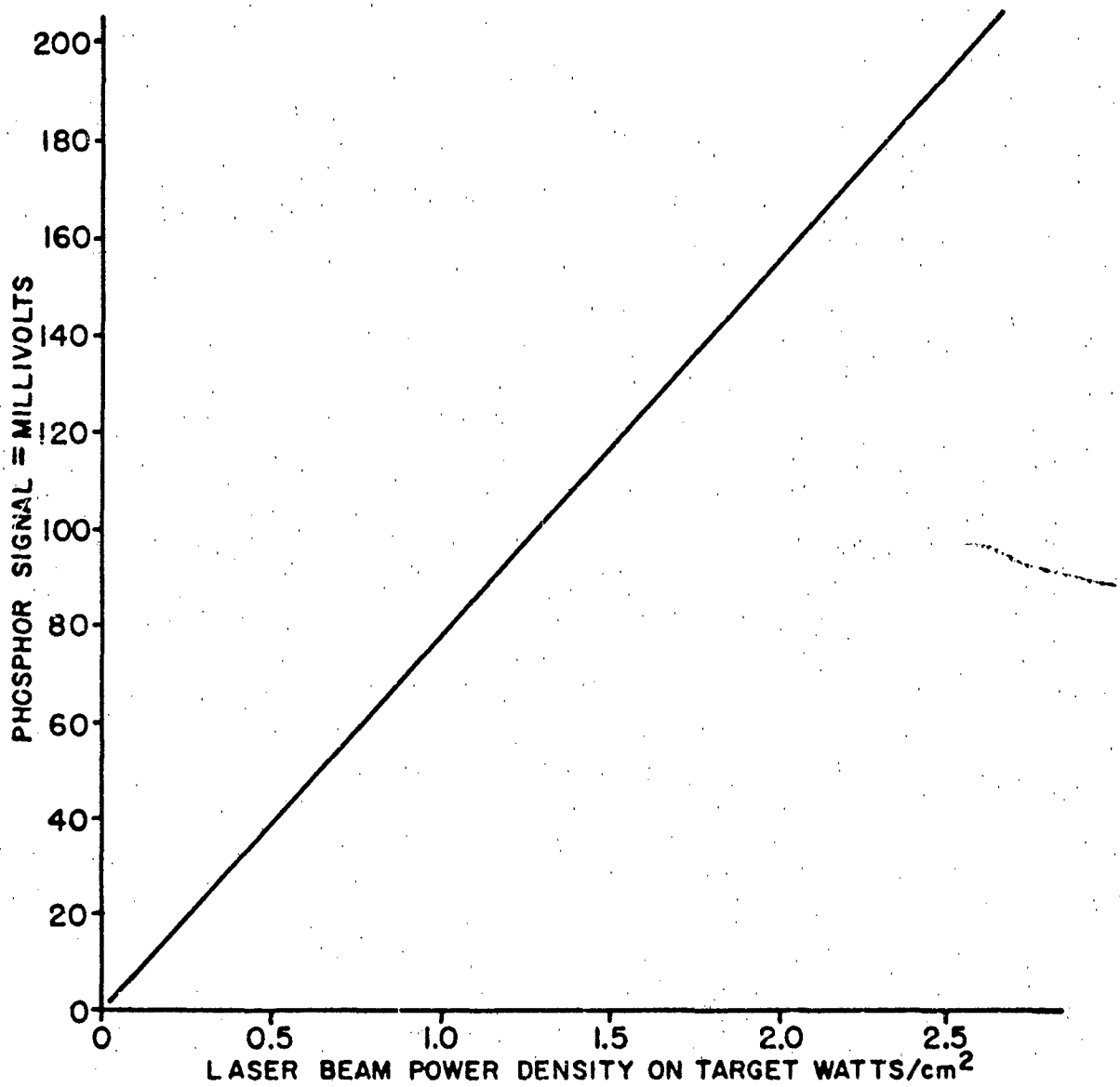

VARIATION OF PHOSPHOR OUTPUT AT 1.8 MICRONS AS A FUNCTION OF INCIDENT LASER POWER AT 1.06 MICRONS

FIGURE 6

$$P_o(t) = K_e \int_o^t \frac{P_1(\alpha)\, e^{-(t-\alpha)/T}}{T}\, d\alpha \qquad (7)$$

where K_e = the ratio of energy out to energy in.

$P_1(\alpha)$ = the variation of pump power with time, the shape of the laser pulse.

T = the phosphor decay time.

Assuming a rectangular pumping pulse, a good approximation can be obtained for the variation in output power with pulse width.

The equation for a rectangular input pulse is

$$\begin{aligned} P_1(\alpha) &= 0 \text{ for } t < 0 \\ &= P_1 \text{ for } 0 \leq t \leq \Delta t \\ &= 0 \text{ for } \Delta t < t \end{aligned} \qquad (8)$$

where Δt = pulse width

By substituting equation (8) into equation (7) the output power is given by:

$$P_o(t) = \frac{PK_e}{T} e^{-t/T} \int_o^t e^{+\alpha/T}\, d\alpha \quad \text{for } 0 \leq t \leq \Delta t \qquad (9)$$

and

$$P_o(t) = \frac{PK_e}{T} e^{-t/T} \int_o^{\Delta t} e^{+\alpha/T}\, d\alpha \quad \text{for } \Delta t \leq t \qquad (10)$$

The maximum value of $P_o(t)$, the peak output power, is found by equating t to Δt so that the power effieiency, K_p, becomes:

$$K_p = \frac{P_o(\Delta t)}{P_1} = K_e\,(1 - e^{-\Delta t/T}) \qquad (11)$$

This equation has been compared to the data taken by plotting P (peak) on the data plot. As expected, equation (11) shows that for pulses much longer than a time constant, the power and energy radiation efficiencies are equal, ($K_p = K_e$).

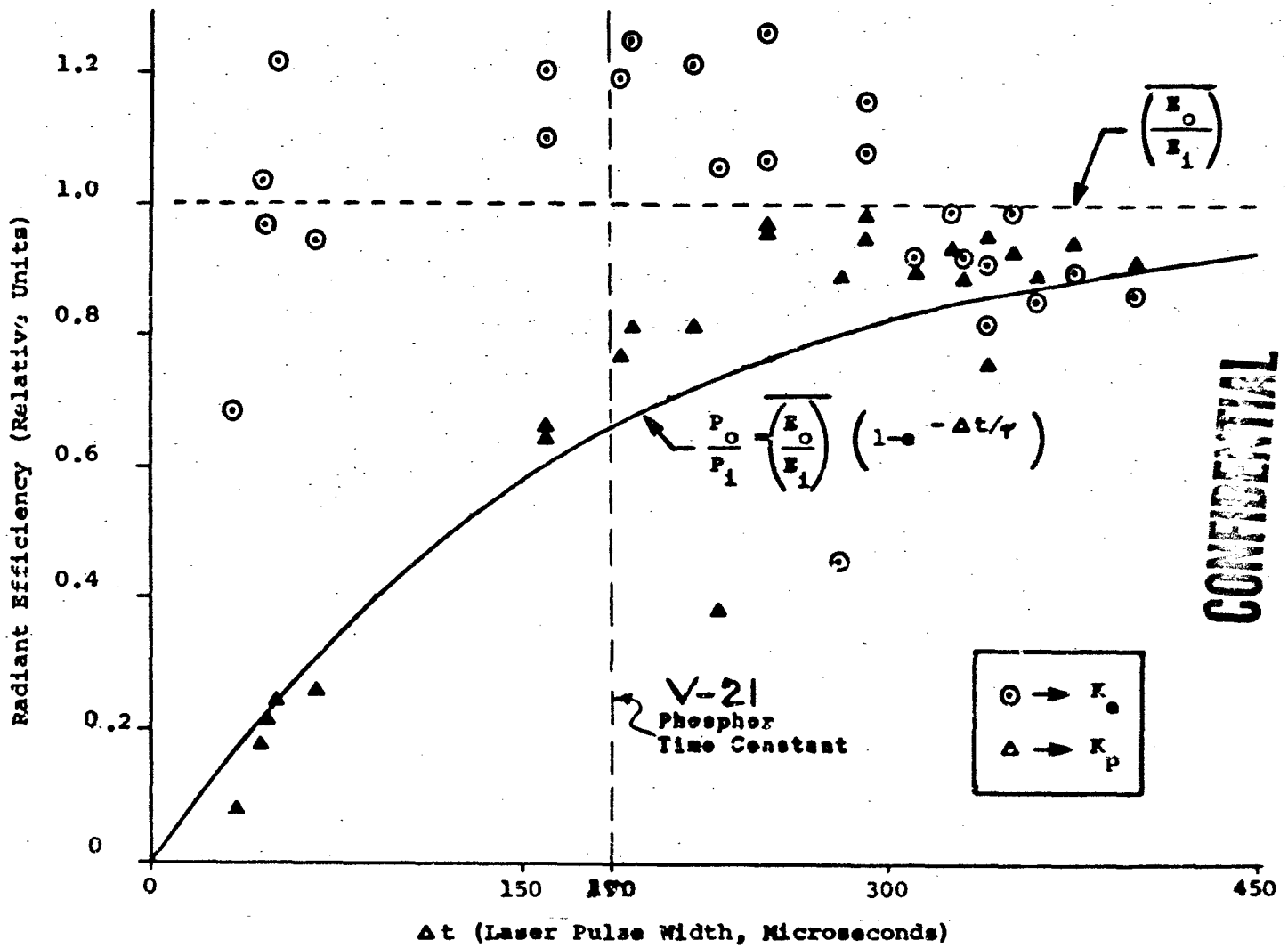

FIGURE 7. Radiant Efficiency as a Function of Laser Pulse Width

The ratios of the output to input energy and peak output to input power measured as function of laser pulse width are plotted in Figure 7. The energy ratio varied slightly with input pulse width. The experimental accuracy accounts for the major variation in the energy ratio. Such a variation would have a minimal effect on the system performance. The power ratio variation with pulse width was found to follow approximately the same curve as predicted in equation (11). The net result of this measurement is the verification of the constancy of K_e with variation in the pulse width and the reduction in K_p for laser pulses narrower than two phosphor time constants.

3.1.12 Phosphor Absorption and Excitation Spectra

Initial attempts to measure the absorption spectra of the phosphors were made by using the Beckman DK-2A with the fluorescent attachment and comparing the reflectivity of a white card with that of the phosphor card with a tungsten lamp used as the source. The output of the tungsten lamp showed considerable variation with wavelength and although strong absorption in the visible was noted, no significant structure could be observed in the region of interest at about 1 micron.

The Beckman was eventually modified so that it could be used as a monochromator, where the intensity of illumination over the wavelengths of interest was reasonably constant and equal, and the fluorescent emission as a function of wavelenght could be measured and recorded. The Ge photometer was used, with filters to pass the fluorescent wavelengths and reject the exciting light. This technique gave an accurate measure of the useful excitation spectra of the phosphor used for the field tests. The curve for the phosphor is shown in Figure 8.

3.1.13 Phosphor Return Signal Evaluation

A Krohn-Hite Model 310-AB variable bandpass filter was used to analyze the relative amplitudes of the frequencies present in a simulated phosphor return signal. The typical phosphor return consists of a 50 microsecond rise time ramp followed by an approximately exponential decay of 170 microsecond to the 1/e point as shown in Figure 9.

The shaped pulse of known amplitude was applied to the variable bandwidth filter and the amplitude of the damped sine wave output (peak-to-peak) recorded for various center frequency settings of the filter. The peak-to-peak voltage was then

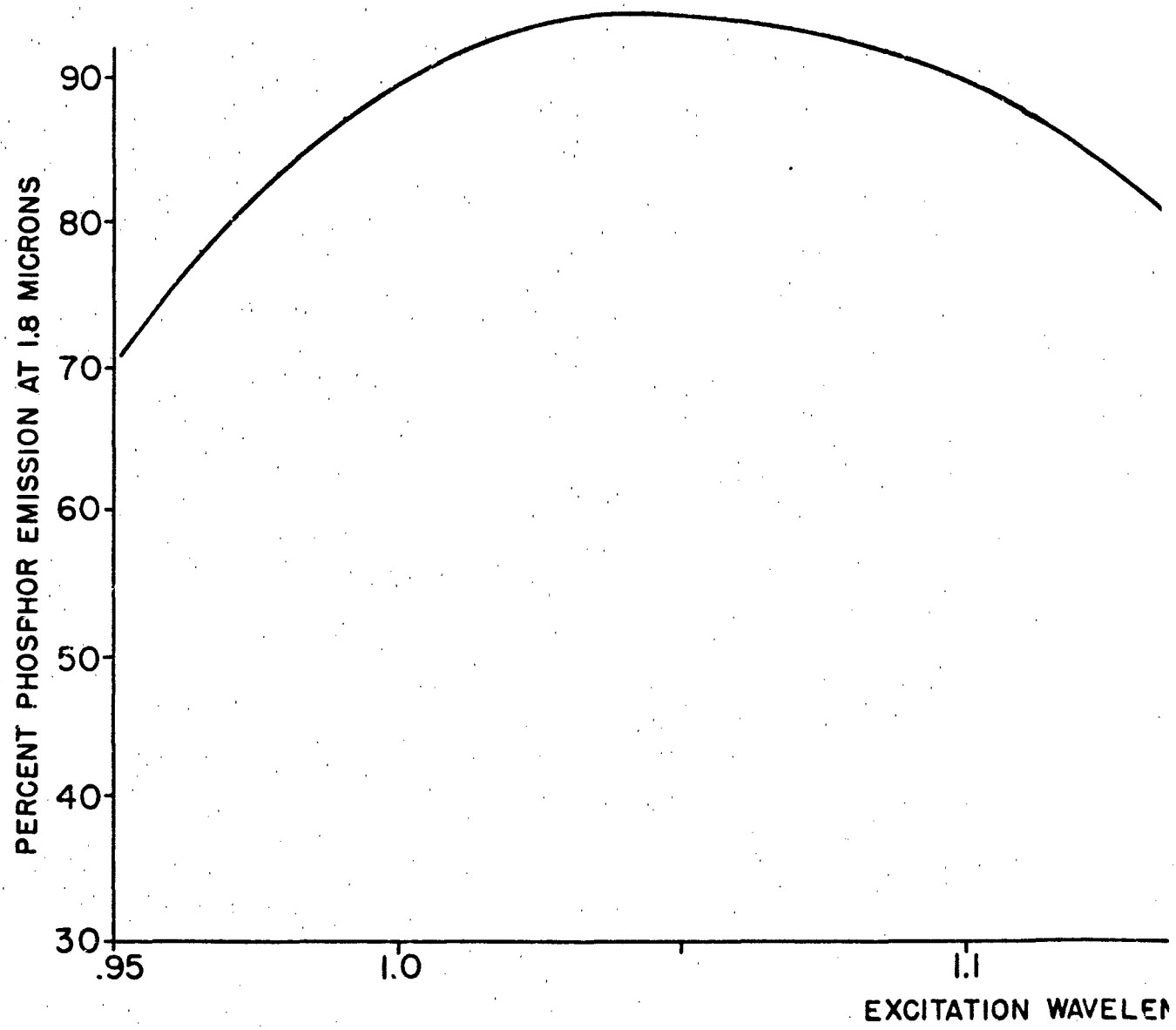

V-21 PHOSPHOR EMISSION AT 1.8 MICRONS AS A FUNCTI

1

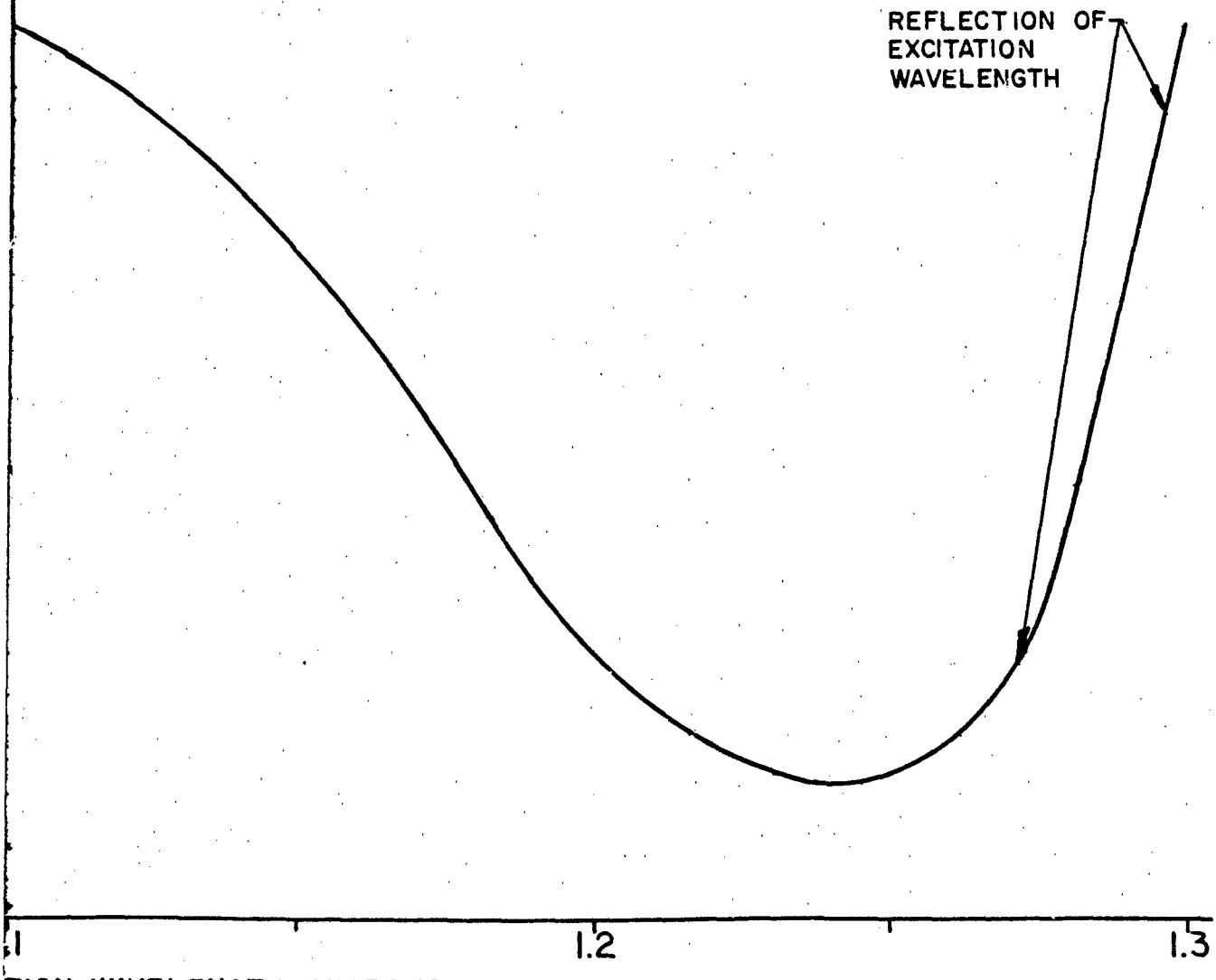

TION WAVELENGTH - MICRONS

S A FUNCTION OF EXCITATION WAVELENGTH

FIGURE 8

2

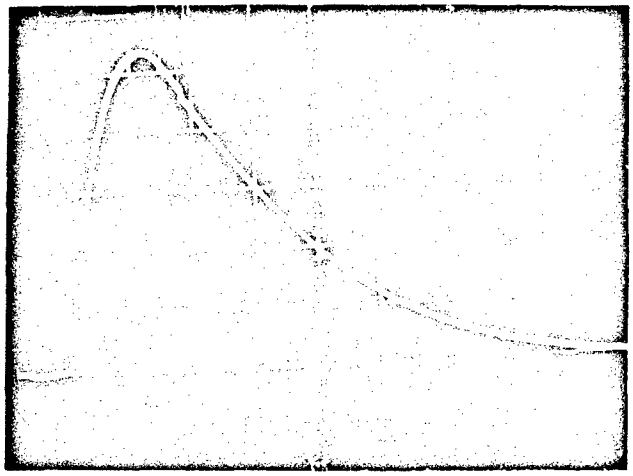

FIGURE 9. Typical Phosphor Return Signal, V-21 Phosphor,
Scale: (0.2V/cm
100usec/cm)

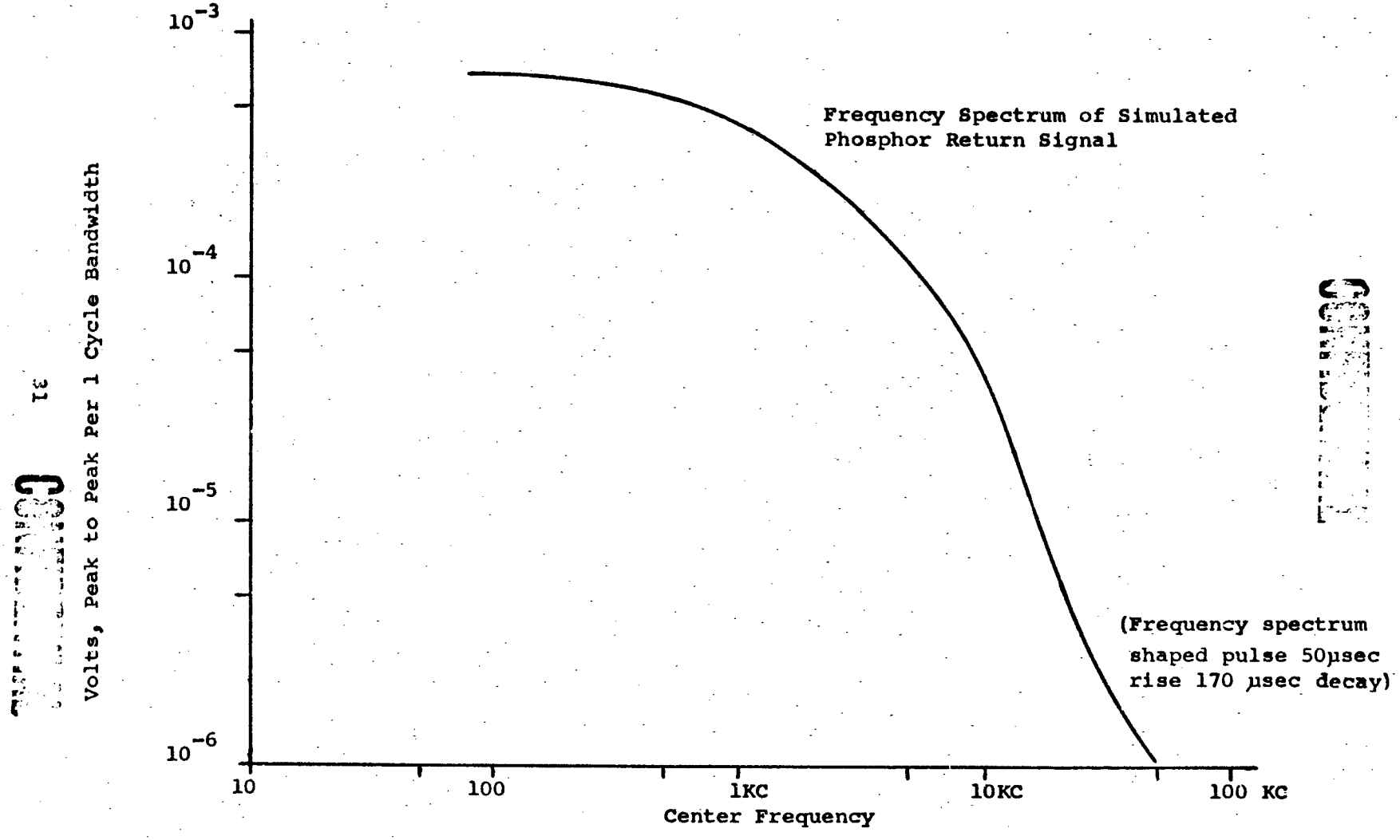
Frequency Spectrum of Simulated
Phosphor Return Signal
(Frequency spectrum
shaped pulse 50μsec
rise 170 μsec decay)
Volts, Peak to Peak Per 1 Cycle Bandwidth
10^{-3}
10^{-4}
10^{-5}
10^{-6}
10
100
1KC
10KC
100 KC
Center Frequency

FIGURE 10

divided by the bandwidth for a given center frequency to normalize the curve to a one cycle bandwidth for ease of interpretation. Figure 10 shows the volts peak-to-peak per one cycle bandwidth as a function of the center frequency. The curve thus represents the frequency content of a typical phosphor return signal and indicates the range of frequencies which will produce maximum signal if a narrow band amplifier (1 cps bandwidth) is used. For instance, at 100 cps, which is the curve center frequency, the output signal would be about the maximum possible. On the other hand, if the amplifier was centered at 2 KC, the output signal would be about 42.7% of the maximum. If noise were not a factor in this system, the choice of a 100 cps center frequency would be obvious. Unfortuntely, the greatest noise amplitudes occur at low frequencies because of the 1/f effect, i.e., the lower the frequency, the higher the noise. For this reason, a tradeoff in signal amplitude had to be made against noise. The optimum center frequency therefore was found to be located between 1.5 KC and 3 KC. The preamplifier was accordingly adjusted to have a center frequency within the 1.5 KC to 3 KC band.

3.1.14 Preparation of Large Batch ZnS-AgV Phosphors

Prior to the preparation of large batch phosphors, some small samples were made with varying amounts of Ag and V. The concentration of Ag was varied from 0.5 to 6 x 10^{-4} molar. Vanadium was varied from 0.5 to 3 x 10^{-4} molar. The data for these phosphors as well as the final large batch phosphor are shown in Table 4. As indicated previously, the concentration of V and Ag do not produce radical changes in efficiency as is the case for the ZnS(Cu,V) phosphors. The decay time is not significantly dependent on composition.

For large batch phosphors of ZP-1B and ZP-6B series the efficiency was found to be lower than the small batch samples of the same composition. This was discovered to be due to heat treatment at 1000°C instead of 950°C. When the temperature was corrected, the efficiency of the large and small batches were equivalent.

The large batch phosphor used for most of the targets (all excpet target #1) was ZP-7B-2. The details of the large batch preparation are given in Section 3.1.15.

3.1.15 Preparation of ZP-7B-2 Phosphor

The preparation procedures for the large batches of ZP-7B-2 used in field testing are described here in detail.

TABLE 4

Large Batch Phosphor Preparations

No.	Dopant Ag*	Dopant V*	ZnS	Furnace In	Heat Time	Efficiency %	(Microseconds) Decay Time
ZP-1	2	2	0.1 moles	Small 950°C	4	2.90	
ZP-1R	2	2	0.1	Small 950°C	28	3.75	180
ZP-2	0.5	0.5	0.1	Small 950°C	4	1.96	200
ZP-3	4	4	0.1	Small 950°C	4	2.90	170
ZP-4	2	6	0.1	Small 950°C	4	1.03	190
ZP-5	6	2	0.1	Small 950°C	4	3.74	
ZP-5R	6	2	0.1	Small 950°C	28	3.74	
ZP-7-1	6	2	0.1	Small 930°C	2	2.05	
ZP-7-2	6	2	0.1	Small 930°C	4	2.61	
ZP-11-1	6	1	0.1	Small 930°C	2	2.42	
ZP-11-2	6	1	0.1	Small 930°C	4	1.45	
ZP-1B-1	2	2	4	Large	4	2.34	170
ZP-1B-2	2	2	4	Large	12	2.34	190
ZP-1B-3	2	2	ZP-1B-1	Small N_2	2	0.93	150
ZP-1B-4	2	2	4	Large	4	1.77	180
ZP-1B-5	2	2	4	Large	28	1.4	
ZP-6B-1	2	0.5	4	Large	7	0.93	
ZP-6B-2	2	0.5	ZP-6B-1	Small	24	3.74	
ZP-7B-1**	6	2	4 moles	Large	2	2.47	
ZP-7B-2	6	2	4	Large	4	2.47	200
ZP-8B-1	6	1.5	4	Large	2	1.96	
ZP-8B-2	6	1.5	4	Large	4	2.89	
ZP-9B-1	6	2.5	4	Large	2	1.87	
ZP-9B-2	6	2.5	4	Large	4	2.47	
ZP-10B-1	6	3	4	Large	2	1.31	
ZP-10B-2	6	3	4	Large	4	1.87	
ZP-11-1	6	1	0.1	Small	2	2.42	
ZP-11-2	6	1	0.1	Small	4	1.45	

* Concentration x 10^{-4} molar

** Phosphor used in field tests

CONFIDENTIAL

Materials: Phosphor grade zinc sulfide was obtained from Radio Corporation of America, RCA Electron Tube Division, Lancaster, Pennsylvania. Reagent grade ammonium metavanadate and silver nitrate were used to make 0.01 molar aqueous solutions in distilled water for activating.

Apparatus: The firings of the phosphors were carried out in a horizontal tube furnace consisting of a resistance ceramic core 3 feet in length and 2-3/8 inches in internal diameter which was insulated with glass wool and fire brick. A vitreosil tube 4 feet in length and of 1-3/4 inch I.D. passing through the furnace provided a chamber within which a hydrogen sulfide atmosphere was maintained. The sample boat, made of clear vitreosil tubing 18 inches long and of 35 mm O.D., rested on the bottom inner surface of the larger vitreosil tube.

A PT-PtRh thermocouple and a West "Guardsman" controller were used to achieve the desired temperature. The correct controller setting to achieve the chosen temperature at the position of the sample boat was determined in preliminary tests.

Procedure: For each batch, 389.6 grams (4 moles) of dry powdered ZnS were weighed out and placed in a large procelain mortar. Appropriate volumes of 1.01 M ammonium metavandate and silver nitrate solutions were added, the mixture mixed well and evaporated to dryness overnight in a 110° drying oven. The cake was broken up and ground well in a mortar. Enough water was added to thoroughly moisten the material and thereby promote uniform distribution of the activating agents under further grinding. The drying, grinding, moistening, grinding sequence was repeated twice more, then the preparation was finally dried and ground and loaded into the sample boat for high temperature firing.

The firing cycle consisted of placing the sample boat into the furnace at room temperature, starting the flow of dry H_2S, heating to 950°C, holding for 2 hours and cooling to room temperature with H_2S still flowing (a rate of a few bubbles per minute after an initial flushing was used). The phosphor sintered to a hard cake during firing. It was broken up and ground with the mortar and pestle and the firing cycle repeated. Final size reduction was achieved by ball-milling and screening.

3.1.16 Phosphor Paint Preparation

Several formulations of phosphor bearing paints were prepared and evaluated for use in the measurements program.

Placing the phosphor in a binder is desirable for obtaining a test target with stable characteristics. That is, the phosphor stays in place and is not affected by handling during experiments. It is emphasized that a paint vehicle is not necessary in an operational system. The following characteristics of a phosphor paint are desirable: transparency in appropriate spectral regions, easily prepared, applicable by spraying, and economical in phosphor content yet giving good phosphor cover.

Clear lacquer, thinned with acetone, and methylmethacrylate polymer, thinned with acetone, were both evaluated. These materials were found to have the necessary transmission bands for phosphor excitation and emission when applied in thin layers. Unfortunately, neither material could be used as a phosphor vehicle because of improper wetting and drying characteristics of the lacquer and uneven coverage of the polymer.

Attention was then turned to formulating linseed oil based paints. The constituents used were boiled linseed oil, turpentine, Japan dryer, and phosphor. Several test batches without phosphor were mixed to evaluate transmission and drying characteristics. The best mixture ratio for the binder alone was found to be 10 parts of linseed oil to 7 parts turpentine to 3 parts dryer by weight.

A 40 gram batch of phosphor paint was made with a one to one phosphor to binder ratio. The mixture was rotated in a cooled ball mill for approximately sixteen hours. The finished paint was found to settle overnight, but stirring soon restored it to the desired uniform consistency.

The paint sprayed easily and gave a dense, uniform matte finish. Although the solvent (turpentine) evaporates out in a matter of minutes, the linseed oil, as in most oil base paints, takes a few days to completely polymerize. This, however, is not considered to be a drawback since, even in this unpolymerized state, the paint samples could be handled and tested with no difficulty. Comparative measurements were made of a painted sample and of a phosphor powder layer on double coated scotch tape, using the Beckman DK-2A as discussed in Section 3 of this report. No difference was observed between the paint and the pure phosphor.

A similar formulation was used to provide 500 grams of phosphor paint for field test targets. This batch differed from the previous formulation (designated Batch 2) only in that

it contained ZP-7B-2 instead of V-21 as a phosphor. It was noted that the ball-milling time required by the batch containing ZP-7B-2 was several days longer than that required by the V-21 bearing Batch 2. This was attributed to a larger particle size of the ZP-7B-2 powder, compared to V-21, prior to ball milling.

3.1.17 Preparation of Test Targets

Several targets were prepared for field testing as outlined in Table 5. Items of various shapes and textures were sprayed with the phosphor bearing paints by means of an airbrush using dry nitrogen as a propellant. Undercoatings were also applied to certain targets to change the surface reflectivity for both exciting and emitted radiation. Target No. 7 had to be undercoated because the phosphor paint binder attacked the plastic of the air inflated sphere.

In the case of Target No. 10, fabricated in the shape of a tetrahedron, each side received phosphor paint layers of a different thickness. This was accomplished by allowing a coating to dry and then respraying. In this manner, side 1 received one layer, side 2 two layers, and side 3 three layers. In each application the same amount of paint was evenly distributed over equal areas.

3.2 Lasers

To optimize the range and power capabilities of the test set as well as the compactness and portability of the equipment, it was necessary to measure laser power as a function of type of laser, dimensions of the laser, output mirror transmission, laser beam divergence, flash lamp energy and pulse shape. The latter two measurements are described in Sections 3.1.10 and 3.1.11.

3.2.1 Comparison of Ruby, $CaWO_4(Nd^{3+})$ and Nd Doped Glass

The initial design goals for the portable test set called for an input energy of approximately 100 joules. No data were available in the literature on the performance of $CaWO_4$ at these energy levels. To obtain this information, comparative output measurements were made of Nd doped $CaWO_4$ and Nd doped glass relative to ruby laser rods.

The laser output was monitored using a photometer with a silicon photodiode detector, filtered with a 0.69 micron spike

TABLE 5

Target Description

Target No.	Item	Phosphor	Undercoating	Substrate Surface
1	Batch 2 Control Card	V-21	None	Smooth tempered masonite
2	ZP7B-2 Control Card	ZP7B-2	None	Smooth tempered masonite
3	100 cm^2 card	ZP7B-2	None	Electropolished aluminum (Alzak)
4	100 cm^2 card	ZP7B-2	None	Rough tempered masonite
5	100 cm^2 card	ZP7B-2	White Krylon	Smooth tempered masonite
6	100 cm^2 card	ZP7B-2	Clear Krylon	Smooth tempered masonite
7	Sphere	ZP7B-2	White Krylon	Air inflated plastic
8	Field Jacket	ZP7B-2	None	Fabric
9	Field Cap	ZP7B-2	None	Fabric
10	Tetrahe-dron	ZP7B-2	None	Smooth tempered masonite

transmission filter for ruby and a 1.06 micron spike transmission filter for $CaWO_4$ and Nd doped glass. The photometer viewed the beam reflected from a diffusely reflecting white card. Measurements were also made using an MgO plate to insure that the white card was really "white". The signals were corrected for filter transmission and the relative response of the photometer at 0.69 and 1.06 microns. The laser cavity output mirror transmission had not been optimized for each of these materials. The data was adequate to indicate that, with some optimization of resonator variables, $CaWO_4$ would be the most adequate material for use in the test set.

3.2.2 Oscillator - Amplifier Experiments

The output of a laser is a linear function of the flash lamp input, with the threshold and the slope of the curve dependent on the transmission of the output mirror, as shown in Figure 5. To get increased output energy at a more than linear rate, it is possible to combine a laser oscillator with a laser amplifier. The characteristics of this combination were investigated. The experimental set up is shown in Figure 11. The output of a 1/4" diameter x 2" long $CaWO_4$ laser was directed into the amplifier, a 1/4" diameter x 3" long Nd doped glass rod. The laser oscillator input was kept constant with a flash lamp input energy of 20 joules. The signal, after going through the amplifier, was reflected from an MgO plate and monitored by a photometer. The output was displayed on a Tektronix scope and photographed. The pulse duration of the laser was about 150 microseconds. The amplifier pulse duration was approximately 50 microseconds, and reached its peak shortly before the laser signal was maximum. The gain of the amplifier was measured over a range of pump energies from 32 to 63 joules. The gain was calculated by measuring the area under the scope trace over the time interval when the amplifier was being pumped and comparing it with the energy out of the laser over the same time interval.

$$\text{Gain} = \frac{\text{area under Osc and Amp Output}}{\text{area under Osc output}}$$

From this the gain coefficient, α, of the amplifier was calculated. The gain coefficient, is defined by the following equation:

$$\text{Gain} = \frac{E}{E_o} = e^{\alpha l} \qquad (12)$$

where E_o = oscillator energy

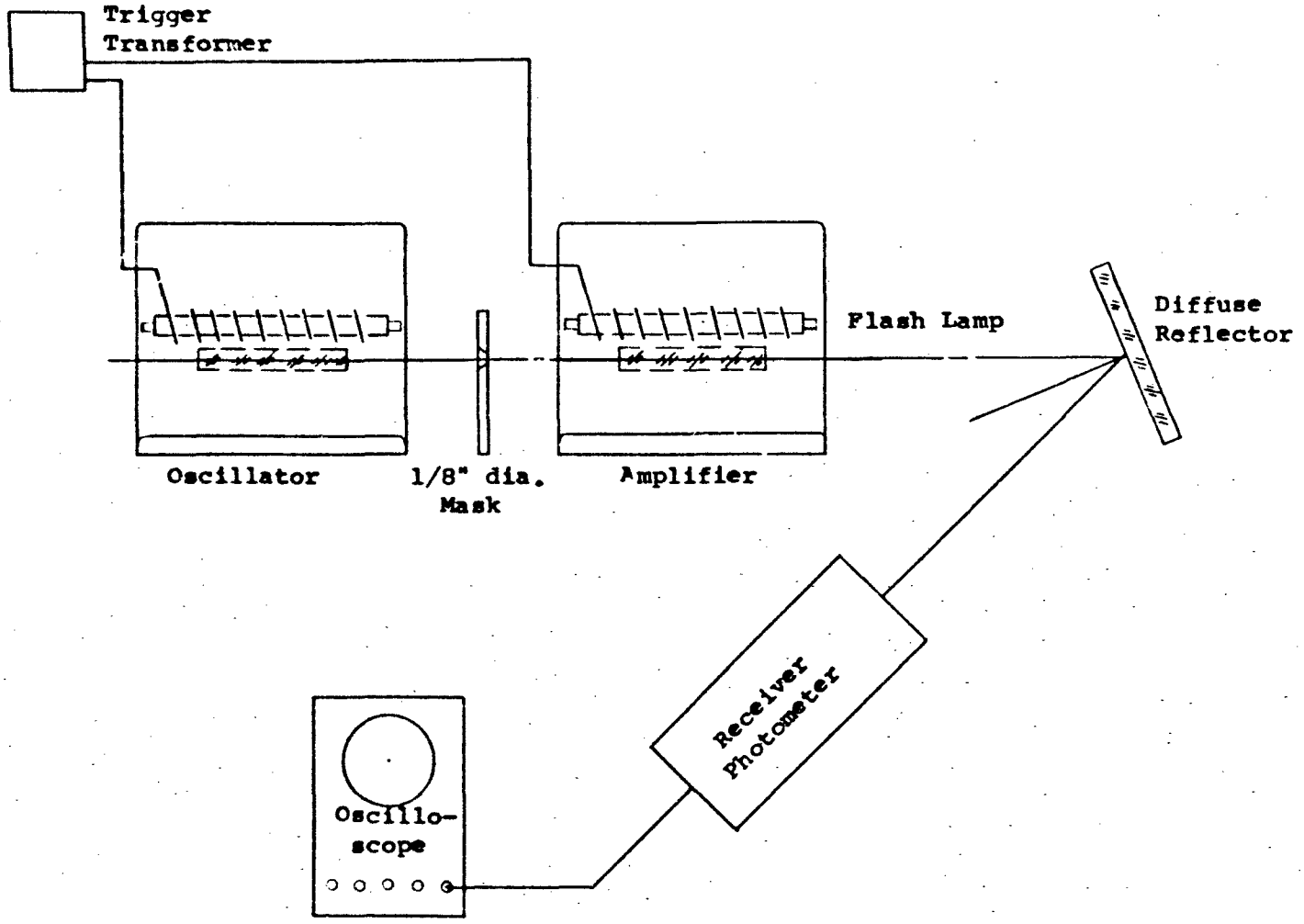

Figure 11. Oscillator-Amplifier Experimental Setup

where E = total output energy
ℓ = length of the amplifier in cm
α = the gain coefficient

The variation of the gain coefficient obtained as a result of testing the oscillator-amplifier is plotted in Figure 12.

Although the results show that the oscillator-amplifier arrangement was feasible, it was decided that the necessity of having two separate cavities and pulse shapes with appropriate delays between trigger pulses was too complicated to be used for the field test set and would require too much additional investigation of the means necessary to optimize such a system.

3.2.3 Laser Output vs. Mirror Transmission

The optimum output mirror transmission for the lasers to be used in the test set was determined by measuring the laser output by means of a photometer, at a constant input to the laser of 160 joules, as the reflectivity of the output mirror was varied. For a 1/4" diameter x 3" long $CaWO_4$ rod with 0.75 atom percent Nd this was found to be 50 percent. The data are plotted in Figure 13. This value is equivalent to having a 6" rod without an external front reflector (Fresnel reflection from the front surface). Based on this fact, this field test system was designed for a 6" laser without an external mirror on the output end. Two 3" laser rods were used instead of a single 6" rod since a 6" rod of required optical quality could not be grown with high neodymium concentrations. These performance characteristics were later verified experimentally using two 1/4" diameter x 3" long $CaWO_4$ rods. The output energy was 10% higher for the two rods with no external output mirror, compared with a single rod with 50% transmission on the output end of the laser, at the same input pump level, 195 joules. At 405 joules input, two 1/4" diameter x 3" long laser rods showed an output 1.85 times the output of a single rod with a 50% transmitting mirror.

3.2.4 Laser for Test Set

The laser that was finally chosen for the test set consisted of two 3/8" diameter by 3" long rods in series, with a 100% reflecting multiple dielectric coated mirror on the back end of the rear rod and no coating on the output end of the laser.

The dichroic coating used on the laser consists of alternate layers of zinc sulfide and chiolite. Although no significant deterioration of the coating occurred during field tests at Isomet, these coatings are known to deteriorate with time,

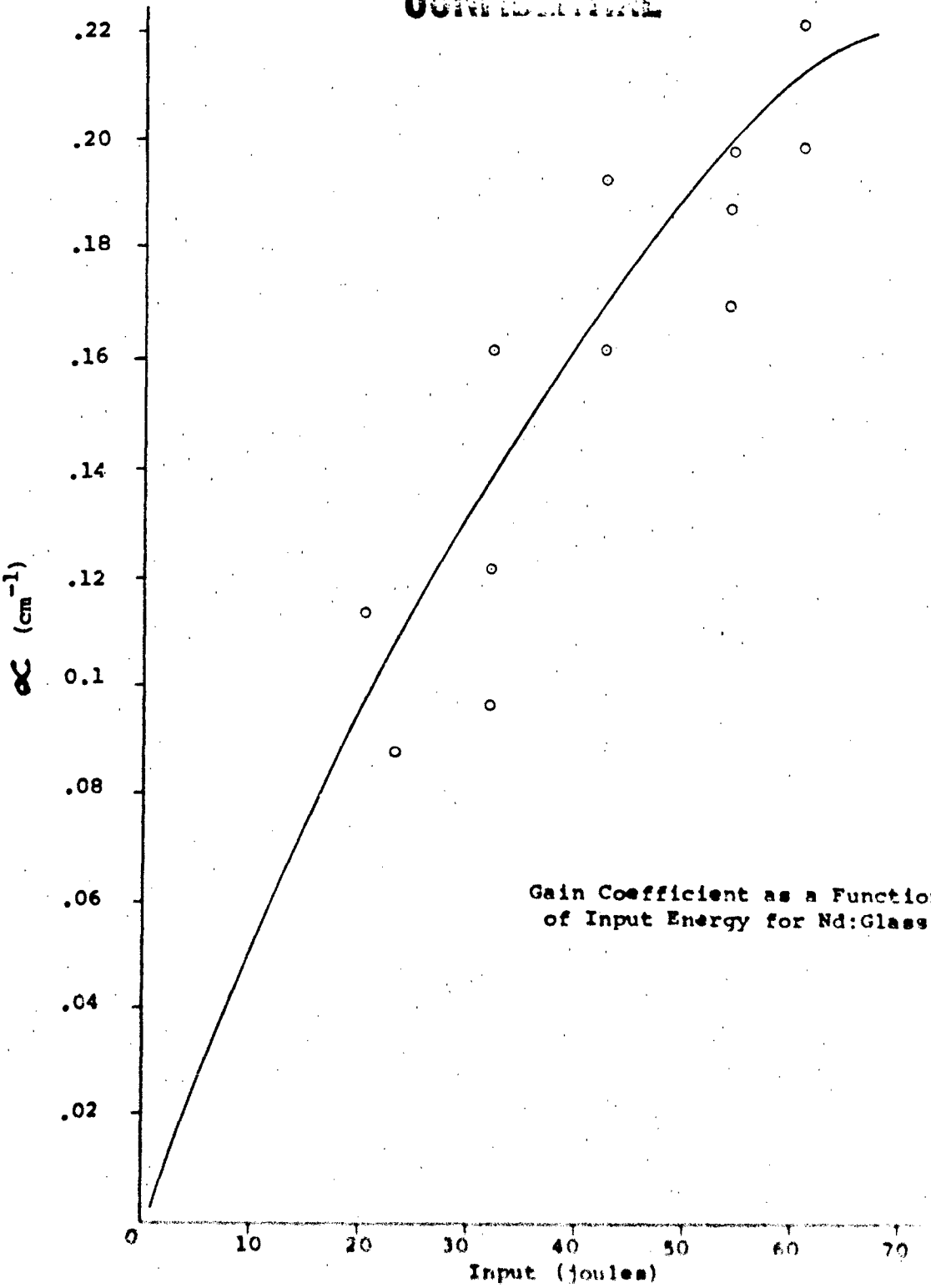

Gain Coefficient as a Function of Input Energy for Nd:Glass

FIGURE 12

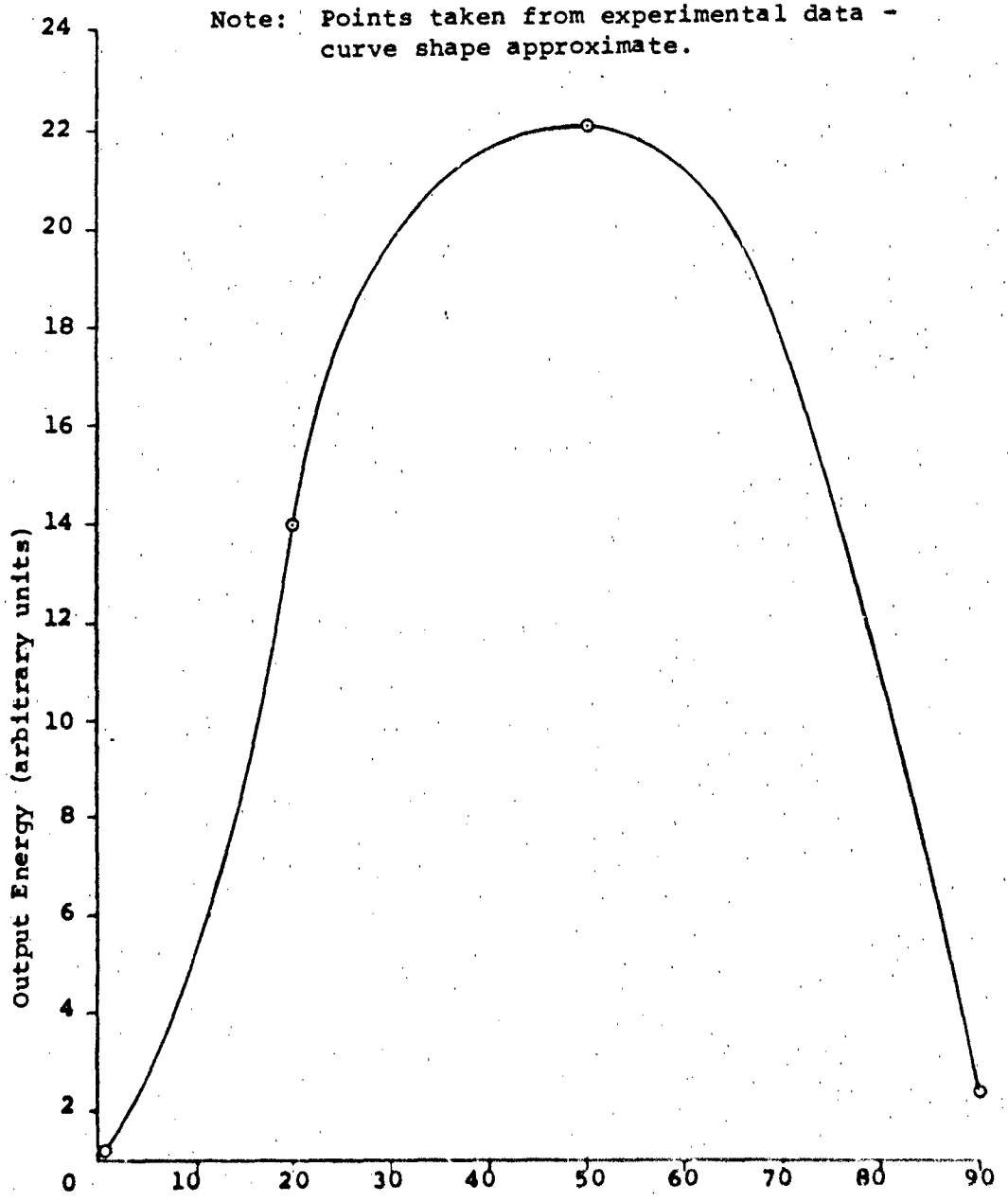

Figure 13. Mirror Transmission % (for 150 usec light pulse)

particularly in humid atmospheres. Therefore, a backup external mirror was included in the field test accessories.

The optimum concentration range for minimum threshold in $CaWO_4$ doped with Nd^{3+} is between 2 and 5 atomic percent Neodymium[3]. Over this range there is a decrease in fluorescent lifetime and an increase in fluorescent line width which wouldnormally increase threshold. These variations appear to be overshadowed over a large concentration range by a direct concentration effect . . .[4]. Where Nassau defines a direct concentration effect on maser action as " . . . more ions per unit volume are present to absorb and emit radiation."[5] A concentration of 0.75% was used, since this was the highest level of doping which would not impair the optical quality of the laser.

The boules from which the rods were fabricated were pulled from the melt at the rate of 1/4" an hour into an after heater held at 1100°C to minimize thermal shock and strain. The rods were annealed at a temperature of 1100°C for 12 hours and then cooled to room temperature at the rateof 15° an hour. Work at Isomet has shown that crystals with Nd concentrations in this range grown at the standard rate of 1/3" an hour and without an after heater resulted in crystals which frequently fractured, and had considerable optical distortions and strain. In the earlier part of this project, several crystals (1/4" dia. x 3" long) were grown at 1/4" an hour with an after heater and compared with a rod grown under standard conditions (0.5% Nd). The threshold of these rods was lower than the standard rod and had comparable or slightly better optical quality.

The laser rods were pumped by an FX-47B Xenon flash lamp at a maximum input energy of 500 joules. The lamp was fired without an external inductor so that the light pulse duration was as short as possible, about 200 microseconds. This is comparable to the phosphor decay time. The effect of the duration of the pump pulse on the phosphor signal is given in Section 3.1.11.

3.3 Detectors

The task of exciting an infrared emitting phosphor with an infrared laser beam and detecting the phosphor emission places the following requirements on the detector:

---

3. K. Nassau, Effect of Growth Parameters on the Threshold of $CaWO_4$:Nd Crystals in Proceedings of the Symposium on Optical Masers, Polytechnic Press, New York, 1963 p. 456.
4. Ibid p. 456
5. Ibid p. 454

a. It must be sensitive in the spectral region where the phosphor emits.

b. Its speed of response must be equal to or greater than that of the phosphor emission.

c. It should be capable of detecting low level signals.

Optimum, overall system performance requires that the laser and the phosphor emit in a spectral region corresponding to an atmospheric window. That is, emission should be in a spectral region of minimum attentuation. Windows of particular interest occur at 1.0, 1.25 and 1.7 microns. Over a distance of 2,000 yards, the atmosphere containing 17 mm of a precipitable water, will transmit approximately 75% of the energy in the radiation bands centered at 1.0 and 1.25 microns and approximately 80% at 1.7 microns.

During the course of the program, efficient phosphors were prepared which emitted at 1.2, 1.8 and 2.1 microns. The first two spectral regions match reasonably well with the atmospheric windows. The 2.1 micron phosphor was set aside due to the higher absorption. The 1.2 micron phosphor was toxic and presented technical problems in obtaining adequate filters for rejecting the 1.06 micron laser energy. The 1.8 micron phosphor was deemed best and was used.

Based on the considerations of spectral match, sensitivity and response time, the most promising detectors were lead sulfide and germanium. The choice of germanium was made early in the program because of germanium's greater peak sensitivity and faster response time (of the order of 1 microsecond). Since the effort in phosphor development was concentrated on obtaining not only higher efficiencies but also faster decay times, the use of germanium was mandatory. When it appeared that the faster phosphors would not be available for field testing, lead sulfide again appeared attractive for use with the phosphor peaking at 1.8 microns.

Ge detectors of the type considered exhibit maximum sensitivity at 1.5 microns. This sensitivity decreases several orders of magnitude at approximately 2.0 microns. At the wavelength of peak phosphor emission, 1.8 microns, the sensitivity of germanium is down to about 34% of its maximum value. Lead sulfide, on the other hand, exhibits peak sensitivity at 2.1 microns and decreases to approximately 90% of peak at 1.8 microns.

The relative spectral sensitivity of these detectors is shown in Figure 14. The curves are plotted to show the spectral response of each detector. The peak sensitivities of Ge and PbS are not the same.

Comparative testing was performed to provide data as to which detector was best suited for use in the final system. The results of these tests indicated that the particular PbS detectors used were inferior to Ge for the pulsed signal operation, and roughly equivalent to Ge on a repetitive low frequency signal basis.

3.3.1 Detector Measurements

Sensitivity measurements were made on a prospective germanium detector, the RCA 7467. This particular device was chosen on the basis of published data which indicated that the sensitivity was higher, by a factor of 4, than similar devices. Initially, several of these germanium detectors were checked directly with a black body source, low noise amplifier, and readout equipment. When a photometer assembly became available, similar sensitivity measurements were made with the detector mounted behind photometer optics. This procedure permitted detectors to be easily evaluated for end use with the laser system and allowed correlation with initial detector data. Initial data were obtained from the following measurements and calculations.

A black body radiation source at 1000°K was used to irradiate the detector. The radiation was chopped at 350 cps by a mechanical chopper. The output of the detector was amplified by a low noise preamplifier, passed through a frequency determining band pass filter, amplified further by a post amplifier, and displayed on a Tektronix scope and a Hewlett-Packard RMS voltmeter. Both the signal and noise were measured. The results for RCA 7467 germanium detector #1 are based on the following conditions:

r = range = 100 cm.
S = signal = 125 mv. peak-to-peak
A_s = area of source = 0.206 cm^2
T = temperature of source = 1000°K
N = noise = 0.4 mv. rms.
f = electrical bandwidth = 500 cps, centered at 350 cps
k = fraction of black body energy in detector spectral region = 4%.

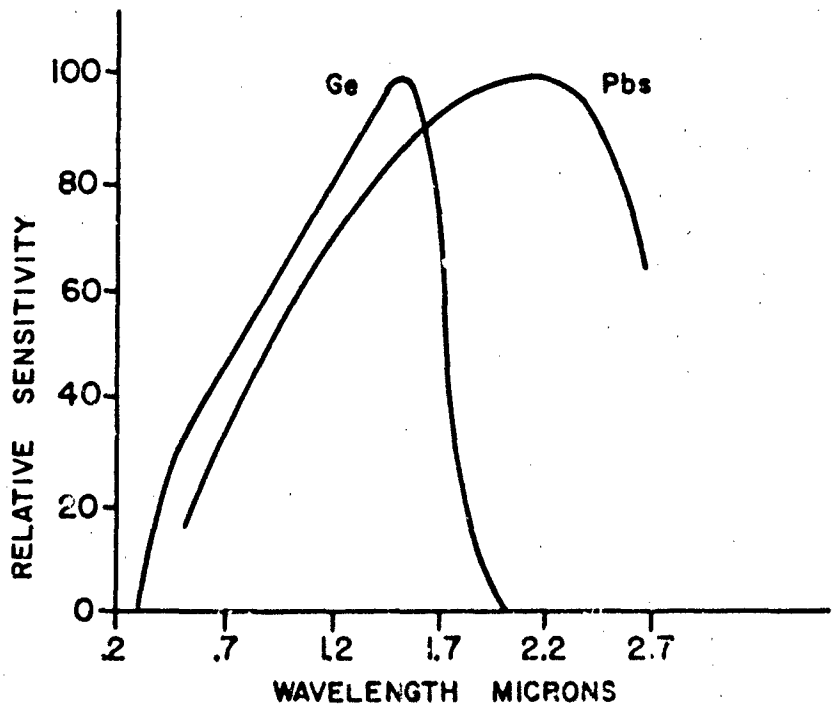

SPECTRAL SENSITIVITY
OF Ge AND Pbs DETECTORS

FIGURE 14

The power density, "H", falling on the detector within its spectral region is

$$H = \frac{N_s A_s k}{\pi r^2} \qquad (13)$$

where N_s = 1.7 watts/cm^2 at 10^3 ^oK = black body source intensity

$$H = \frac{1.7\ (0.206)(0.04)}{10^4}$$

$$H = 1.4 \text{ microwatts/cm}^2$$

$$S/N = 125/0.4 = 312$$

The NEPD for a 500 cps Δf is:

$$NEPD = \frac{H}{S/N} = \frac{1.4 \times 10^{-6}}{312} = 4.48 \times 10^{-9} \text{ w/cm}^2 \qquad (14)$$

Where NEPD, the Noise Equivalent Power Density, is the minimum radiation power density on the detector which will produce a signal to noise ratio of unity.

If we assume a white noise distribution, the NEPD for a one cycle bandwidth is:

$$NEPD_{1 \text{ cps.}} = \frac{4.48 \times 10^{-9}}{(500)^{1/2}} = 2 \times 10^{-10} \text{ w/cm}^2 - \text{cps}^{-1/2}$$

The D* of a detector is defined as

$$D^* = \frac{(\Delta f)^{1/2} A_d^{1/2}}{NEP} \text{ (cm) (cps)}^{1/2}\text{/watt} \qquad (15)$$

where A_d = detector area, and NEP is the Noise Equivalent Power related to NEPD by the detector area. D* is a quantity describing the detectivity of the detector in such a manner that the detector area and amplifier bandwidth do not affect the result. The detectivity is thus normalized.

$$NEP = (NEPD)(A_d),$$

$$D^* = \frac{1}{NEPD_{1 \text{ cps.}}} (A_d)^{1/2} \qquad (16)$$

Computing D* for $A_d = 0.01\ cm^2$ (7467 detector)

$$D^* = \frac{1}{2 \times 10^{-10}}$$

$$D^* = 5.0 \times 10^{10}\ (cm)\,(cps)^{1/2}/watt$$

It should be noted that these detector measurements were made at room temperature.

Four 7467 detectors were checked in the above manner and their sensitivities calculated. The values are given in Table 6.

TABLE 6. D* of RCA 7467 Germanium Detectors

RCA 7467 Detector No.	D*(cm $cps^{1/2}$/watt)
1	5.0×10^{10}
2	4.8×10^{10}
3	9.1×10^{10}
4	7.2×10^{10}

This data indicated that the RCA 7467 detector was sufficiently sensitive for use in the system and that the variation in sensitivity between units was (for the batch tested) minimal and better than anticipated.

An additional test was performed on 7467 unit no. 1 to determine the effect of temperature on the detector dark current. This is the current that flows through the biased detector junction when it is not exposed to radiation. The detector exhibited dark current versus temperature characteristics as shown in Figure 15. The RMS noise current observed is related to dark current by the formula:

$$In = \sqrt{2\ q\ Id\ \Delta f} \qquad (17)$$

where In = RMS noise current
Id = dark current (average)
Δf = amplifier electrical bandwidth in cps.
q = electronic charge = 1.6×10^{-19} coulomb

For Detector No. 1, the theoretical noise was calculated from equation (17) in the following manner:

For a detector operating temperature of 23.5°C, Figure 15 shows that the dark current is 15×10^{-6} amps. Testing with

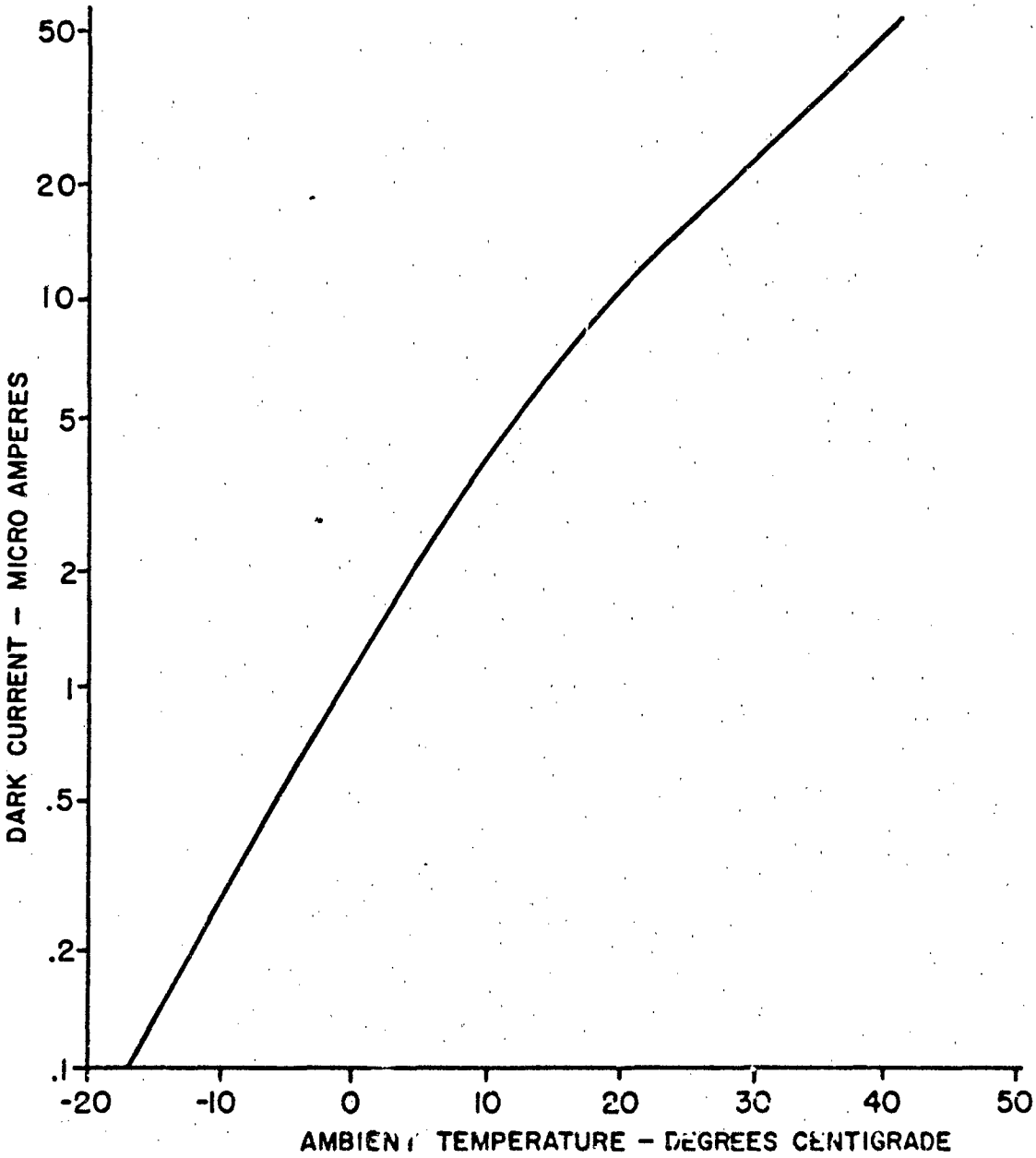

DARK CURRENT CHARACTERISTIC OF GERMANIUM ALLOY(p-n) PHOTOJUNCTION DIODE, RCA 7467, UNIT NO. 1, 5 VOLTS BIAS

FIGURE 15

an amplifier bandwidth, Δf, of 200 cps, the noise current can be predicted,

$$I_n = \sqrt{2 \times 1.6 \times 10^{-19} \times 15 \times 10^{-6} \times 200}$$

$$I_n = \sqrt{9.6 \times 10^{-22}}$$

$$I_n = 3.1 \times 10^{-11} \text{ amps.}$$

This value was checked experimentally by the following procedure. An unbiased detector and detector load resistor were placed across the input of a low noise, high input impedance amplifier with known characteristics. The output noise voltage level, E_a, was measured. The detector was then biased with a dc voltage and covered to exclude light. The total output noise level, E_t, representing the combined detector and amplifier noise was measured. The amplified noise contribution of the detector, E_d, was calculated from the relationship:

$$E_d \text{ (rms)} = \sqrt{E_t^2 - E_a^2} \qquad (18)$$

The observed value of E_d was divided by the amplifier gain to give the equivalent detector input voltage. The equivalent input divided by the resistive load on the detector gave the noise current of interest. The value calculated in this manner was 3.46×10^{-11} amps, in good agreement with the theoretical value.

It appears from Figure 15 that cooling the cell should improve S/N ratios by one or more orders of magnitude. While this was observed during the initial detector tests, cooling was later found to have a deleterious effect on the life of the particular detectors being used.

When detector testing was initiated, the RCA 7067 units were biased on for periods of roughly ten to twenty minutes at a time while the required tests were performed. Measured noise levels during these periods remained relatively constant, indicating a typical slow increase in noise which leveled off as junction temperature was stabilized. The amount of noise increase was barely measurable (approximately 2%). These same units were later tested to check their sensitivity to phosphor emission with the same low noise amplifier. Because of operations involved in the test, the detectors were biased for longer periods than previously required. The periods ranged up to 3 hours in length. Difficulties were experienced with the first detector after several

days in this mode. The output noise level of the amplifier was observed to increase and reach a point where the output waveshape indicated amplifier saturation. Noise spikes occurred with great frequency. When detector bias was turned off, the level immediately dropped down to the normal level for the amplifier with an unbiased detector across its input. When bias was switched on again after several minutes off time, the output noise was at the low level originally observed. This value was maintained for a short time and then began to slowly increase, reaching the amplifier saturation level within five minutes. The noise frequency spectrum was observed to increase in low frequency content during the process. In all tests, both the detectors and the low noise amplifier were biased with voltages obtained from batteries.

The time required to reach the maximum level appeared to shorten after each run until it took about 10 seconds for the increasing noise to saturate the amplifier. This degeneration occurred slowly over a period of days. When this point was reached, the tests with the detector were discontinued, and the detector was considered to have undergone a complete failure. One interesting point observed during this period was that while the noise increased with time for any measurement and the signal to noise ratio decreased, the signal level obtained from the phosphor remained constant.

The phenomena of increasing detector noise was observed in two other detectors under similar conditions. One of these units had been used to qualitatively determine the effect of detector cooling on dark current noise. Noise was observed to decrease dramatically when the detector was cooled to $-40^{\circ}C$, the minimum operating temperature recommended by RCA. This unit was used later to replace the detector for the measurements described above. Failure from increased noise occurred within a few hours with this unit. At the time, no connection between detector cooling and rapid failure was made.

At that point RCA was contacted about the noise problem. Personnel responsible for design and fabrication of the 7467 claimed that they had become aware of the problem which appeared to be due to surface contamination of the junction and contact bond deterioration or both. A redesign had been instituted to package the junction in a manner which would prevent contamination. The resulting device, the SQ2516, was the basic 7467 junction packaged in a modified TO-5 type transistor case. This design permits end on viewing of the junction. Manufacture of the 7467 was discontinued since the SQ2516 was identical in performance and structurally stronger. A quantity of SQ 2516 detectors were purchased for evaluation.

Tests similar to those performed on the 7467 to obtain D* were also performed on five SQ2516 detectors. Data, in this case, were obtained with the detectors operating in the photometer used for field testing. The photometer NEPD was determined as indicated in Section 3.4.3.1. From the NEPD, the detector D* was calculated from the following relation:

$$D^* = \frac{(A_d)^{1/2}(\Delta f)^{1/2}}{(NEPD)(Aca)(T_f)} \qquad (19)$$

where A_d = detector area, cm^2
Δf = amplifier bandwidth, cps
Aca = clear aperture of photometer, cm^2
T_f = transmission of filters, lenses

For the photometer used in field measurements, (described in Section 3.4.2.1) the variables are as follows:

NEPD = 3.51×10^{-11} w/cm^2 (Detector No. 4)
Δf = 5415 cps
Aca = 3.34 cm^2
T_f = 0.43
A_d = 0.01 cm^2

$$D^* = \frac{(0.01)^{1/2}(5415)^{1/2}}{(3.51 \times 10^{-11})(3.34)(0.43)}$$

$$D^* = 7.0 \times 10^{10}\ cm(cps)^{1/2}/watt$$

The SQ2516 values of D* shown in Table 7 and the 7467 values listed in Table 6 show that the two detector types are equivalent in performance.

Table 7. D* of RCA SQ2516 Germanium Detectors

SQ2516	D* $cm(cps)^{1/2}/watt$
#1	2.6×10^{10}
#2	6.1×10^{10}
#3	1.1×10^{10}
#4	7.0×10^{10}
#5	6.4×10^{10}

The frequency distribution of noise generated by an SQ2516 was obtained by connecting the detector to a low noise preamplifier. The system was detector noise limited. A Krohn-

Hite Model 310-AB, Variable Band Pass Filter was connected to the preamplifier output to sample the output noise voltage. The filter high and low frequency cutoff points were adjusted to give a net bandpass, Δf between 0.77 fc and 1.30 fc where fc was the center frequency being checked. To find the noise in a one cycle bandwidth, the noise voltage, N, at a given center frequency fc, was divided by the bandwidth at the 50% points of the filter bandpass. These points are 6 db down on the slope of the filter characteristic curve and occur at 0.68 fc and 1.45 fc. The noise voltage obtained at each center frequency was divided by the gain of the preamplifier at that frequency. The resultant quantity, plotted in Figure 16, is the detector noise voltage per one cycle bandwidth over the range of frequencies of interest.

The SQ2516 response for levels of background and signal anticipated during field test conditions was found to be linear when operated with a bias voltage of 45 volts. Because of the detector junction deterioration previously described at this voltage, the bias was reduced to 9 volts. This reduction affected the linearity of the detector such that the unit appeared to be between 1.3 and 2.5 times more sensitive at night when a low background condition exists. During identical day and night measurements, the signal was found to have consistently decreased within this range of ratios. The fluctuation from 1.3 to 2.5 was due to variations in cloud cover, haze, and background in the immediate target area. Additional comparative testing of the 7467 and SQ2516 detectors was abandoned when the remaining 7467 became excessively noisy.

Tests were performed on two randomly chosen SQ2516 units at various bias conditions. Identical tests were run on Pbs detectors to determine their characteristics and to obtain comparative data. The test setup, shown in Figure 17, consisted of a high intensity tungsten light source chopped at a 300 cps rate. Water and gelatin filters were utilized to remove light excitation at wavelengths shorter than 1.0 micron. The filtered light beam was aimed at a 6.5 x 8.5 inch card coated with V-21 phosphor. Detectors were located in a metal enclosure containing the necessary bias batteries and resistors. The entire enclosure was aimed at the phosphor card from a 45° angle to the plane of the card. The detector output was applied to a low noise amplifier and the amplified signal displayed on an oscilloscope and measured on an RMS voltmeter. Focusing lenses were not used in front of the detectors. Filters, similar to those included in the final system, were utilized to limit the detected energy to the spectral region of 1.5 microns. The filtering used gave some advantage to

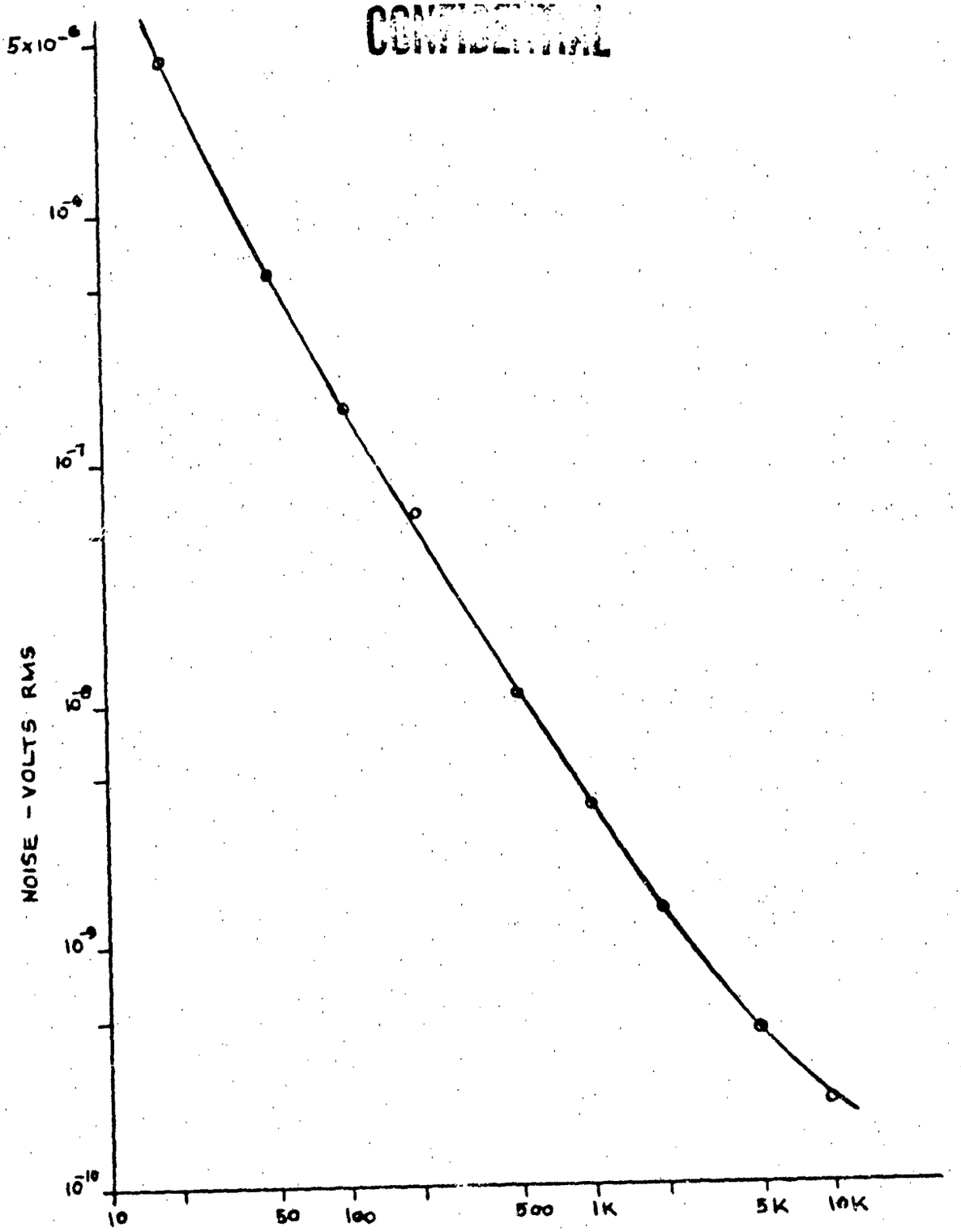

FIGURE 16. SQ 2516 DETECTOR NOISE VOLTAGE PER ONE CPS BANDWIDTH

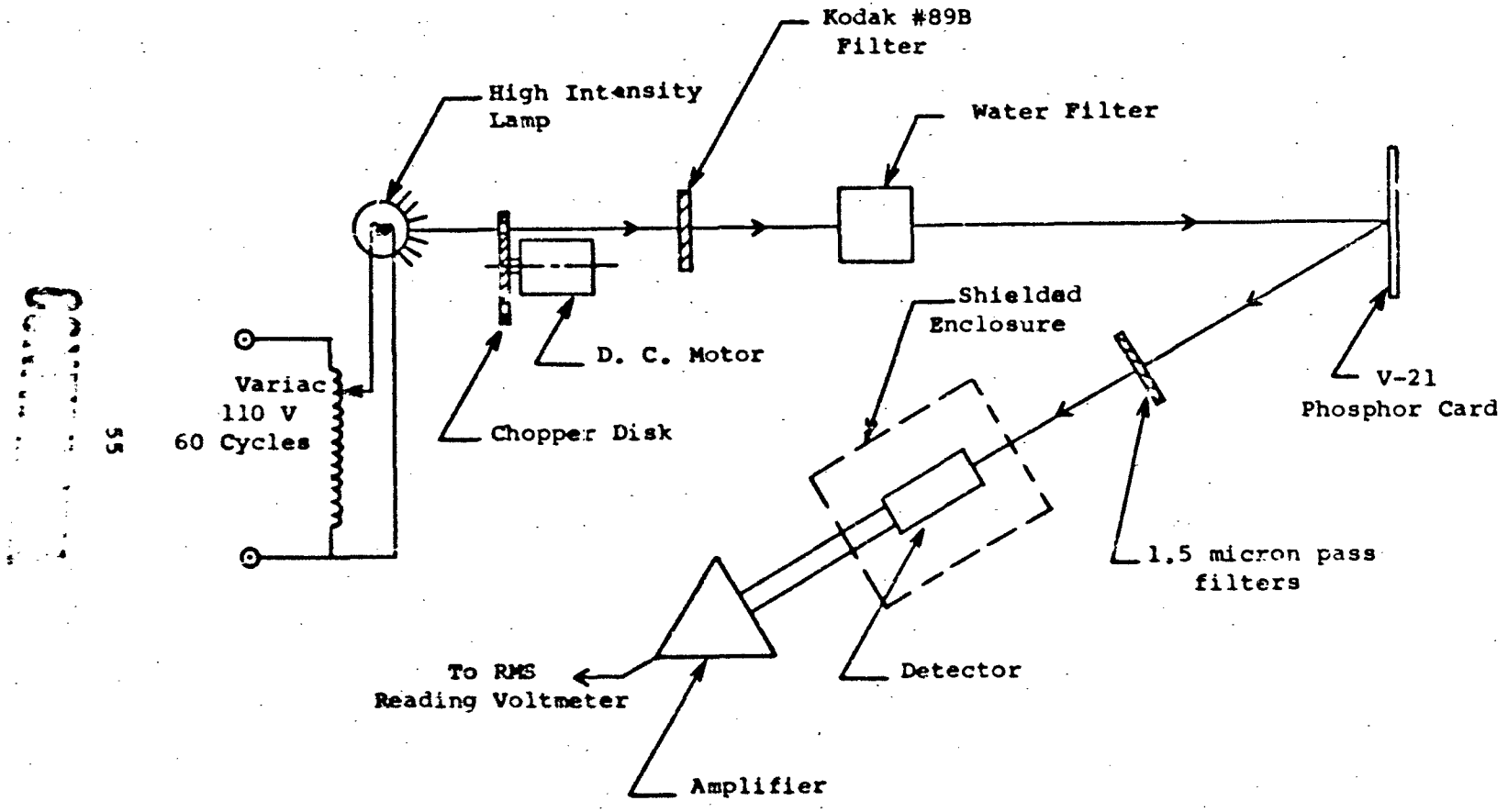

Figure 17. Detector Test Setup

the PbS detectors which are sensitive up to the 3 micron region while the long wavelength cutoff for the SQ2516 is approximately 2.0 microns.

Results of the tests which are shown in Table 8 are not completely definitive since only a small number of detectors were tested. However, important information was obtained on detector signal to noise variation with bias voltage and load resistance. For the SQ2516, it became obvious that the best S/N occurred when the bias voltage was reduced from 45 volts to 9 volts and the load resistor was 22 thousand ohms for the particular amplifier used. It appeared, therefore, that use of the lowest possible bias voltage consistent with detector linearity would substantially improve detector performance. In addition, the use of lower bias voltage improved the operational lifetime of the SQ2516. This fact was partially borne out by the tests performed on SQ2516, unit 3. Initially, unit 3 performed well and, in test 7, the data compared satisfactorily with test 4, performed on SQ2516 No. 1. In test 8, as the detector was being positioned the voltmeter pointer began pulsing, indicating large spikes of noise. This was confirmed on the oscilloscope. Circuit connections were rechecked and found to be satisfactory. With the detector aperture blocked, both pulsing and the wide band noise level were observed to have increased by 20%. The detector was then disconnected from the 45 volt battery and connected to 22 volts with the same 22 thousand ohm load resistor (test 9). With this combination, wide band noise was reduced to normal and the frequency of noise spiking somewhat lessened. Initially, with the exception of the spiking, performance was similar to that of SQ2516 No. 1 under the comparable conditions of test 2. During test 9 there was an observable, slow increase in spiking and wide band noise. This is due to increased junction temperature and is normal in all junction devices. With a defective junction, the temperature effect is accentuated and may not stabilize.

At the completion of test 9, the detector was connected to a 47Kohm load resistor and the 22 volts battery (test 10). While adjustments were being made, noise and spiking increased to the point where it was impossible to obtain readings. The unit was then reconnected, as in Test 9, to determine if detector performance was as previously observed. Noise and spiking were again excessive and it was concluded that Ge detector No. 1 had experienced a catastrophic junction failure.

As a possible means of improving system sensitivity, the same tests were run on three PbS detectors to determine their

TABLE 8

Test Results of Germanium and Lead Sulfide Detectors

Test No.	Detector	Unit No.	Amplifier Noise (mv RMS)	Total Noise (mv RMS)	Detector Noise (mv RMS)	Max. Signal Obtainable (mv RMS)	Detector S/N Ratio	Bias Conditions
1	SQ2516	1	6.7	9.0	6.01	70	11.65	R_L = 47K, E_C = 22V
2	"	1	6.7	12	9.96	42	4.22	R_L = 22K, E_C = 22V
3	"	1	6.7	17	12.0	45	3.75	R_L = 22K, E_C = 45V
4	"	1	6.7	30	29.24	70	2.39	R_L = 47K, E_C = 45V
5	"	1	6.7	5.0	Amplifier noise limited	35	Amplifier noise limited	R_L = 22K, E_C = 9V
6	"	1	6.7	7.5	3.38	65	19.2	R_L = 47K, E_C = 9V
7	"	3	6.7	35	34.35	75	2.18	No spiking R_L = 47K, E_C = 45V
8	"	3	6.7	40	39.4	50	1.27	Spiking apparent R_L = 22K, E_C = 45V
9	"	3	6.7	10	7.42	39	5.26	Spiking apparent R_L = 22K, E_C = 22V
10	"	3	6.7	Too noisy to continue tests			--	R_L = 47K, E_C = 22V
11	B1SA3	1	6.7	12.5	10.54	135	12.8	R_L = 470K, E_C = 45V
12	B1SA5	2	6.7	13.0	11.4	180	15.8	R_L = 470K, E_C = 45V
13	B1SA5	3	6.7	10.0	7.42	178	24.0	R_L = 470K, E_C = 45V

CONFIDENTIAL

characteristics. The devices were manufactured by Infrared Industries, Waltham, Massachusetts. Unit 1, a type B1SA3, had an area of 0.0016 square inches, comparable to the SQ2516 in active area. This unit performed better in test 11 than did SQ2516, with the exception of test 6 when the bias voltage was reduced to 9 volts. Bias voltages were not reduced with the PbS detectors as in the Ge units since there is adequate published data to show that both signal and noise vary in the same manner with bias voltage changes. That is, S/N remains constant over a wide range of bias voltages for PbS detectors.

Two B1SA5 units were checked in tests 11, 12 and 13. These detectors have active areas of 0.0060 square inches, about 3.75 times the active areas of SQ2516 and B1SA3. It has been shown[6] that the output signal of a lead sulfide detector is normally independent of detector area if the detector materials are identical and incident radiant flux density is constant. Since the PbS detector material and the incident flux met this criteria, it was expected that the three units would have fairly close output signal voltages and that the noise voltage E_n, would vary inversely with the square root of the cell area. The observed deviations from these predicted parameter changes are most likely due to manufacturing tolerances. Taking this into consideration, unit 3 is better than units 1 and 2, while all are within the manufacturer's sensitivity tolerances.

The detector tests showed that increasing bias voltages on either type of Ge detector did not improve signal to noise ratio. Although the SQ2516 was rated for operations at 50 volt bias, it was not advisable to even approach that voltage range for low noise detection. In addition, the excellent results obtained with the PbS detectors required that further tests be undertaken to compare the Ge and PbS units in pulse applications where sensitivity, and therefore S/N, decrease as the response times involved approach the detector time constant. For both the B1SA3 and B1SA5, the time constant (time required for the detector output signal to reach 63% of maximum) was found to be approximately 85 microseconds, although the manufacturers specification calls for less than 60 microseconds.

To determine the suitability of PbS for pulsed application, one B1SA5, unit #3, was installed in a photometer and calibrated with a black body source. The responsivity for the

6. Lead Sulfide Photoconductors; A state of the Art Report Technical Bulletin 2, Infrared Industries, Inc. Waltham, Mass. 1960, p. 5

photometer with this detector was calculated to be 182 x 10^6 v-cm^2/w for the spectral band of interest and for the following conditions:

Range - 104 inches
Source Temp. = 1000°C
Source Aperture = 0.025 inches diameter
Chopping Frequency = 360 cps
Noise voltage - 16 millivolts
Signal voltage = 1.25 volts peak to peak

The photometer was then targeted on a 1.8 micron emitting phosphor sample at a range of 24 feet. Phosphor return signals were recorded when the sample was irradiated by a Nd doped $CaWO_4$ laser beam (1.06 microns radiation).

The same procedure was followed with an SQ2516. The responsivity for identical calibrations conditions was calculated as 431 x 10^6 v-cm^2/w. The ratio of the Ge and PbS responsivities are:

$$\frac{R_{Ge}}{R_{PbS}} = \frac{431}{182} = 2.37$$

which would indicate that in the spectral region being used, the Ge detector would provide 2.37 times the signal of PbS for identical illumination. The experimental results for identical illumination indicate a ratio of:

$$\frac{V_{Ge}}{V_{PbS}} = \frac{1060 \text{ mv}}{380 \text{ mv}} = 2.79$$

The discrepancy between the calculated and experimentally determined ratios may be due to the time constant factor in PbS which did not permit full output signal to be obtained. The positioning of detectors in the test set photometer was fairly critical and was a source of apparent sensitivity variation between detectors.

The sensitivity advantage of Ge over PbS would probably disappear if:

1. A PbS device was selected with a time constant of less than 10 microseconds and highest sensitivity.

2. A smaller detector area was utilized.

A low time constant would permit the output voltage to be generated with little or no signal degeneration. A high sensitivity, coupled with the PbS spectral response, which "sees" more of the phosphor emission spectrum than Ge, could result in a higher responsivity in pulsed operation. The PbS detector output signal and S/N are functions of detector area as indicated below:

Signal = C/A for constant incident radiant power
where C is a constant, therefore:
Signal/Noise = C^1/A
where C^1 is a proportionality constant

It is evident that use of a detector with the smallest area would improve photometer performance. One limitation on the detector is imposed by the photometer design parameters. A wider field of view requires a larger detector. In a final system, this limitation can be overcome by use of a larger clear aperture objective lens or an array of several detectors.

A complete evaluation of the degree of possible improvements was not made because of the lead time involved in obtaining the required detectors. However, from the data obtained, it appears that PbS in a photometer specifically designed for a small area detector would perform as well as Ge and perhaps somewhat better depending upon the availability of fast (rise time less than 10 microseconds), high sensitivity devices (D* greater than 1×10^{10}). System performance and reliability would benefit from use of PbS because of the stability of the detector material. In addition, if multiple detectors are required on a final system, the use of PbS would be highly advantageous because of the ease in obtaining detector arrays.

Germanium detectors appear, at the present time, to be best for the ultimate application where fast phosphors would require a high speed response (up to 10^{-6} seconds). In this case, the predominant, low frequency (1/f) noise would be eliminated.

3.4 Test Set

The engineering model test set, developed to perform measurements in the field, consisted of three separate units; the laser power supply, the signal processing electronics, and the transceiver. The latter contained the laser (transmitter) and the photometer (receiver). The processing electronics and laser power supply were packaged in portable, weather-proof cases. A functional system block diagram is shown in Figure 18. A schematic circuit diagram of the complete system is shown in

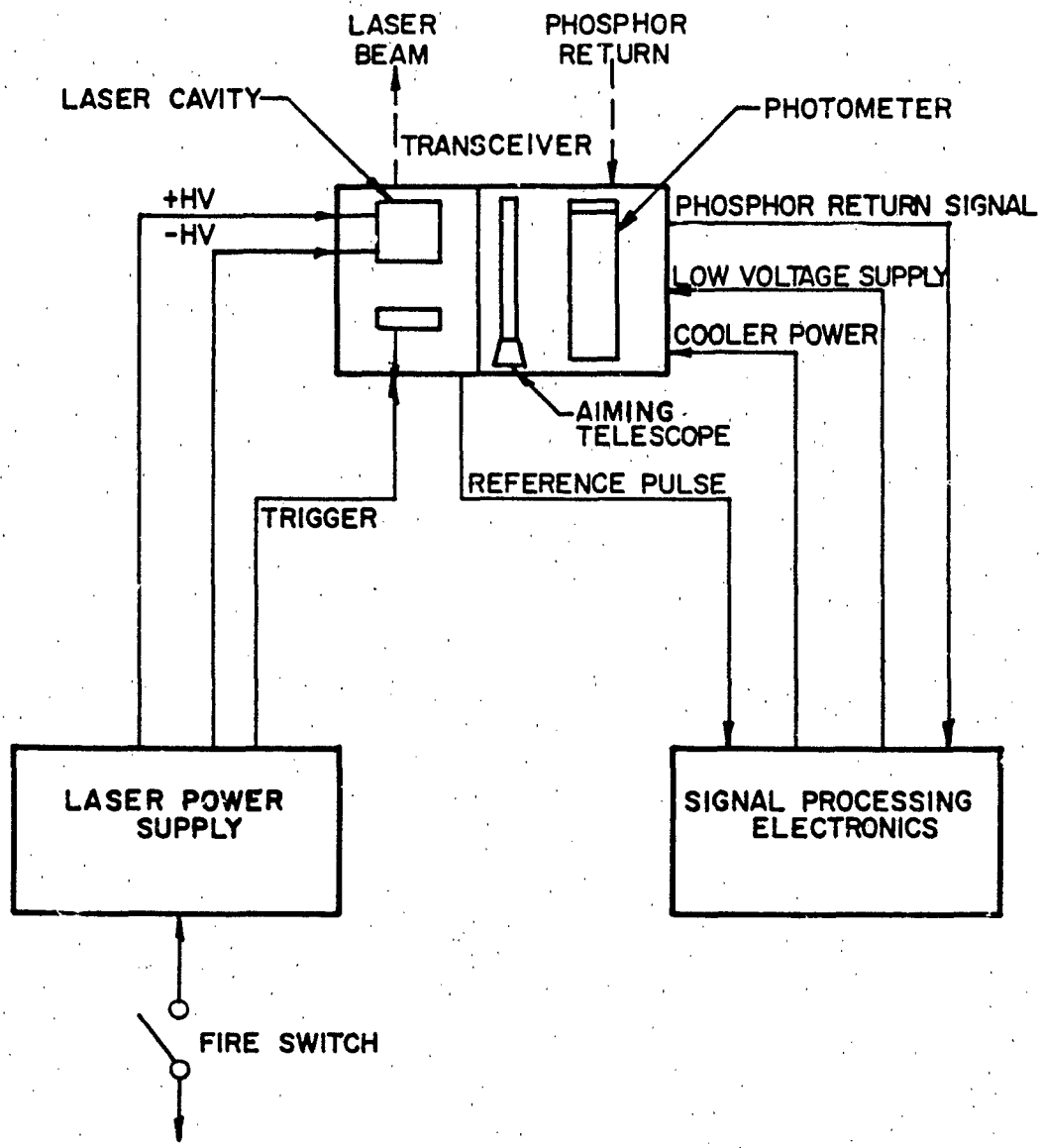

TEST SET BLOCK DIAGRAM

FIGURE 18

Appendix I. The test set was self-contained, except for AC power, and permitted interrogation of a target with visual and audible alarms for signaling phosphor return signals. A brief system description and instructions for its operation are included in Appendix I.

3.4.1 Processing Electronics Package

The processing electronics provided a means of automatically discriminating between phosphor return signals and reflections of laser energy from highly reflective surfaces. The circuits also provided some enhancement of signal in the presence of noise through the use of gating circuits in which a phosphor return signal could be sampled for a short interval after the laser turned off. The significant S/N advantage of these circuits was established during the field measurements when data was being obtained close to dense brush where relatively large amplitude reflections were observed. When the highly reflective greenery was illuminated by the laser at short (5 to 10 feet) ranges, the return reflection came close to saturating the amplifier, in spite of the flash lamp and laser energy filtering. However, no phosphor presence gate signal was generated. The system was able to distinguish between real signal and large background returns.

The functional block diagram of the processing circuits is shown in Figure 19. As indicated, the circuits may be divided into two channels. The amplification and signal shaping channel was utilized for increasing the phosphor signal level and adjusing the waveform for further processing. The gating channel provided the timed and delayed gating voltages to sample the phosphor signal in a discrete time interval after the laser turns off. Gating was initiated by an RCA SQ2516 detector identical to that used to detect phosphor return signals. An SQ2516 was utilized in this application since a fast response to the laser output waveform was required for properly timing the gating circuits. A lead sulfide detector in this usage would introduce excessive delay time due to the longer time constant of the material. The SQ2516 detector generated a signal which was referenced to the laser beam. The detector was "on" when the laser was on; when the laser beam was off, the detector also switched off. The change in detector state from "on" to "off" triggered the timing and gating functions that permitted the received signal to be evaluated and then rejected or transmitted to the readout electronics. Typical waveshapes generated in the system are shown in Figure 20. Operation and processing was as follows:

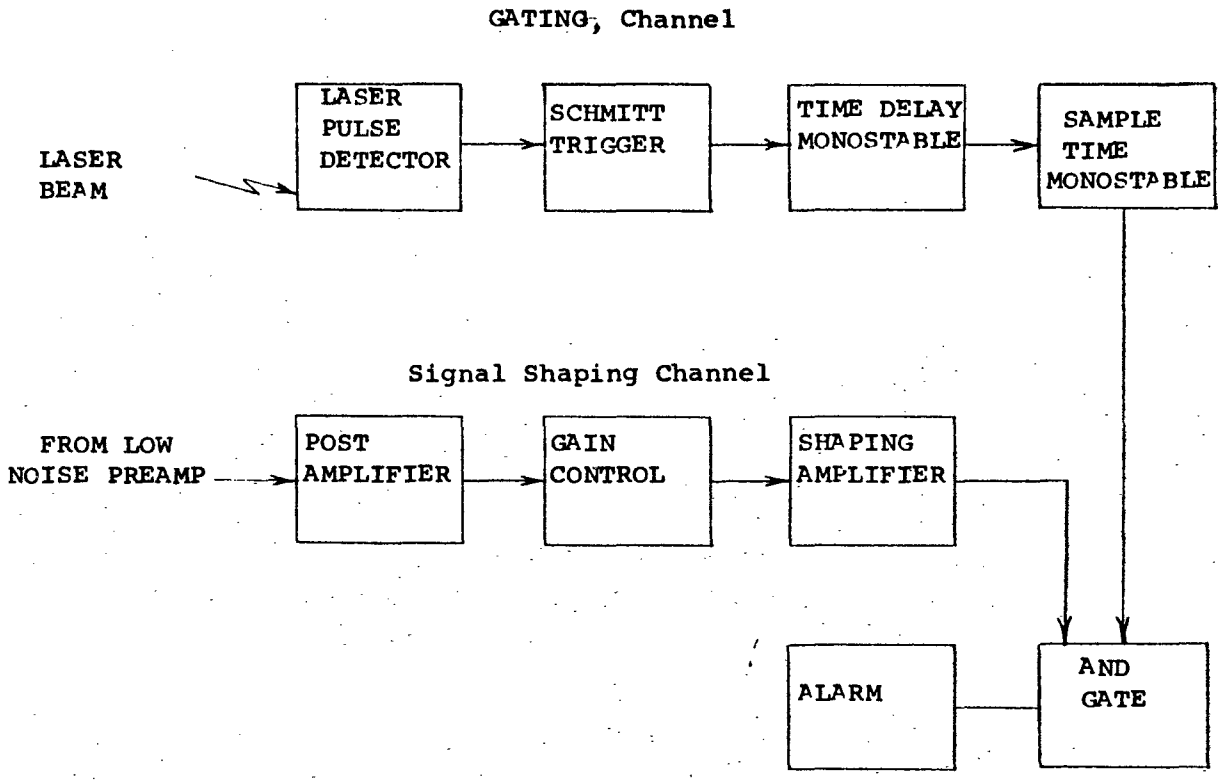

FIGURE19. Processing Electronics Block Diagram

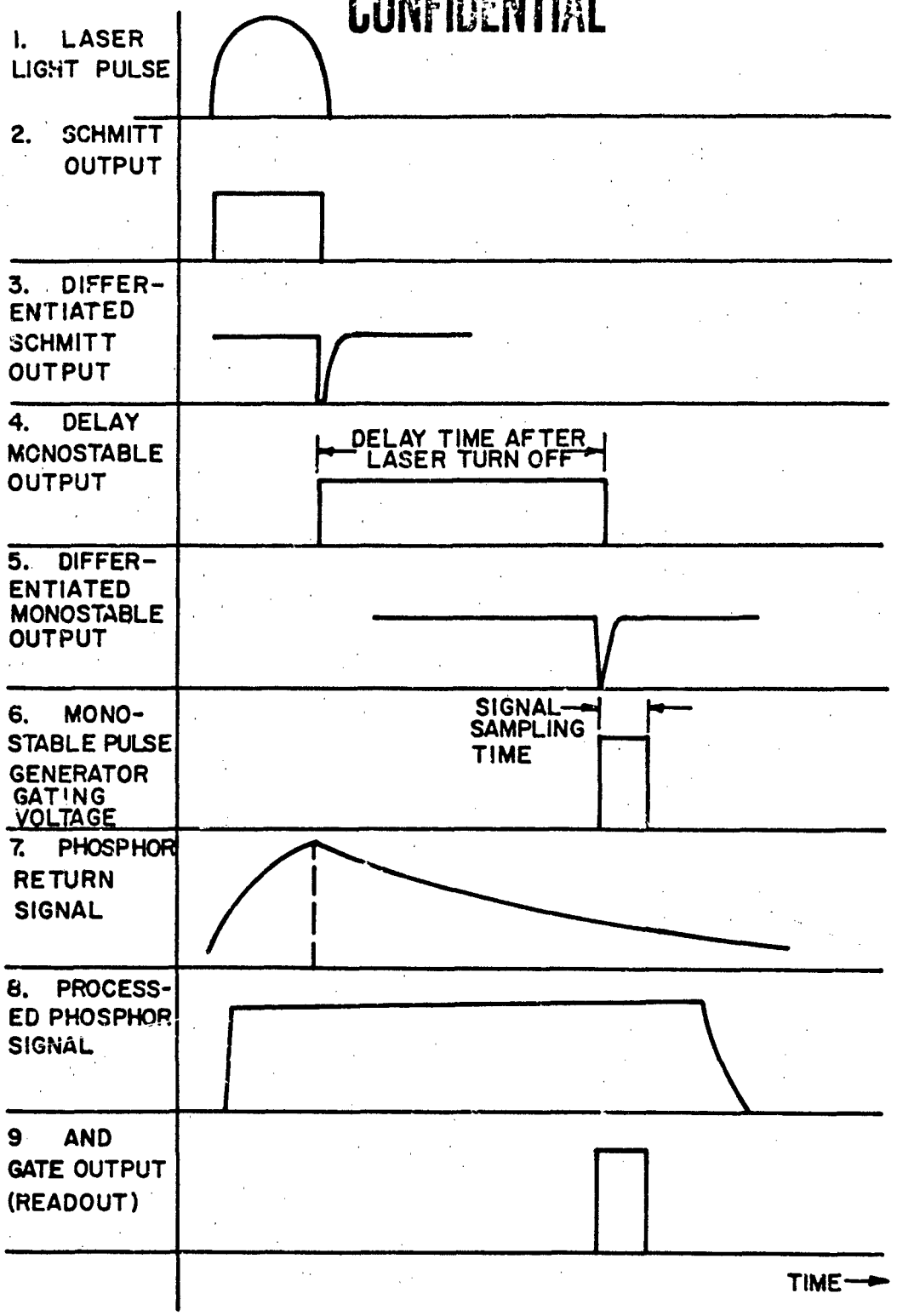

ELECTRONIC WAVEFORMS
FIGURE 20

When the laser "fired", the laser output beam was detected in the transceiver by the laser pulse detector, generating waveform (1) of Figure 20. This signal turned on a Schmitt trigger circuit, waveform (2). The Schmitt trigger output voltage was then differentiated, producing a negative pulse (3) corresponding in time to the laser beam turn off. This negative pulse triggered a monostable multivibrator (MV) which functioned as a delay element remaining in its "on" state as shown in (4) for a preset period of time. For field measurements, a 20 microsecond delay time was used between laser turn off and signal sampling time. The trailing edge of the delay MV waveform was differentiated to produce a negative pulse (5) that was in turn applied to a second monostable multivibrator circuit. During its "on" time, this circuit produced a gating voltage (6) which corresponded to the desired signal sampling time. This gating voltage was applied to one input of an AND gate. The other input was driven by the amplified and shaped phosphor return signal obtained from the signal shaping channel. Shaping consisted of setting a bias level corresponding to the smallest phosphor signal anticipated. Any phosphor signal above the bais level was amplified and referenced to a specific voltage which was applied to one gate input. Signals below the bias level did not trigger the gate circuit. The unprocessed phosphor return signal and its shaped equivalent are indicated as waveforms (7) and (8) respectively. When the gating signal and the shaped return signal were applied to the AND gate inputs at separate times, no output signal was obtained. The AND gate output could be obtained only when the two inputs were applied simultaneously. When this occurred, the gate output voltage (9) was generated. This voltage was applied to the readout alarm circuits consisting of a buzzer and a light to give a go or no-go indication of phosphor presence.

As shown in Figure 21, an illustration of how a phosphor return is differentiated from a reflection, the value of this gating technique lies in the fact that strong reflections of the laser beam, which could otherwise be interpreted as phosphor returns, were locked out of the readout circuits thus preventing false alarms.

A power supply for energizing the thermoelectric coolers in the photometer assembly was located, for convenience, in the processing electronics package. The circuit supplied adjustable high currents at low voltages. One circuit was necessary for powering each cooler. The larger area cooler, a Cambion 3950-1, required up to 7.0 amperes dc at 2.6 volts, the small cooler, Cambion 3950, required up to 1.5 amperes at 2.6 volts. Both units

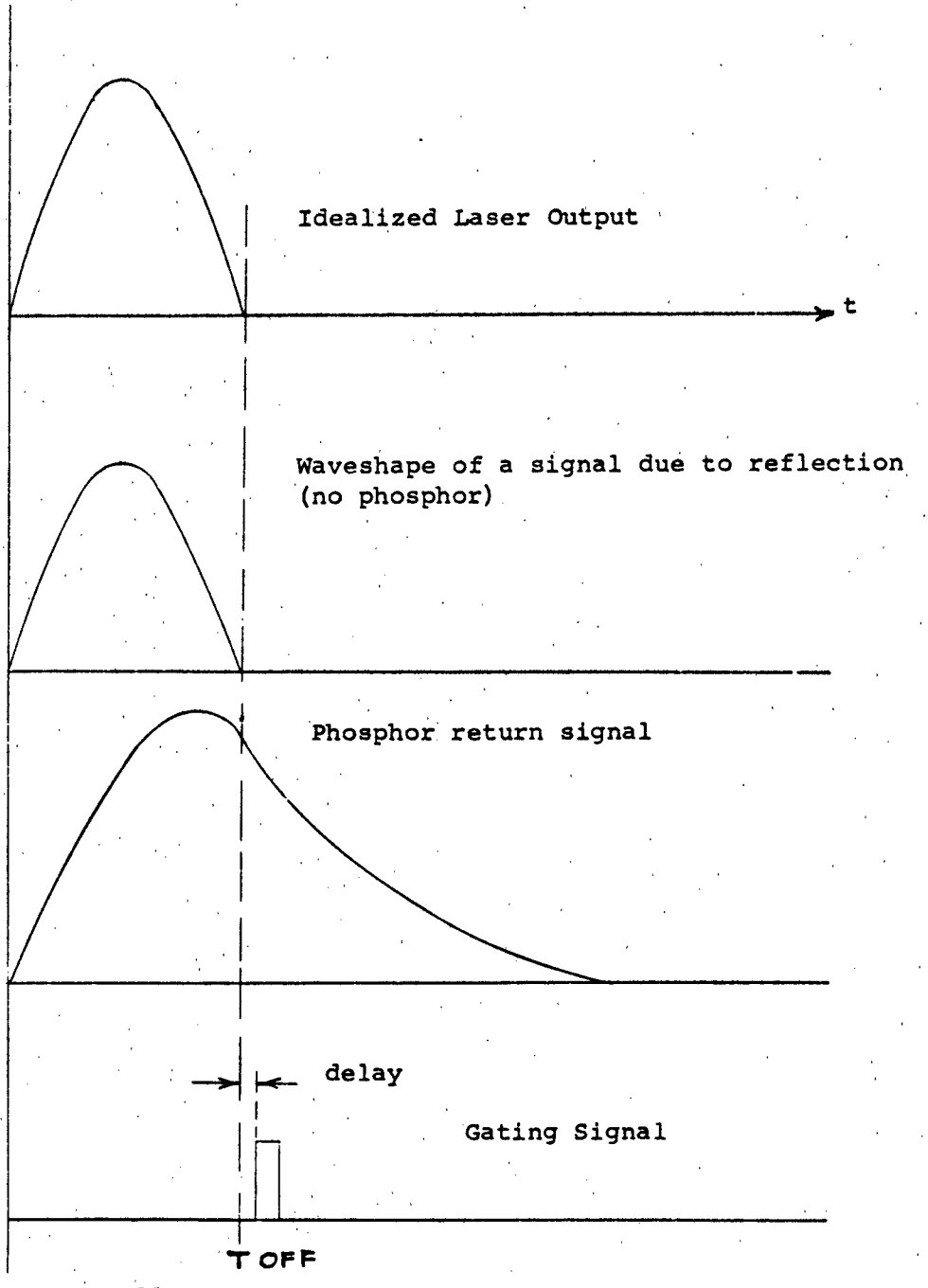

Figure 21. Illustration of Experimental Data Showing How a Phosphor Return is Differentiated from a Reflection

were run at a maximum of 80% of these ratings to provide a margin of safety in case of line voltage fluctuation.

3.4.2 Transceiver Package

The transceiver contained the two elements required to interrogate targets and receive the phosphor return information. A laser consisting of two 3/8 x 3 inch $CaWO_4$ (Nd) rods in series was used as the source of 1.06 micron excitation power. A photometer, consisting of refractive optics, filter to limit the spectral bandwidth to 1.8 microns and a germanium detector, was utilized to sense the presence of stimulated phosphor emission. A telescope was provided as an integral part of the photometer for use in aiming the entire transceiver assembly. A heavy duty tripod was supplied as portable support. The laser and the photometer were packaged in close proximity. To minimize pickup from the large amount of current used in firing the flash lamp, careful attention was paid to grounding and shielding. Pickup was reduced to an almost negligible level by shielding both the laser cavity and photometer with Conetic metal. Additional design details are given below.

3.4.2.1 Photometer

The photometer, designed for detection of the phosphor return signal, utilized an RCA type SQ2516 germanium detector. The detector was located in the photometer, as shown in Figure 22, in the focal plane of a five and one half millimeter focal length field lens. The objective lens is a 220 millimeter focal length lens which when assembled in the photometer gives a 1-13/16 inch clear aperture. The infrared filters, used to limit the photometer spectral response to the region required, consist of a silicon disc in front of the field lens, and a group of two inch diameter dichroic disc filters fabricated at Isomet. The filters are held in standard Kodak series VII filter mounts attached at the front aperture of the photometer. All optical elements, excluding the detector, were antireflection coated for the phosphor emission spectrum. The photometer field of view shown in Figure 23 was determined to be approximately 47.5 minutes (half maximum points).

The effective spectral response of the photometer is indicated in Figure 24. The curve is obtained by combining the experimentally determined response curves of the filter system and response characteristic of the RCA SQ2516 detector. The

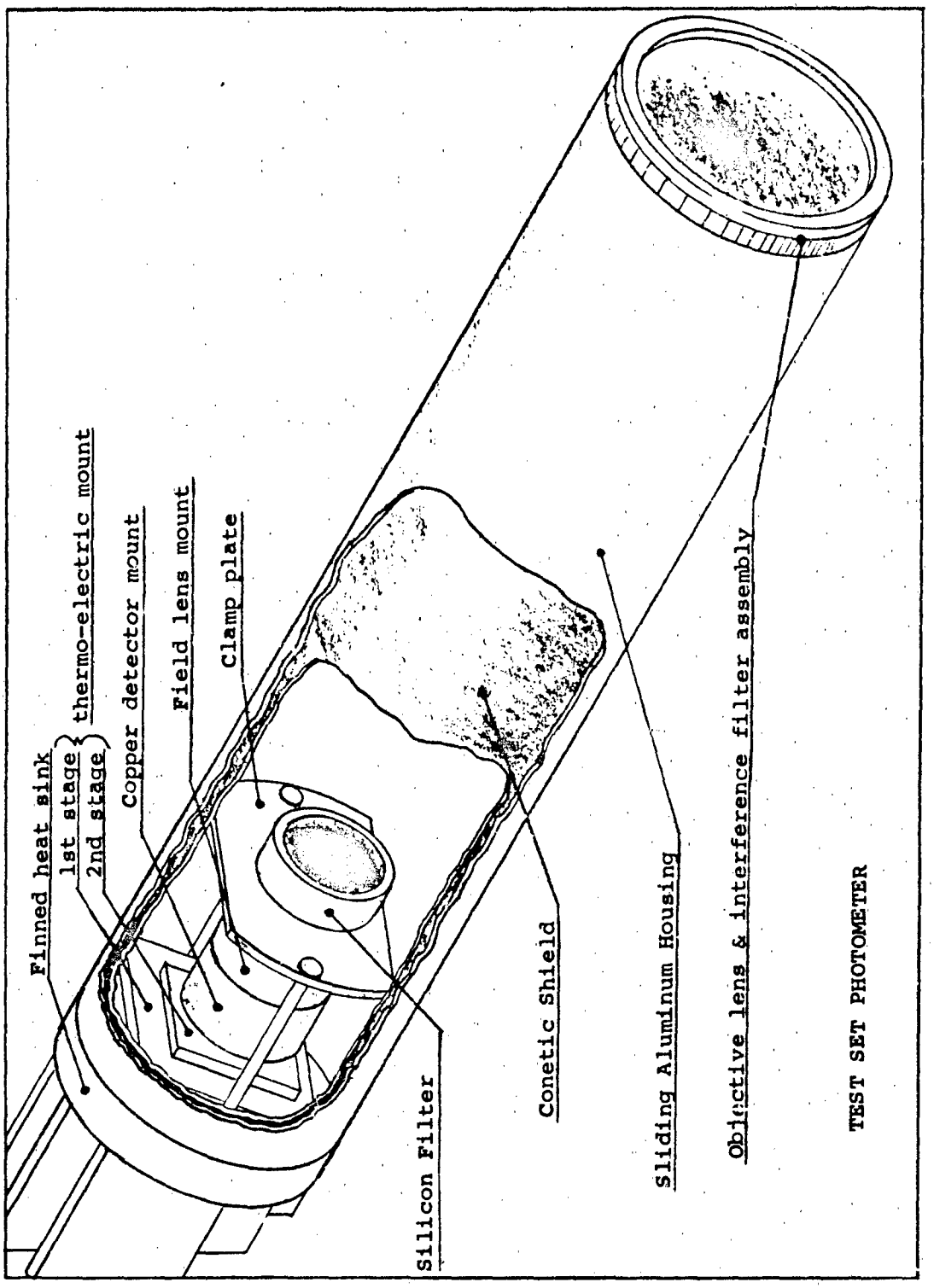
Finned heat sink
1st stage
2nd stage
thermo-electric mount
Copper detector mount
Field lens mount
Clamp plate
Silicon Filter
Conetic Shield
Sliding Aluminum Housing
Objective lens & interference filter assembly
TEST SET PHOTOMETER

FIGURE 22

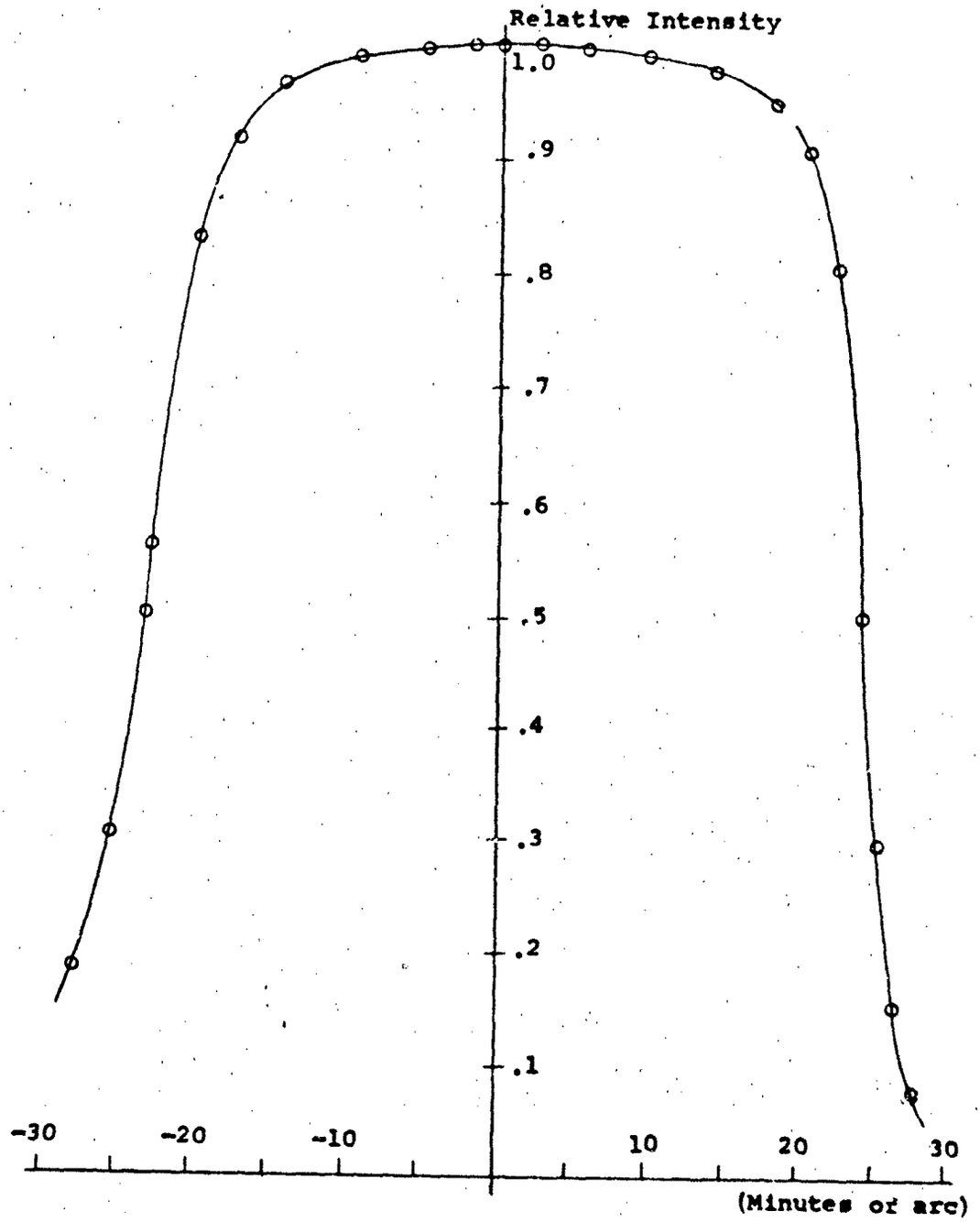

Figure 23. Receiver - Photometer Field of View

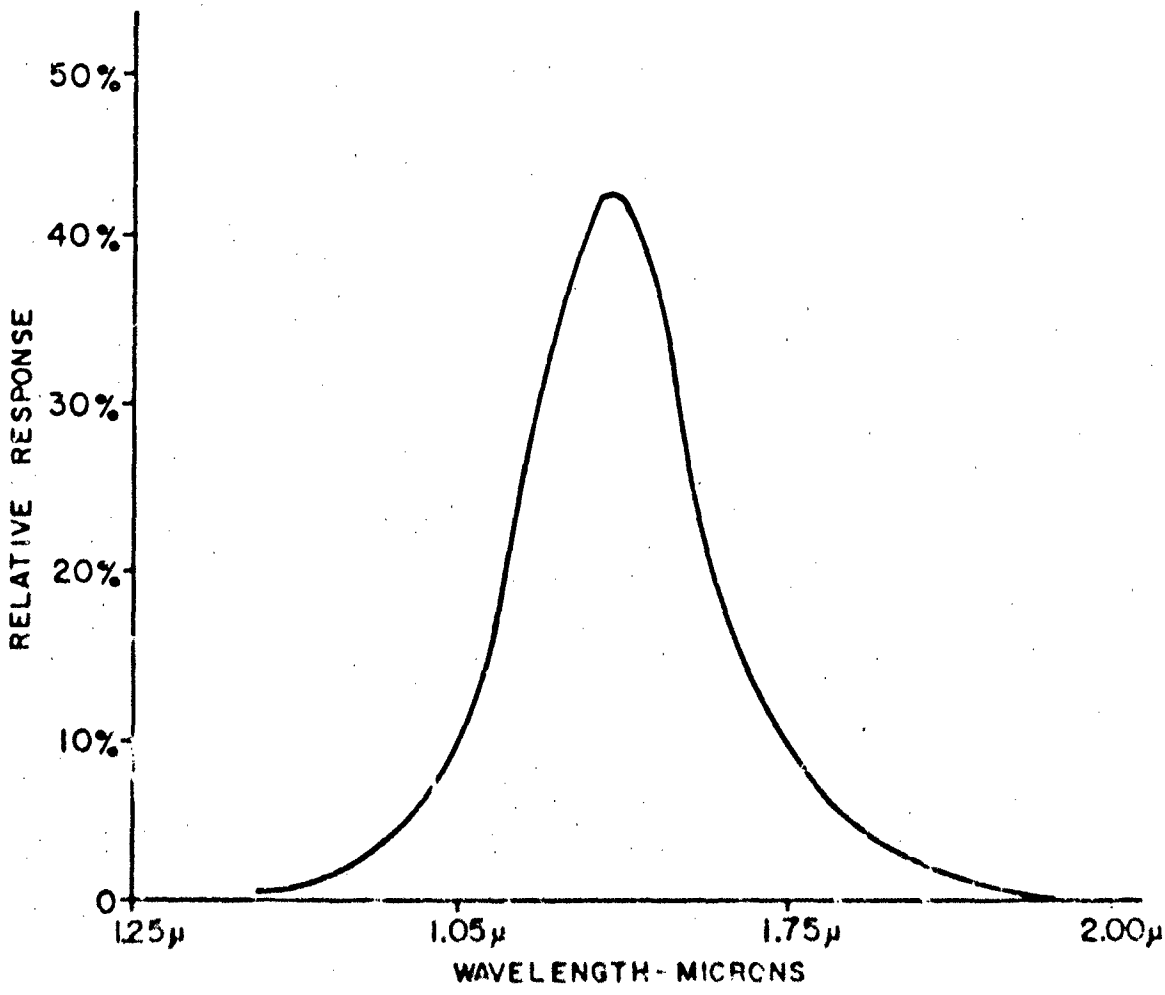

EFFECTIVE PHOTOMETER SPECTRAL RESPONSE

FIGURE 24

combination forms an almost symmetrical curve centered at 1.6 microns. For the detector used, a peak photometer response at 1.6 microns combined with the phosphor emission curve produces maximum detection efficiency. A curve indicating the relative response of the photometer to the phosphor output emission is shown in Figure 3, Section 3.1.8.1.

The photometer circuits provide the initial amplification of the phosphor return signal. The noise characteristic of the preamplifier is such that the output signal is detector noise limited. That is, the noise generated by the detector is greater than that generated by the first transistor in the circuit. For the average detectors and low noise input transistors checked during the program, detector noise was observed to be approximately two to three times greater than transistor noise. The input transistor used was a Fairchild 2N2484, NPN silicon device selected for its low noise characteristics. The unit, as used in the test set, was biased to operate in its lowest noise generating region. The output of the 2N2484 was applied to a Fairchild uA-702 integrated circuit amplifier which provided the additional gain and bandwidth limiting required. The basic circuit diagram for the low noise amplifier is shown in Figure 25. The gain-frequency response is given in Figure 26.

A curve of the relation between preamplifier input and output signal is shown in Figure 27. The curve indicates an amplifier output saturation level, where the curve departs from a linear relationship by 10%, of 1.4 volts. This means that large phosphor signals from either large targets or small ranges will not be amplified as much as lower level signals from distant or small area targets. A side effect of the saturation characteristic is the time required by the amplifier to become unsaturated or recover after being driven into the non-linear region. If a large signal saturates the amplifier, the excess signal generates voltages which are stored in the circuit capacitors. When the signal is removed, the capacitors discharge at a rate dependent upon the circuit configuration and time constants involved. Therefore, in some cases, a large signal existing for 100 microseconds can produce an output lasting for 200 microseconds or more. Because of these characteristics, care was taken to obtain phosphor signals within the linear range of operation. For a final system, the preamplifier design would be modified to provide the larger dynamic range of signals experienced during field measurements.

Characteristics of the preamplifier are as follows:

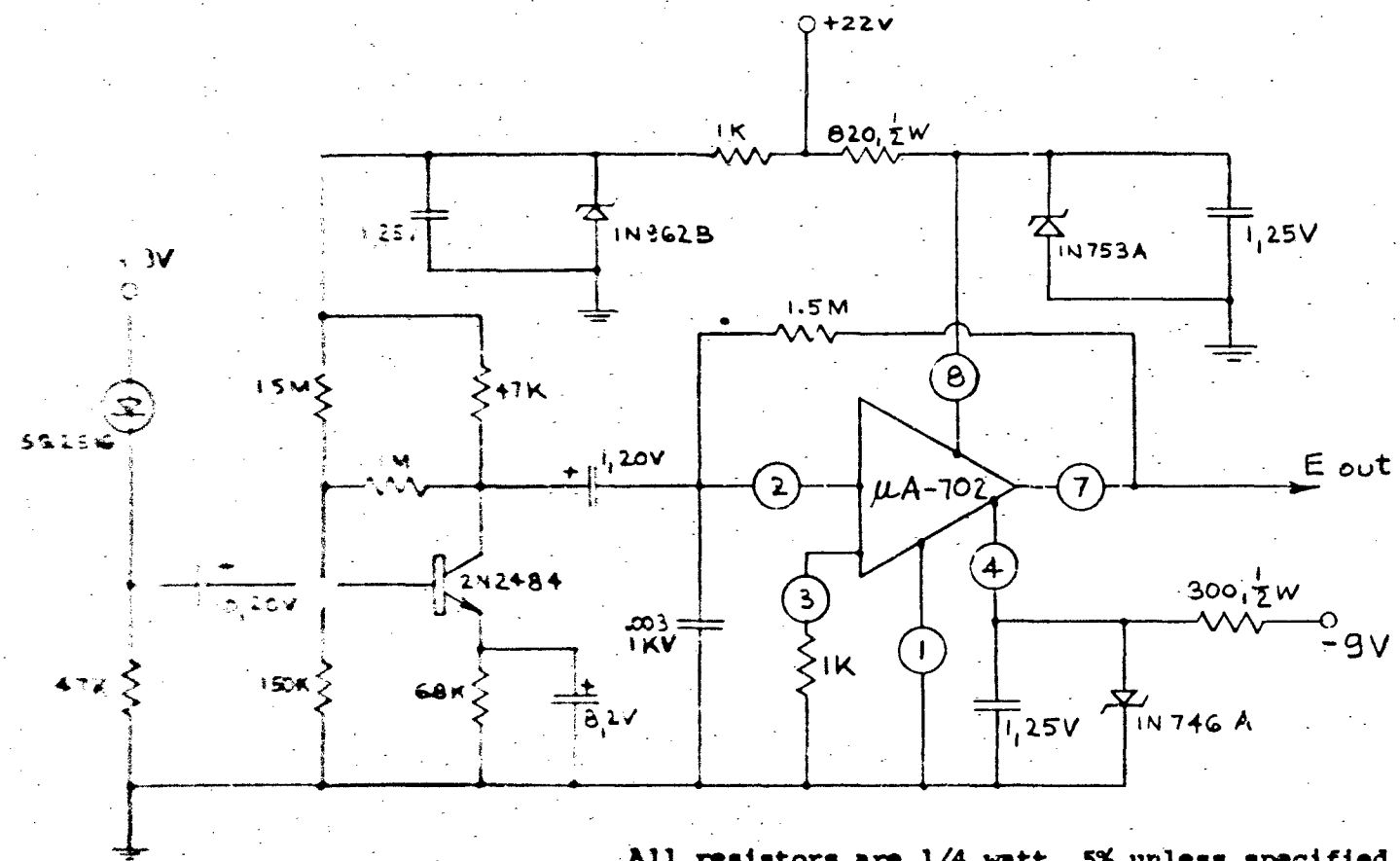

All resistors are 1/4 watt, 5% unless specified otherwise
All capacitors are in microfarads

FIGURE 25. Low Noise Photometer Preamplifier

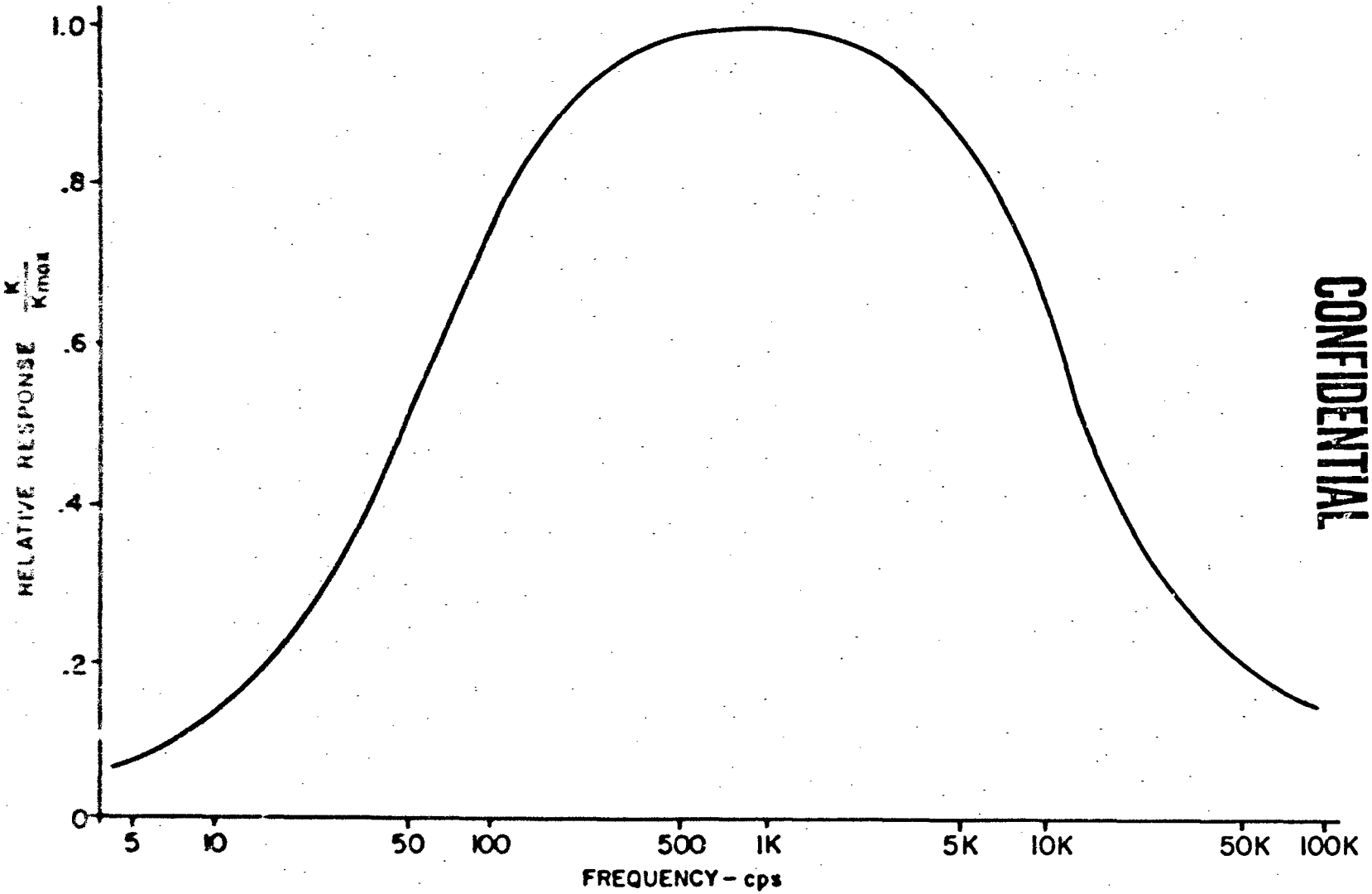

PHOTOMETER PREAMPLIFIER RESPONSE

FIGURE 26

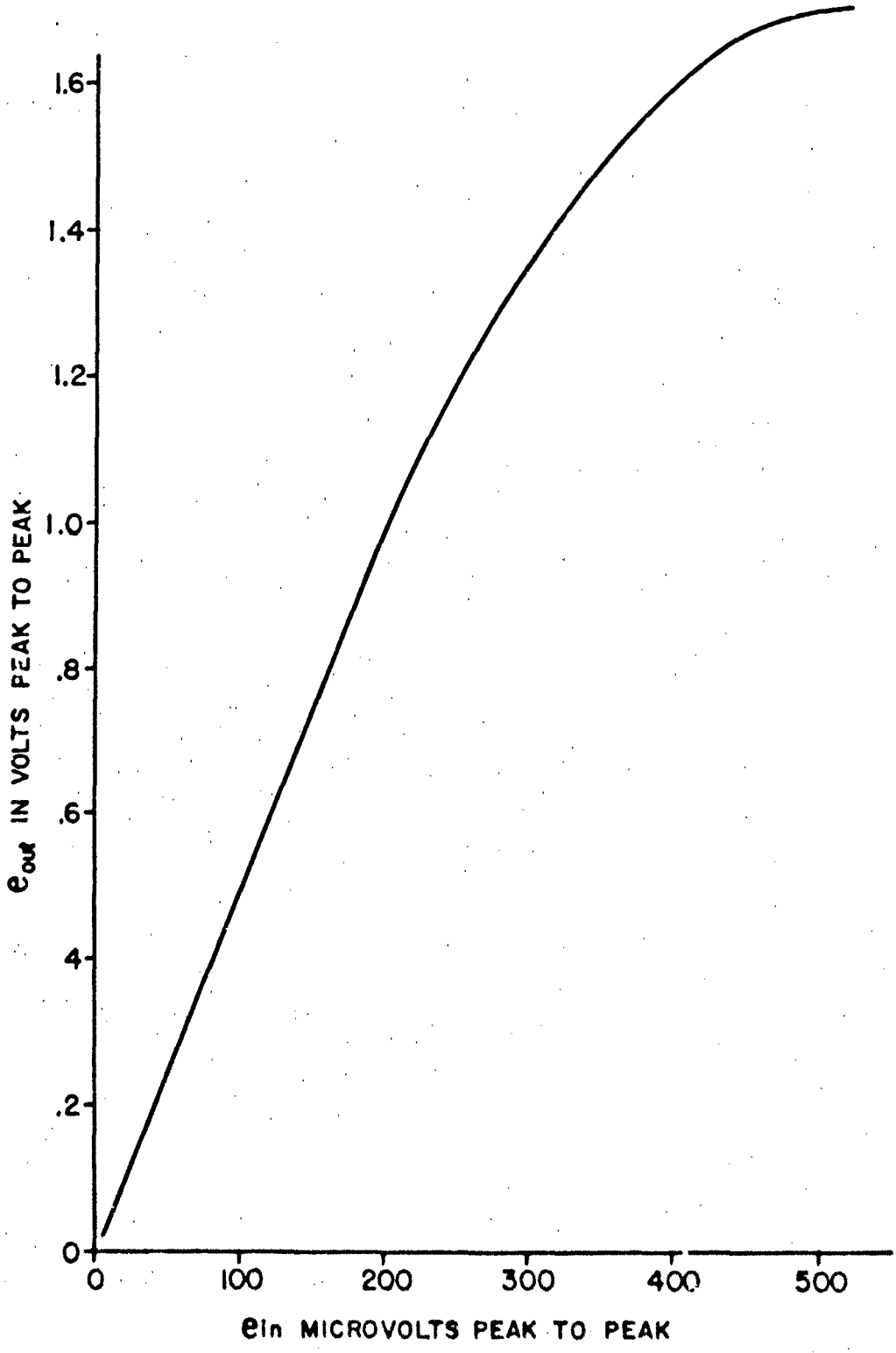

PREAMPLIFIER LINEARITY CURVE

FIGURE 27

Gain at center frequency of 1000 cps	5720
Bandwidth (3db points)	90 cps to 9.0 KC
Equivalent noise input with 47K ohm source	1.14 μVRMS
Feedback	18 db
Output saturation level (10% deviation from linearity), 10 K load, rectangular single pulses, 150 microsecond width	1.4 volts

Overall sensitivity of the photometer was checked prior to field measurements. The detector used was unit #4 with a bias of 9 volts. The values of responsivity and NEPD were calculated from the following conditions:

Black Body Temperature	930°C
Chopping Frequency	370 cps
Range, r	605 cm
Aperture area, Aa	1.26×10^{-2} cm^2
Noise voltage, En	15×10^{-3} volts RMS
Signal voltage, Es	1.5 volts P-P
Filter 50% Transmission Points	1.50 and 1.69 microns
Filter Center Wavelength	1.615 microns

From the black body temperature used, the source intensity in the spectral band defined by the filter set is determined by use of a Radiation Slide Rule. The source intensity No, was found to be:

$$No = 0.322 \text{ watts/cm}^2$$

The photometer responsivity R is calculated from:

$$R = \frac{Es\, \pi\, r^2}{No\ \ Aa} \qquad (20)$$

$$R = \frac{1.5\ (3.14)\ (605)^2}{0.322\ (1.26 \times 10^{-2})} = 427 \times 10^6 \ \frac{V\text{-cm}^2}{\text{Watt}}$$

NEPD for the photometer is found from the relation:

$$NEPD = \frac{En}{R} = \frac{15 \times 10^{-3}}{427 \times 10^{-6}}$$

$$NEPD = 3.51 \times 10^{-11} \text{ watts/cm}^2 \qquad (21)$$

It was anticipated that detector cooling would improve the performance of the photometer. After preliminary tests, a fixture was designed for attachment to the basic photometer housing. Detector cooling was provided by a two stage cooler consisting of two Cambion coolers: a type 3952 mounted on a 3950-1. The combination of these two devices permitted temperatures as low as -22°C to be obtained. Temperature was measured at the solid copper detector mounting block and in a pressure contact with the upper cold junction. Silicon grease was used between all bearing surfaces to improve thermal conductivity. There was no measurable temperature difference between the copper in the immediate detector area and the cold junction surface. The hot junction of the large cooler (3950-1) was fastened to a finned copper fixture at the rear of the photometer. A small cooling fan mounted on the rear wall of the transceiver enclosure provided air cooling of the fins. Because of detector noise problems due to junction degradation, the coolers were seldom used in measurements. It was felt that cooling contributed to junction degradation. The problem became apparent in measurements made outdoors in humid weather. Frost formed on all cooled surfaces including the detector aperture. As described in Section 3.3, the presence of water vapor in the detector case may have contributed to detector failure if cooling caused even minute amounts of water to deposit on the junction.

Since a hermetically sealed photometer assembly would not solve the problem of entrapped water vapor in the detector, the photometer was not sealed. Cooling was therefore limited to only a few short duration tests under field conditions. In these cases, noise was observed to decrease, as predicted, and then increase until it was higher than the initial value at room temperature. Test data obtained with the cooled detector in the field could not be used for evaluation since the coolers were not left on long enough for the junction temperature to stabilize. This led to large variations in signal to noise ratio in the data obtained.

3.4.2.2 Laser

The laser used for field measurements consists of two 3/8" x 3" $CaWO_4$ (Nd) rods in series. The rods are mounted in a closely coupled cylindrical cavity. The cavity is fabricated from an aluminum casting based on Isomet's "clamshell" design and lined with high reflectance electropolished aluminum (Alzak). As indicated in Section 3.2.4, two 3/8 x 3 inch rods were used because 3/8 x 6 inch rods with the necessary optical quality and

high Nd content were not available. Although the rear rod had a 100% reflective coating on the non-transmitting end, an external reflector was provided as a backup in case the rod coating was damaged by the high lamp energy. During the course of field measurements at Eglin A.F.B., the coating did become sufficiently deteriorated to warrant use of the external reflector. The external reflector is not subjected to the full lamp energy and therefore is usable for an extended period of time. An additional optical element found to be necessary for making measurements at close range with high laser input energies was a 1.06 micron spike transmission filter. This unit was located in the exit aperture on the front panel and was required to attenuate the energy produced by the flash lamp. The wide band energy, although not collimated, had a sufficient output between 1.5 and 1.8 microns to produce reflections which occassionally obscured phosphor return signals. This would occur when the laser beam was aimed at a reflective surface at ranges up to approximately 50 feet. While not all of this radiation was filtered, the energy was reduced sufficiently to prevent amplifier saturation with all but the closest reflective objects.

One factor effecting the maximum operation range is the divergence, or cone angle, of the laser beam. As the beam diverges with increasing range, the power density (watts/cm^2) decreases. To increase the operational range of the system, to permit specific small area targets to be illuminated, and to obtain data on effects of varying beam angle, a set of telescopes was provided with the test set. The initial beam divergence is decreased by the magnification of these telescopes. Three Galilean telescopes with magnification of 5.75, 2.88 and 1.67 were fabricated. Each unit consisted of two simple lenses, one negative and one positive. The ratio of the focal length of the latter to the former is the magnification. All optical surfaces were antireflection coated at 1.06 microns.

The beam divergence of the laser was measured using two different telescopes at ranges of 47 feet and 12 feet. The beam size was measured by viewing the beam reflected from a white card using a metascope as in image converter. The data are given in Table 9. The average deviation is about 20%, reflecting the subjective nature of the technique used. The method was adequite, however, for our needs.

The laser flash lamp, an FX47B manufactured by Edgerton, Germeshausen, and Grier, Inc., Boston, Massachusetts, was externally triggered by an electrode attached to the wall of

TABLE 9. BEAM DIVERGENCE OF LASER

Test No.	Telescope Magnification	Beam Diam. (inches)	Range (feet)	Beam Divergence (mrad)	Av. Div.	BD x Mag.	Deviation
1	5.75	4	12	12.76		66.5	+ 11.5
		8	47	10.34	11.55		
2	5.75	3.25	12	7.56	7.63	43.8	- 11.2
		7 x 6	47	7.70			
3	1.67	6	12	37.4	32.7	54.6	- 0.4
		16 x 17	47	28.0			

Average 55.0 M rad ± 7.7 mrad

the lamp. A high voltage trigger transformer (delivering 25,000 to 35,000 volts) and pulse drive circuit were located immediately behind the cavity to minimize high voltage cabling and reduce radiative fields. The drive circuit consisted essentially of a silicon controlled rectifier which short circuited a capacitor in series with the primary winding of the trigger transformer to produce the short duration, high voltage spikes required for firing the flash lamp.

The laser output beam is detected within the transceiver by an SQ2516 detector. The output of this detector, properly amplified, is used to trigger the processing electronics gating circuits. Triggering is initiated when the laser is fired. As the laser is turned off, the gating circuits are permitted to function as described in Section 3.4.1. No signal processing may be performed until the laser is off.

The output power of the test set laser was found by measuring the reflection of 1.06 micron energy from a white card using a calibrated photometer. The photometer utilized a high speed detector and wide band amplifier to insure waveform fidelity. The responsivity of the photometer at 1.06 microns and the parameters used in determining the laser peak power output are as follows:

r = Range = 396 cm
V = Signal voltage = 2 volts
R = Responsivity at 1.06 microns = 1.02×10^3 volts-cm^2/watt

The peak output power, Po, is calculated from the equation :

$$P_o = \frac{V \pi r^2}{R} \qquad (22)$$

$$= \frac{2\pi(396)^2}{1.02 \times 10^3}$$

$$P_o = 965 \text{ watts, peak}$$

The power was obtained using an input energy to the flash lamp of 485 joules. Prior to the time the measurement was made, the coating on the rear laser rod had deteriorated so much that it had been removed and was replaced by an external mirror. As discussed in Section 3.5, this was the maximum power used in making the field test measurements, although the flash lamp and power supply were designed to deliver energies up to 600 joules.

3.4.3 Laser Power Supply

The laser power supply serves as a capacitor energy storage bank for powering the laser flash lamp with short duration bursts of current. The unit is capable of providing up to 600 joules of energy at 2000 volts. Pulse width of the flash and discharge was observed to vary slightly between 200 and 220 microseconds depending on power supply voltage and firing rate.

Two modes of operation were built into the power supply. These are automatic or manual initiation of the charging cycle. In the automatic mode, after the laser is fired, recharging of the capacitor bank begins immediately and ends when the preset voltage level is reached. An internal system of relay logic provides all functions automatically except the firing of the laser. The state of the system is shown by a voltmeter recording charge voltage and a series of lighted switches and indicators. In the manual mode, after each firing, the high voltage power supply is disconnected from the ac line, and remains inoperative until a reset button is pushed. In either mode, the supply may be discharged without firing the flash lamp and put into a "safe" condition by depressing a "manual dump" button. When this is done, the high voltage supply is disconnected from the line and the supply is discharged through a high voltage relay and a series of power resistor. An interlock is also provided so that the supply is discharged if the cabinet is opened.

Power for the flash lamp trigger circuit is generated within the laser power supply. This consists of +28 volts dc and +400 volts dc. The 400 volts dc is used to store energy in the capacitors in series with the trigger transformer primary winding. A large series resistor is used to prevent supply damage when the capacitor is shorted to ground by the silicon controlled rectifier (SCR).

The SCR is triggered from the 28 volt dc supply. A push button switch and an external cable are supplied for triggering the system.

3.5 Field Measurements

Field measurements with the engineering model system were performed at several locations in New Jersey from March 15 to April 16, 1965, and at Eglin Air Force Base, Florida from April 26 to May 18, 1965.

The New Jersey measurements were made in cool weather

with backgrounds containing sparse green vegetation except for fir type trees. Measurements in Florida permitted system performance to be checked in an almost totally different climate with heavy ground and tree greenery. Performance of the system at both areas was good and a large quantity of pertinent data was obtained.

Parameters checked during the field measurements were:

a. Absolute signal levels for various ranges and objects.

b. Signal to noise levels and variations with various backgrounds.

c. Go/No-Go indication of phosphor presence

d. Items which cause unusual responses and noise

e. Range equation parameters

Raw data for all measurements were recorded on the reverse side of the oscilloscope trace photographs taken for each data point. A typical set is shown in Figure 28. The data recorded have the information required above.

The phosphor coated targets used for range measurements and for determining the effects of geometry and substrate surface on system performance are described in Table 5, Section 3.1.17. A similar table with additional details is shown in Table 12, Section 4.5.2.

Data was taken in conformance with the Test Plan which is outlined below.

A. Background Studies

The background studies consisted of photometric measurements which would show the effects of various backgrounds on system performance. Characteristics of spurious signals and noise due to emission and scattering were obtained. Measurements were made at different sites with and without laser excitation on the items indicated in Table 10. The table also shows the results obtained for each item. As these items were tested, each was photographed in color. No spurious signals or phosphor scintillation signals were observable when the photometer was statically trained on various objects. The signal levels and characteristics appeared

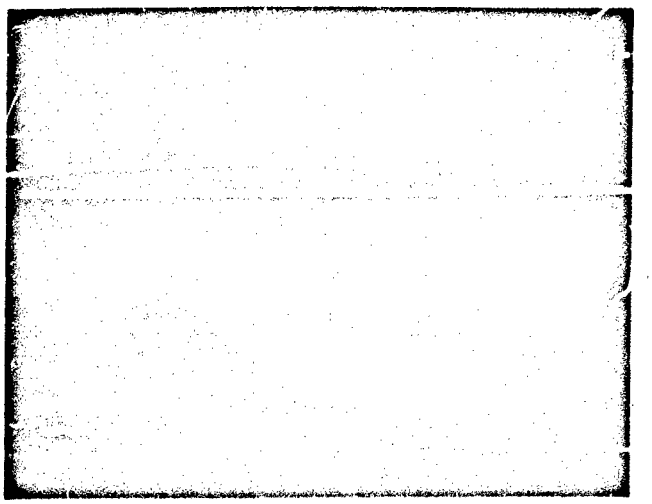

Upper Trace: Gate Channel with Phosphor Presence Signal
Lower Trace: Phosphor Return Signal

Date 5/10/65 Initials [illegible] Photo No. 49 Target Photo No. 2
Voltage 1800 v Cap 300 uF Joules In 785
Top Trace 50 us/cm 10 v/ GATE CHANNEL
Bot Trace 100 us/cm 10 v/ PHOS. RETURN
Location & Weather NIGHT Time 8PM
Range & Target Description 200 FT. TARGETS - FIELD JACKET
Comment BUILDING 1000

FIGURE 28. Oscilloscope Trace Photograph and Reverse Side Indicating Method of Recording Raw Data

TABLE 10

Summary of Field Background Measurements

ITEM	RESPONSE	DESCRIPTION OF RESPONSE
Blue Skies, clouds	Nil	
Trees A. Conifer	Reflection (scattering) No effect from static background.	Reflection of 1.06 micron laser and lamp radiation. No observable emission.
B. Deciduous		Deciduous vegetation gave the larger amplitude reflections of the two tree types.
Ground Vegetation	Reflection No effect from static background.	Reflection of 1.06 micron laser and lamp radiation. No observable emission.
Solar Radiance (reflected from white cards)	Nil	
Water	Reflection. No effect from static background.	Reflections, strongly angle dependent, low levels. No observable emission.
Bare ground, sand, rocks, ree clay	Reflection. No effect from static background.	Mica flecked rock and white sand gave the largest reflections of 1.06 micron laser radiation. No observable emission.
Phosphor coated objects	No static effect	
Clothing	Reflection. No static effect	Reflections of 1.06 micron radiation dependent on color and cloth texture. Low level in any case. No observable emission.
Human Skin	Reflection. No static effect.	Low level reflection. No observable emission

CONFIDENTIAL

to be those generated by the detector alone. No effects from Raman scattering was observed when the terrain was illuminated with the laser beam.

B. Phosphor Range Studies

Measurements were made of the signal returns from a variety of shaped phosphor coated objects at known horizontal ranges to permit verification of the derived range equation. The maximum operating range of the system was determined over an unobscured path. Several sets of measurements were made at Eglin Air Force Base and New Jersey with phosphor coated objects behind varying degrees of cover. Photographs were taken of the target obscuration in each case. Additional testing was performed with the equipment set up in a tower to permit measurements to be taken along vertical and slant paths to simulate an airborne environment. Night measurements were taken at Eglin Air Force Base outside Building 1000 at Field 1 and from a tower located in the southwest corner of Field 1.

3.5.1 Background Study Results

As a result of the background studies, it has been determined that none of the objects or backgrounds viewed by the photometer on a static basis caused a variation in output signal level. No unusual responses were observed in this mode. Detector noise did not change when different objects were viewed but was somewhat affected by ambient temperatures as would be expected from the curve of Figure 15, Section 3.3.

When many of the background items observed by the photometer were irradiated with laser energy, the signals due to reflections (scattered) were recorded. None of these reflections, however, resembled phosphor signals. This reflection phenomenon was observed also with phosphor coated objects. Moreover, each phosphor target was found to have a particular level of reflection. While this is observed to be true for irradiated backgrounds, field conditions did not permit quantitative data to be taken. What was observed were reflected signals that varied with range, background, density, reflectivity, directivity and object shape and size. For example, any reflecting object would give larger reflection than a less dense background of the same material. Finally, high reflectance objects with a degree of directivity (large broad leaves) produce larger return signals than lower reflectance and directivity objects (small fir tree needles.)

During initial field testing in Closter, New Jersey, a 1.06 micron spike transmission filter was placed in front of the laser cavity to reduce the radiation of wide band flash lamp energy from the cavity. The filter was effective at ranges of about 50 feet when the laser beam was reflected from a large tree trunk. At closer ranges the reflection signal became larger. In Florida, the background encountered reduced the effectiveness of the filter because of the higher reflectivity of the greenery. In addition, a higher proportion of 1.06 micron energy was reflected.

Several oscilloscope traces from the Florida measurements are indicated in Figures 29 through 38. These photographs are illustrative of reflections from greenery obtained at ranges of about 50 feet to 2000 feet. The upper trace of the photographs represents the gating channel. For reflections, gating signals were not observed unless the preamplifier saturated or the instantaneous system noise was excessive.

The lower trace shows the reflection signal obtained. In several cases, the beginning of the pulse is slightly obscured by pickup noise but the overall waveshape can be determined if the first two narrow spikes are discounted. Spikes of this type appear in Figures 32, 33, 37 and 38. Signal levels are measured by placing a straight edge along the zero signal line, bisecting the noise. The height from this point to the peak of the signal is measured and multiplied by the recorded oscilloscope scale factor. In many cases, the peak of the signal contains small oscillatory waveforms and the center line of the waveform must be estimated to obtain a peak. It should be noted that all signals contain a pickup level which varies between 20 and 40 millivolts. This appears to be due to the large current pulse in the flash lamp.

Figure 29 is the return obtained from a palmetto bush at a total range of 54 feet from the laser. The laser was located in a clearing 15 feet from the edge of the ground cover surrounding the palmetto. The palmetto was 24 feet in from the edge of the clearing. A thick grouping of low branches were immediately behind the palmetto. The peak signal recorded was 0.75 volts.

Figure 30 was obtained from the reflection of dense underbrush and low hanging tree branches. The transceiver was aimed at a wooden stake at a total range of 100 feet. The stake as observed through the transceiver was barely discernable because of tree branches in the line of sight. Undoubtedly, these branches caused the larger return. The peak reflection voltage

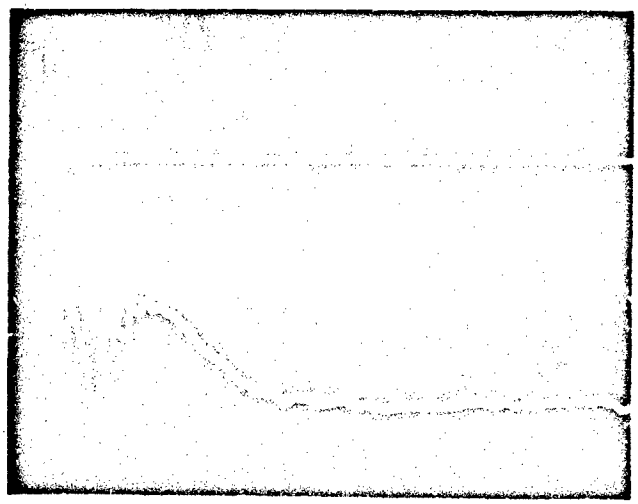

FIGURE 29. Reflection Signal From a Palmetto Bush at 39 Foot Range. (0.5V/cm 100usec/cm)

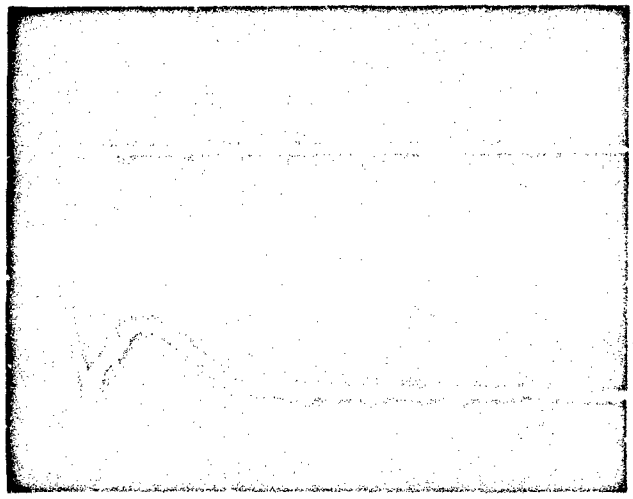

FIGURE 30. Reflection Signal from Dense Underbrush and Low Hanging Trees Branches. (0.5V/cm 100usec/cm)

is approximately 0.55 volts. Figure 31 was obtained when the laser beam was projected into an area similar to that for Figure 30. The transceiver, in this case, was 40 feet from the edge of dense cover, and the area aimed at, a group of unidentified deciduous trees, was 30 feet beyond the edge of cover. The peak reflection was approximately 0.64 volts.

Figure 32 is the reflection recorded from a pine tree over a clear path. Range in this case was 100 feet and the laser beam was targeted on a dense area of pine foliage about 8 feet above the ground. The tree trunk could not be seen. In this photograph, the first two positive pulses are pickup and are extraneous. The peak signal was estimated to be 0.14 volts.

Figure 33 is the reflection obtained from an unidentified deciduous type tree at a range of 100 feet. The laser beam was aimed at a section of the tree about 15 feet from the ground. Blue patches of sky could be seen through the branches. The peak signal observed, discounting the first two pulses, was about 0.070 volts.

Figure 34 is the reflection from an oak tree at a range of 110 feet. Again, height was about 15 feet above the ground and blue sky could be seen through the branches. Peak signal was about 0.140 volts.

Figure 35 was obtained from the reflection of the laser beam from white sand with sparse ground cover at an unobscured range of 190 feet. The target area was sloping upwards at an angle of roughly 30 to 40 degrees. Peak signal was estimated at 0.120 volts.

Figure 36 is a reflection from a white card at a 150 foot unobstructed range. The peak signal is 0.120 volts.

Figure 37 was obtained from the reflection from a light blue cotton shirt and probably a portion of the rear of the subject's head. The clear range was 200 feet. The initial pulse in this photograph is pickup. The reflection is the lower amplitude, second "bump" which has an estimated peak height of 0.060 volts. This may be partly or totally due to electrical pickup. The signal level is sufficiently low to be questionable as qualitative data.

Figure 38 is the reflection from the subject's face and shirt front. The large initial pulse is again due to pickup. The absence of signal thereafter points out the questionability of the signal level obtained in Figure 37.

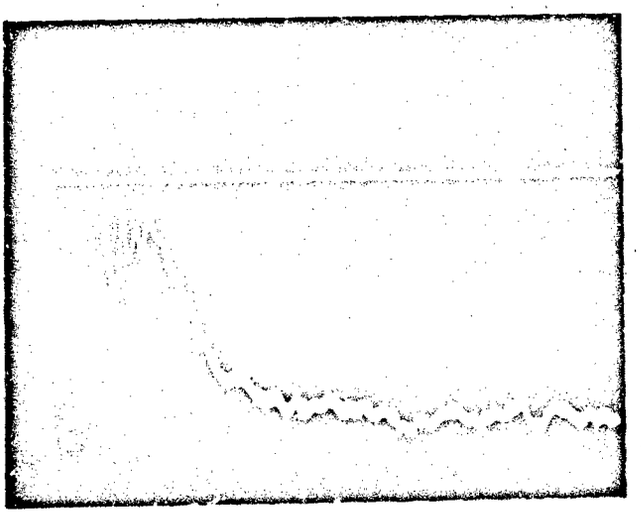

FIGURE 31. Reflection From Dense Vegetation at 70 feet. (0.2V/cm 100usec/cm)

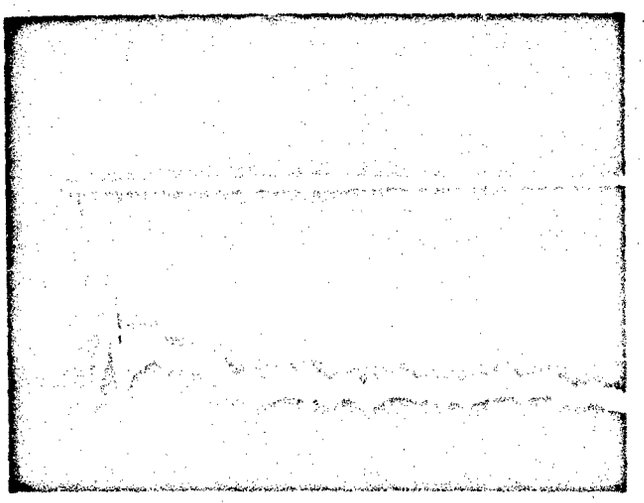

FIGURE 32. Reflection Signal from a Pine Tree at 100 Feet. (0.2V/cm 100usec/cm)

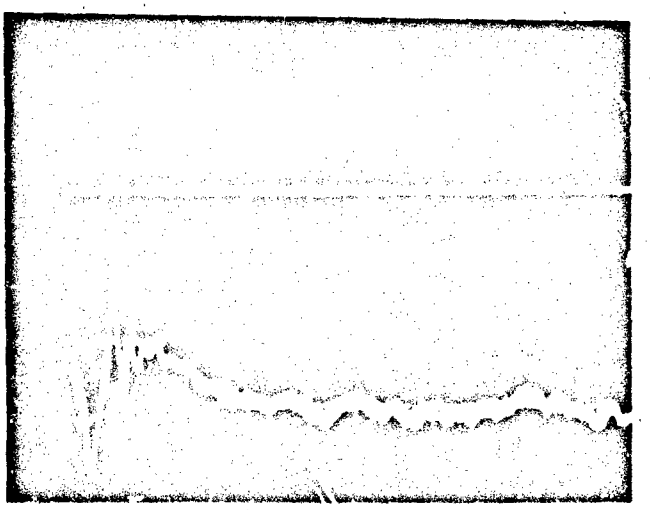

FIGURE 33. Reflection Signal From Foliage of An Unidentified Deciduous Tree. (0.2V/cm 100usec/cm)

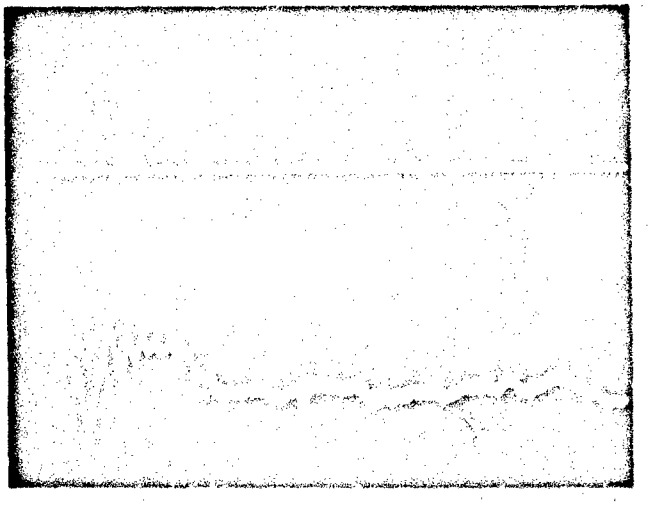

FIGURE 34. Reflection Signal From Oak Tree Foliage At 110 Foot Range. (0.2V/cm 100usec/cm)

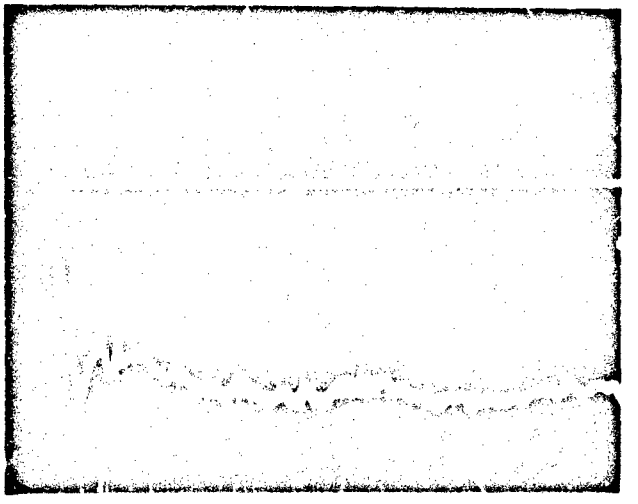

FIGURE 35. Reflection Signal From White Sand and Sparse Ground Vegetation at 190 Feet. (0.2V/cm 100usec/cm)

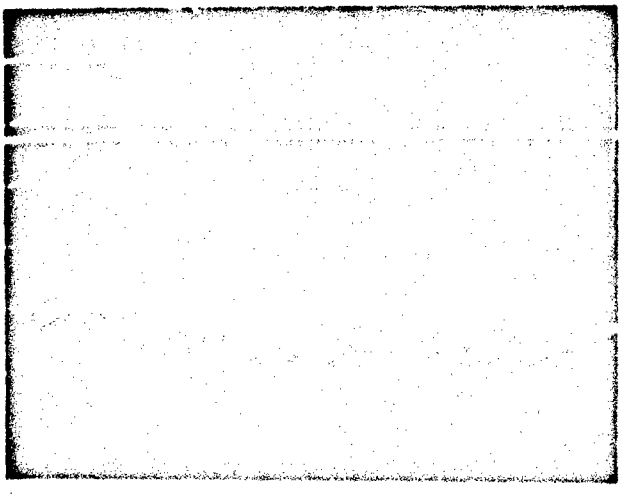

FIGURE 36. Reflection from an 8-1/2 x11 inch White Card at 150 Feet. (0.2V/cm 100usec/cm)

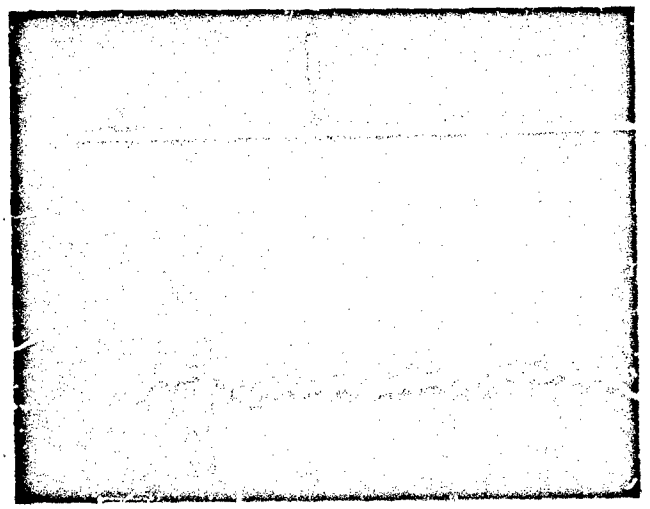

FIGURE 37. Reflection Signal from a Light Blue Cotton Shirt at 200 Feet. (0.2V/cm
100usec/cm)

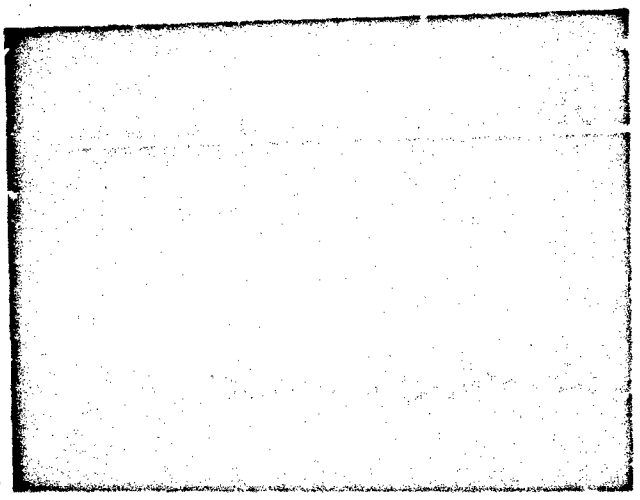

FIGURE 38. Reflection Signal From Skin and Hair (Head) at 200 Feet. (0.2V/cm
100usec/cm)

Similar photographs were made in other areas with similar results. In no case was a return signal observed with phosphor-like characteristics. An important observation, in terms of a future, operational flight system, was that no visible radiation was apparent at the target. There was no visible glow from phosphor fluorescence or the laser beam and there was no visible radiation from the laser cavity aperture. All visible radiation impinging upon the aperture was attenuated by the 1.06 micron spike transmission filter.

3.5.2 Range Measurements Results

Range measurements were performed both in New Jersey and Eglin Air Force Base, Florida. Data from both locations were evaluated and found to be equivalent for the same system operating conditions. The data were, therefor , processed identically. The procedure used in obtaining data as a function of range was to place a series of markers at 50 foot intervals over the desired range which was usually from 150 to 600 feet. At each marker, the complete series of phosphor coated targets was irradiated a minimum of two times and a photographic record made of each return response. If the response was questionable, additional "shots" were made. After the entire series of targets had been tested, the procedure was repeated at the next marker. To provide information on reflection levels, a white card was irradiated at each range. These tests were performed during the day and repeated at night, mainly at Building 1000, Field 1, Eglin Air Force Base. Further testing was performed from a tower to simulate an airborne environment. Tests similar to those performed above were carried out vertically and over a variety of slant ranges. Also, targets were placed flat against the ground to obtain data as a function of effective area. In some instances, targets were suspended at various angles above white cards and irradiated indirectly to obtain signal returns reflected from the underlying card. In all measurements, the laser input power was kept constant at 485 joules.

The maximum daylight horizontal range at which a phosphor target could be identified repeatably was between 300 and 350 feet for small area targets and up to 450 feet for Target B, a green, cotton twill, field jacket. Range was observed to increase by a factor of approximately 1.25 during night measurements. This brought the maximum detection range with Target B out to between 550 and 600 feet. Since this effect was not anticipated, sensitivity measurements previously made at Isomet were repeated to obtain the cause of improved range performance at night. The

results of these measurements are given in Section 3.5.4. Maximum range was again improved when the laser reflector was changed from a dichroic end coating on the rear surface of the rear laser rod to an external reflector. The increase in range for Target 8 was from 600 feet to 850 feet and is due to a more homogeneous and probably lower divergence laser beam. Similarly, proportional range increases were observed with all targets.

3.5.3 Obscured Target and Special Measurements Results

A large number of field measurements were performed with various types and degrees of target cover. Testing was performed in New Jersey and in the early Spring with backgrounds and cover consisting of dry brush and reeds ranging in color from dirty white or gray to dark brown in color. Foliage shapes ranged from long broad leaves (palmetto) to intermediate sizes (oak and ground plants) to small, thin fir tree foliage.

Results of these measurements indicate that within certain limits, obscured phosphor targets can be stimulated to give detectable returns. In the Closter, New Jersey measurements, Target 8 was placed behind extremely dense brush and reed cover alongside a tree trunk. As shown in Figure 39, a small section of the field jacket, roughly 2 inches by 10 inches could be seen through the cover from a distance of 8 feet. As viewed along the laser line of sight, the jacket and exposed phosphor area could not be seen. There were no major obscurations along the line of sight as shown in Figure 40. When the target was irradiated from a distance of 200 feet, a phosphor presence gating signal was generated. The recorded oscilloscope trace, Figure 41, indicates the gate signal and a phosphor signal with a zero to peak value of 520 millivolts. An identical measurement, made when the target was removed, is shown in Figure 42. The combined reflection and pickup level in the signal channel (lower trace) is approximately 60 millivolts zero to peak; there is no gate signal.

A similar measurement, where there were no obscurations over a major portion of the range as shown in Figure 43, was performed at Eglin Air Force Base. Target 1 (V-21 phosphor) was placed in the limbs of a tree, Figure 44 behind cover extending about 15 feet in front of the target. In this measurement, at a 138 foot range, the target could not be seen through the aiming telescope and branches in front of the target had to be temporarily pulled out of the way while the transceiver was aligned. A gate signal was generated when the laser was fired and the phosphor return signal, shown in Figure 45, had a zero to peak

FIGURE 39. Target 8 and Target Area in Closter, N.J., photographed from 8 Feet and to the Right of the Path of Illumination.

FIGURE 40 Target Area Photographed from 35 Feet.

FIGURE 41. Return Phosphor Signal From Obscured Target 8, 200 Foot Range. Top Trace Shows Gate Signal. Signal Channel Scale: (0.2V/cm 100usec/cm)

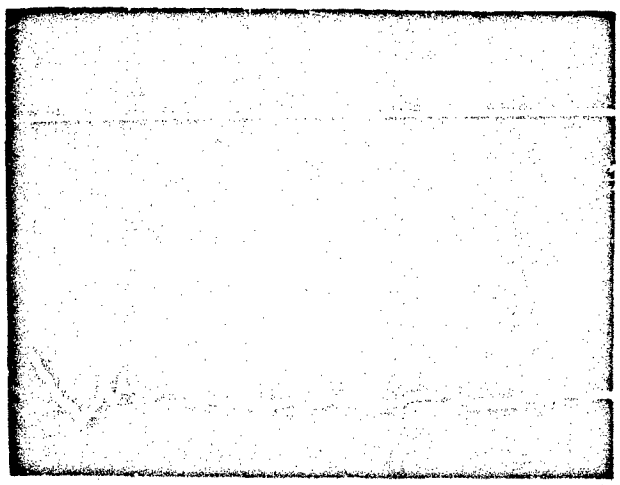

FIGURE 42. Reflection Signal From Target Area. No Phosphor Present. 200 Foot Range. Signal Channel Scale: (0.2V/cm 100usec/cm)

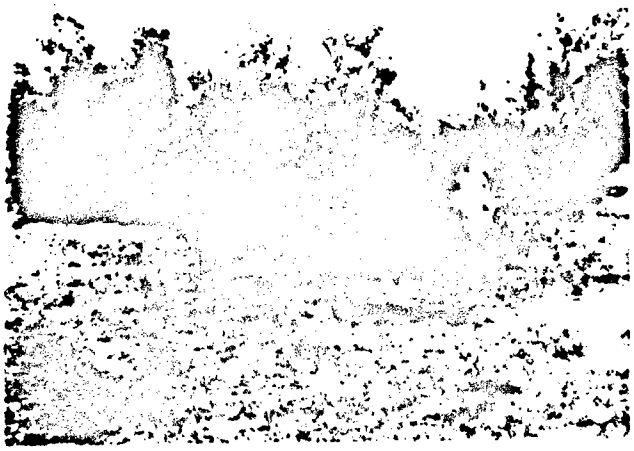

FIGURE 43. Eglin A.F.B. Target Area With Obscured Target Photographed From 35 Feet.

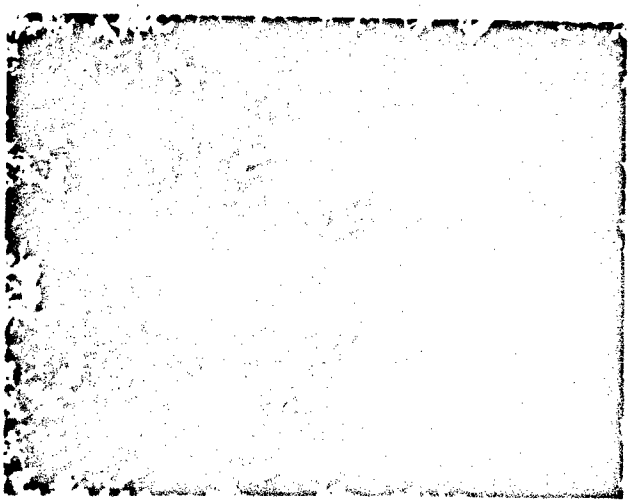

FIGURE 44. Close-Up View of Target Taken From 10 Foot Range and to Right of Actual Illuminated Path.

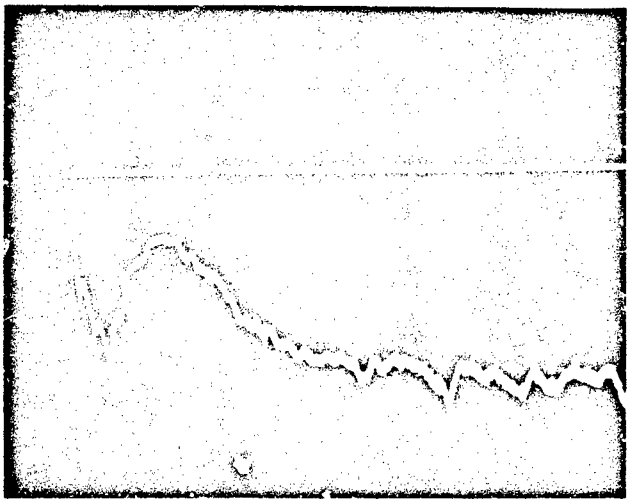

FIGURE 45 Return Pnosphor Signal From Obscured Target, 138 Foot Range. Top Trace is Gate Signal. Phosphor Signal Channel Scale (0.2V/cm 100usec/cm)

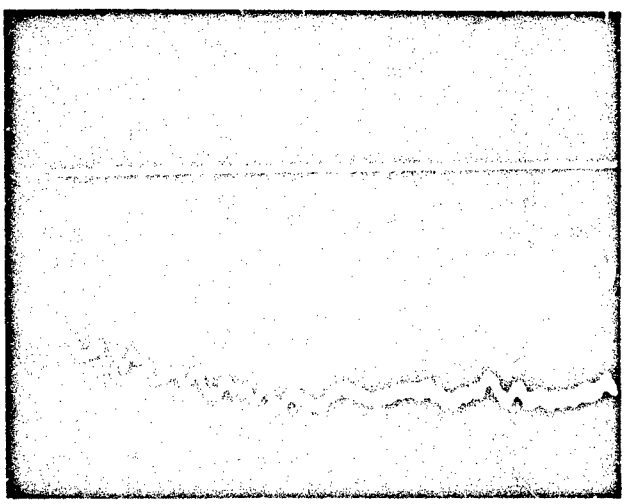

FIGURE 46. Reflection Signal From Target Area, No Phosphor Present, 138 Foot Range Signal. Signal Channel Scale: (0.2V/cm 100usec/cm)

value of approximately 440 millivolts. Another measurement made of the identical area without the target is shown in Figure 46. The background and pickup level was about 110 millivolts zero to peak. No gate signal was generated.

A series of measurements were performed with the field jacket, Target 8, at ranges of 150, 200, and 250 feet. The transceiver was located 100 feet from the edge of a wooded area. Stake markers were placed at 50 foot intervals into the woods in a straight line with the transceiver. The jacket was worn by a person who stood by designated markers while the measurements were performed. The results are tabulated in Table 11.

TABLE 11

Target 8 with Varying Degrees of Cover

Measurement No.	Range, Feet	Signal Level, Volts	Gate Signal	Comments
1	150	1.5	Yes	Subject standing. Photometer saturated.
2	150	1.5	Yes	Subject standing. Photometer saturated.
3	150	0.50	Yes	Subject standing. Solid signal
4	200	0.60	Yes	Subject standing. Solid signal
5	200	0.56	Yes	Subject standing. Solid signal
6	200	0.60	Yes	Subject standing. Solid signal
7	250	0.08	No	Subject standing.
8	250	0.14	No	Subject standing. Low level phosphor signal.

TABLE 11
(Continued)

Measurement No.	Range, Feet	Signal Level, Volts	Gate Signal	Comments
9	250	0.12	No	Subject sitting. Low level phospho signal.
10	250	0.16	No	Subject sitting, Low level phospho signal.
11	250	0.165	Yes	Subject sitting. Low level phospho signal.

At the 150 foot range, the jacket and subject were clearly visible through the aiming telescope. A large area of phosphor was irradiated by the laser and the resultant return signal saturated the photometer preamplifier. At the 200 foot mark, a tree branch was in the field of view, reducing the return signal to an averaged value of 0.360 volts. For comparison, at 200 feet, the signal level with an unobscured target 8 was large enough to saturate the preamplifier. When the range was increased to 250 feet, only the lower portion of the persons' body was observable. The upper sections of the jacket which contained the phosphor were completely blocked. Of the two measurements taken at this range with the subject standing, one indicated only background and the other a low level phosphor signal too low in level to trigger a phosphor presence gate signal. The subject then sat on the ground at the 250 foot range and three measurements were made. In this case, the phosphor dusted area of the jacket was barely discernible through the aiming telescope because of heavy brush and bush cover. In the three measurements made, low level phosphor signals were apparent but only the third irradiation produced a gating signal.

The variation in signal levels as indicated in measurements 7 and 8 of Table 11 was observed to be due to light winds which randomly changed the degree of target cover. The variation indicated above is not dramatically large but one series of measurements, which was to be performed with the transceiver only 15 feet from the edge of a wooded area, had to be discontinued because of this effect. While operation this close to background

is not anticipated in an operational flight system, these tests were performed to determine the effects of large background reflections in the presence of phosphor signals. At any range, the laser beam diameter is defined by its beam divergence angle. At close range (15 feet), the beam has not expanded greatly and for the 10 milliradian divergence experienced with the 5.75 magnification telescope, the beam is approximately 4 to 5 inches in diameter. The measurements could not be performed because densely leaved branches within thirty feet of the laser were blown back and forth along the line of sight. If the branches were in the line of sight when the laser was fired, most or all of the energy was prevented from impinging upon the target. A specific branch was identified, by means of a "metascope", as intermittently blocking the entire beam and when the leaves were removed a larger proportion of signals were obtained. Measurements were discontinued, however, because of the same situation further down the line of sight. The measurements made, however, point out the fact that best results are obtained when the laser beam is somewhat spread out. The entire beam cannot then be blocked by one or two leaves.

3.5.4 Equipment Performance in the Field

3.5.4.1 Flash Lamp Triggering

With the exceptions indicated below, the test set performed well permitting a large quantity of useful data to be accumulated. For the most part, anamolous behaviour such as the rare presence of a gating signal when the system was aimed and fired at a background, was due to a poor trigger pulse. It is possible that occasionally during triggering, if the flash lamp did not breakdown and begin conducting immediately, the trigger pulse voltage increased above normal causing an audible arc from the trigger wire to the cavity wall. In this instance, the radiation from the arc could produce a signal in the photometer preamplifier. On all occasions where an unexpected phosphor presence gating signal appeared, the measurement was rerun several times without a gating signal being generated. The arcing experienced above can be avoided by use of an in-line trigger transformer. This element generates a pulse which is internal to the circuits and the flashlamp. Unlike the situation with external trigger wire, arcing can occur only through a good deal of insulation. An in-line transformer was not used in the test set in an attempt to keep the laser discharge circuits simple and versatile.

3.5.4.2 Signal Level Variations

Occasionally, a large difference in signal level was

observed between photographs taken consecutively with the same target. This is attributable to a loss in discharge voltage across the energy storage capacitors in the laser power supply. The loss is caused by the slow discharge of the capacitors through the voltage monitoring circuit since continuous charging was not utilized in the test set. If the flash lamp is not fired within a 20 second interval after the preset charge level is attained, the voltage will have decreased enough to noticeably effect the laser output power and, therefore, the return signal level. When data of this type were observed, several additional measurements were made to establish the proper signal level.

During the course of field measurements some equipment characteristics were encountered that had not previously been observed. The least expected was the increase in operational range observed at night with tests identical to those performed during the day. At first the effect was through to be due to phosphor saturation or quenching by the sun, although laboratory tests had shown the phosphors to be linear with power levels available.

Phosphor linearity was reconfirmed at Isomet after completion of the field tests by testing a sample of the phosphor used in the field measurements with the same background intensity and incident laser power observed in the field. There was no phosphor saturation observable. Photometer detector linearity was then measured over the same range of background and laser intensities. The variation of detector output signal with and without background on a wide band diffuse reflector was found to be approximately 2.5. That is, without a solar background, the output signal was 2.5 times higher than when the background was present.

Early detector measurements did not indicate a non-linear effect in the range of signal levels encountered and it is believed that the detector bias of 45 volts then used provided a large linear range. When the bias voltage was reduced to 9 volts to improve detector S/N, the linear range of response became limited. The net effect of operating with a bright background and 9 volts detector bias is, therefore, a decrease in sensitivity of about 2.5. At night with no background illumination, the range of the system increased roughly by a factor of 1.25 as would be expected from the range equation (fourth root of 2.5). In addition, an increase in range was obtained when the laser rod reflective coating was replaced by an external reflector. The improvement is primarily due to the quality of the external reflector. The reflective coating on the rod had deteriorated over a period of time and several areas of the coating

contained pinholes. This would reduce the area over which lasing could occur. This condition became apparent when the laser beam was reflected from a large white card and viewed with a Metascope. The beam appeared to have patches of high and low intensity. Furthermore, it was found that phosphor return signal levels could be increased as much as 2 to 1 by small shifts in the laser beam position. As viewed through the aiming telescope, the position shifts required were between 1 and 2 inches on the target. When the external reflector was installed, beam uniformity improved and changes in phosphor return signal with aiming level were minimal.

Four days prior to completion of the field measurements, the photometer detector began to fail. Failure was evident from the increasingly large noise level. The detector, unit #4, was replaced by an auxiliary detector, unit #5, whose operating characteristics were close to unit #4. Unit #5 performed as well as #4, which was shown by comparison with previous field measurements. Detector #5 performed well until the last day of testing when it too exhibited the characteristic of increasing noise.

4. SYSTEM ANALYSIS

The basic concept of covert marking with an IR-IR phosphor and covert detection by an IR laser transceiver can be implemented in many ways. The maximum range and V/H characteristics of any particular system will depend primarily on that system's design goals and not on the basic laser M & D concept. One working M & D laser system has been designed and built to measure the basic variables and characteristics of this laser concept. In the following sections, this system is analyzed theoretically and compared with the results of three man-months of field measurements.

Some of the possible techniques of implementing the basic concept are also analyzed, showing the major advantages and their limitations. The theoretically predicted system characteristics based on the derived range equation have been verified.

4.1 Basic Systems Analysis

The basic system,consisting of a laser, a target and a photometer, is shown in Figure 47. The laser transmitter projects an IR beam at the marked target. An IR sensing photometer (receiver), boresighted with the laser, detects the stimulated radiation from the target. Ideally, the laser beam is physically confined to the photometer field of view. Any target illuminated by the laser can be "seen" by the receiver. The laser transmitter radiates a narrow spectral line beam centered at a wavelength λ_L. The receiver is insensitive to the laser illumination and detects only those wavelengths, λ_P, given off by the phosphor marking agent in response to stimulation by λ_L. The presence of reflectors in the field of view has not interfered with the system operation.

4.2 Flat Targets

This system analysis is for the field measurements test set. The difference between this particular analysis and a more general treatment is that the beam angle is small (less than 10 degrees). The narrow beam angle was a necessary design requirement. By building this type unit, discrete small targets were measurable at long ranges.

The intensity at the target, H_L, is measured in a plane normal to the laser beam. The ratio of the laser power, P, to the illuminated area is H_L where,

$$H_L = (P/Br^2)e^{-\alpha_1 r} \quad (\text{watts/cm}^2) \qquad (23)$$

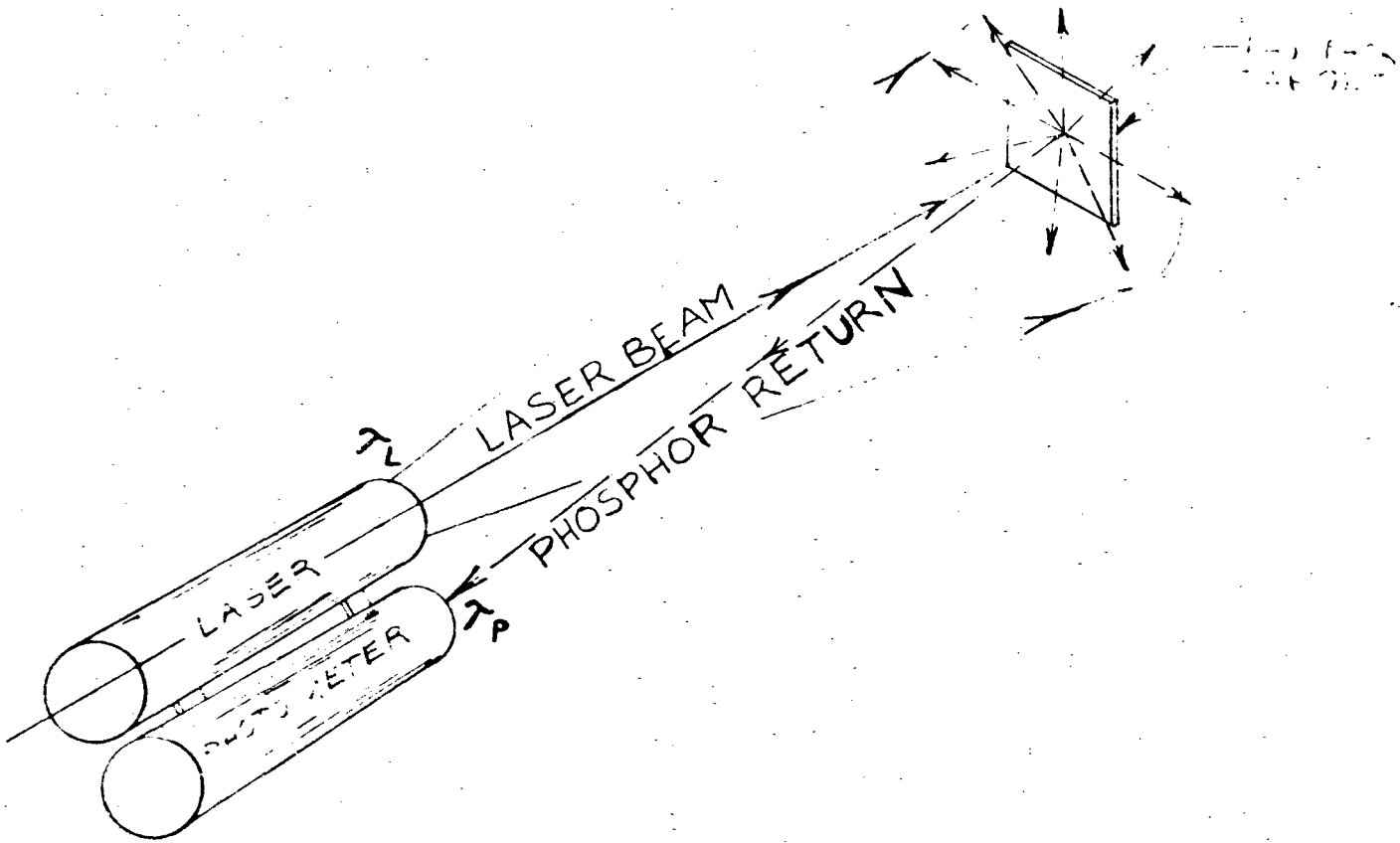

Figure 47. Basic System

where, α_1 is the absorption and scattering coefficient of the atmosphere for the laser beam (cm^{-1}),

r is the range from the target to the laser,

B is a function determined by the beam geometry (steradians).

$$B = \begin{cases} \frac{\pi \phi_L^2}{4} & \text{(for a circular beam)} \\ \phi_L \psi_L & \text{(for a rectangular beam)} \\ \phi_L^2 & \text{(for a square beam)} \end{cases} \quad (24)$$

where ϕ_L and ψ_L are angular dimensions of the laser beam (radians) as shown in Figure 48.

Consider a flat phosphor marked target at distance r from the transceiver. The brightness of the target surface at the wavelength of phosphor emission can be given as:

$$N(\text{watts/cm}^2) = 0, \text{ if no phosphor is present}$$

$$= H_r K \cos\theta, \text{ if the laser beam impinges on a proper phosphor} \quad (25)$$

where K is the radiant efficiency of the phosphor surface, θ is the angle between a normal to the phosphor plane and the laser beam (radians).

The power density at the photometer aperture, H_r, determines the signal level, and for a given photometer, the signal to noise ratio. The return signal is given by

$$H_r = \frac{N \cos\theta A_I}{\pi r^2} e^{-\alpha_2 r} \quad (26)$$

where α_2 equals the absorption and scattering coefficient of the atmosphere at the phosphor wavelength and A_I is the illuminated area of the target as given by,

$$A_I = A_t, \text{ if full target area is illuminated}$$

$$= Br^2/\cos\epsilon, \text{ if target area is larger than beam dimensions.} \quad (27)$$

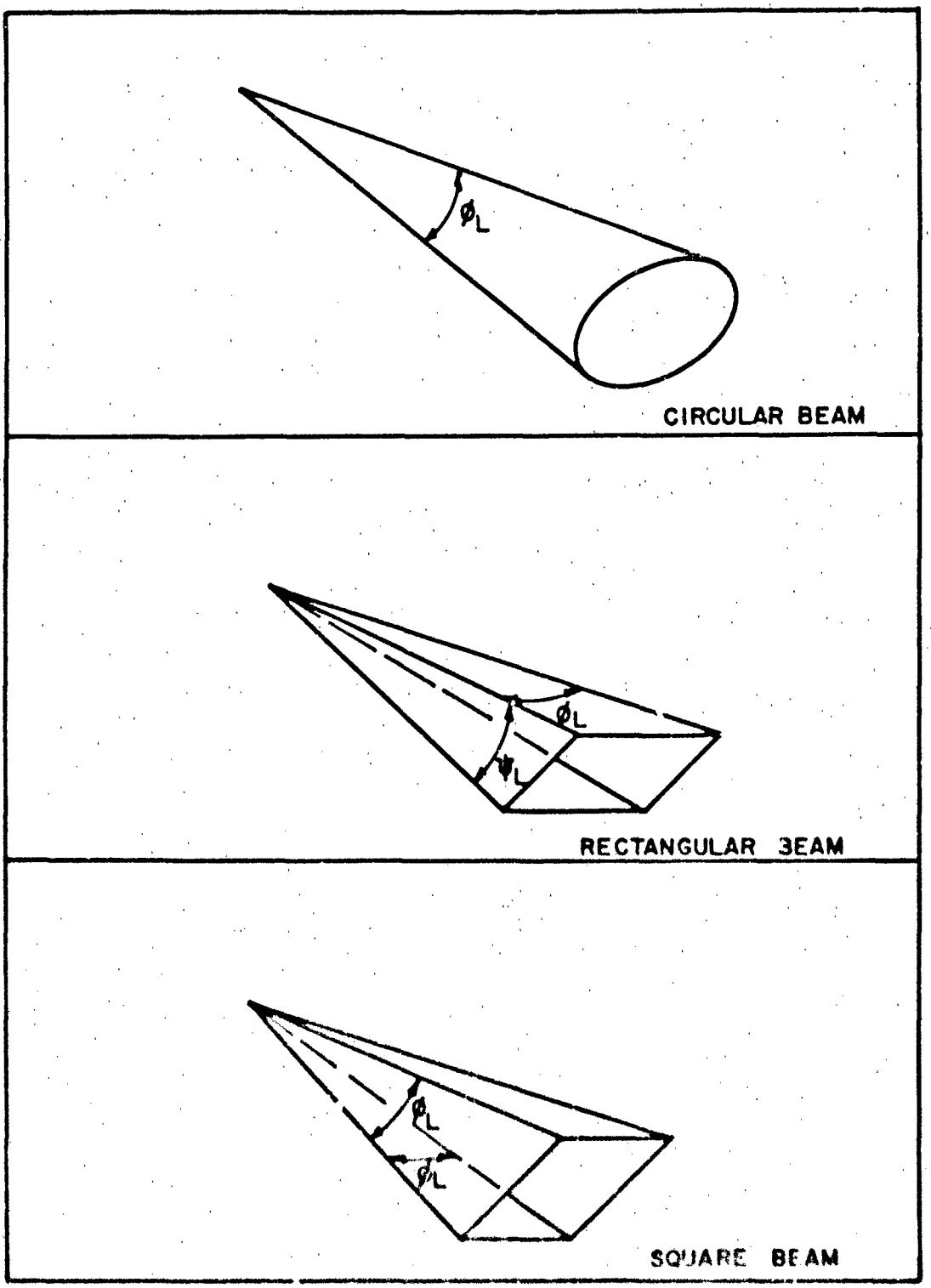

BEAM GEOMETRIES FIGURE 48

(This page is Confidential)

Where A_t is the actual target area.

The first case will be referred to as the small target condition, the second as the large target condition.

Combining equations (23) through (25) yields the power density at the receiver for a flat target,

$$H_r = \frac{PK \cos^2 \theta A_I e^{-(\alpha_1 + \alpha_2)r}}{B \pi r^4} \quad (\text{watts/cm}^2) \tag{28}$$

The signal to noise ratio (S/N) at the receiver is the ratio of the signal density to the noise equivalent power density (NEPD) of the photometer. The NEPD is defined as the equivalent amount of light signal density at the appropriate wavelength, required to cause the photometer to generate a signal voltage equal to its output noise voltage. The S/N ratio is, therefore,

$$S/N = H_r/(NEPD) \tag{29}$$

Besides the inherent photometer noise which determines the NEPD, there are several other potential sources of false signals and of noise which could interfere with proper system operation. The sources of false signals would be natural phosphors in the target area, bright reflections of the laser beam which are not completely rejected by photometer filters, reflection of radiation which is emitted by the laser system in the spectral region detected by the photometer, fast variations in the intensity at λ_p in the field of view of a scanning photometer and bright flashing light sources in the field of view. External noise would be due to the random distribution of scattered solar photons.

The range equation for the test set can be derived by combining equations (28) and (29),

$$r = \left[\frac{4PK \cos^2 \theta A_I}{(S/N)\pi^2 \phi_L^2 (NEPD)} \right]^{1/4} \tag{30}$$

where the effect of $(\alpha_1 + \alpha_2)r$ is negligible and is equated to zero for the ranges used in field measurements.

The relationship between the NEPD, D* and the photometer

dimensions, which were part of the original range equation is verified in the section of this report dealing with the photometer. The range equation is experimentally verified, therefore, when equation (28) is verified.

The photometer signal voltage, V_s, resulting from an IR power density, H_r, at the appropriate wavelengtn is determined by the responsivity $R(\lambda_p)$, a constant for a given photometer,

$$V_s = H_r R(\lambda_p) \text{ (volts)} \tag{31}$$

By using the equations derived above, the anticipated signal for a given flat target can be computed. These relationships have been used in the analysis of the field test data.

4.3 Shaped Targets

The signal return from the targets with complex shape can be predicted on the basis of the flat target derivations. Several non-flat targets were measured in this program; a sphere, a pyramid, a field cap and a field jacket. The general equation for any target shape and the two equations for the geometrical shapes are derived below.

The surface of any object may be divided into small differential flat areas. The brightness of each elemental area is essentially given in equation (25) as

$$N = \begin{cases} H_L \cos\Theta & \text{for } -\pi/2 \leq \theta \leq \pi/2 \\ 0 & \text{for } \pi/2 \leq \theta \leq \pi/2 \end{cases} \tag{32}$$

where Θ is the angle between a normal to the elemental area and integral

$$P_r = \int_S N(\Theta) \cos\Theta \, dA \tag{33}$$

4.3.1 Spherical Target

Consider now a spherical target such as shown in Figure 49. The signal will be derived for a sphere which is entirely within the laser beam. The elemental area, shaded in Figure 49, is given by

$$dA = 2\pi r_s^2 \sin\Theta d\Theta \tag{34}$$

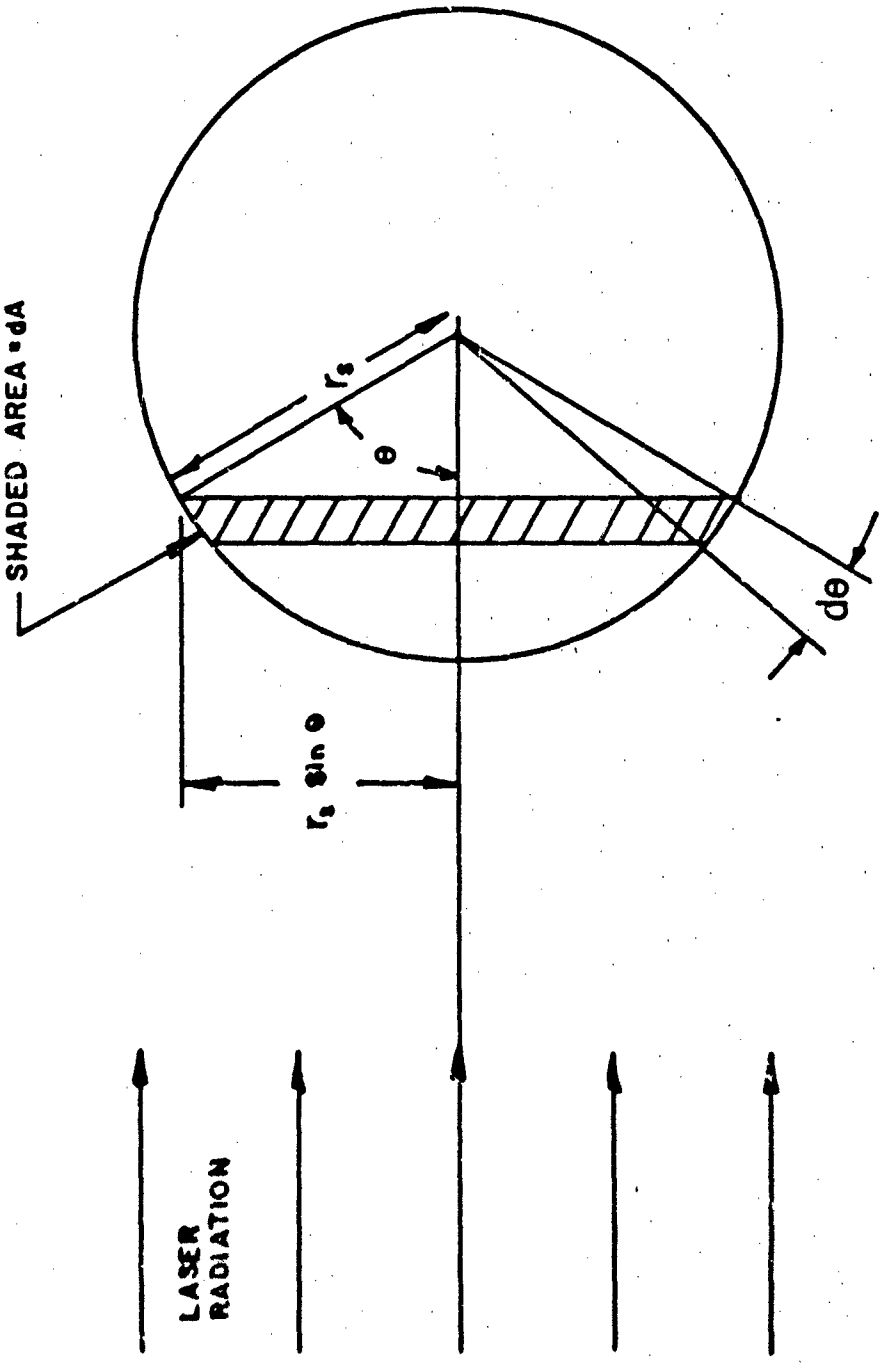

SPHERICAL TARGET GEOMETRY

FIGURE 49

where r_s is the sphere radius. Substituting equations (32) and (34) into equation (33) yields the value of P_r for a sphere.

$$P_r = \int_0^{\pi/2} NdA \cos\theta \tag{35}$$

$$= \int_0^{\pi/2} (H_L K \cos\theta)\ (2\pi r_s^2 \sin\theta) \cos\theta d\theta$$

$$= 2H_L K \pi r_s^2 \int_0^{\pi/2} \sin\theta \cos^2\theta d\theta$$

$$= \frac{2H_L K \pi r_s^2}{3} \tag{36}$$

As a basis of comparison, consider a flat disc of radius r_s oriented so that $\theta = 0$. The return from this target is,

$$P_{(disc)} = H_L K \pi r_s^2 \tag{37}$$

The return signal for a sphere is, therefore, 2/3 of the return from a disc of equal radius. When a flat disc of equal radius is tilted so that θ is greater than thirty five degrees, the sphere will give the stronger return. The amount of phosphor required to coat the sphere is only twice that required for the disc (both sides coated).

4.3.2 Pyramid Target

Consider the equilateral pyramid shown in Figure 50. The radiation incident on the side of the pyramid facing the laser is given by:

$$H_I = H_L \cos\theta \tag{38}$$

The return power is given by

$$P_R = (A \cos\theta)\ H_I K$$

$$= H_L \frac{l \times h}{2} K \cos^2\theta \tag{39}$$

Since $\theta = 60^\circ$, $\cos\theta = \frac{\sqrt{1}}{2}$ and $P_R = H_L K \left(\frac{3\sqrt{1}}{16}\right) l^2$ (40)

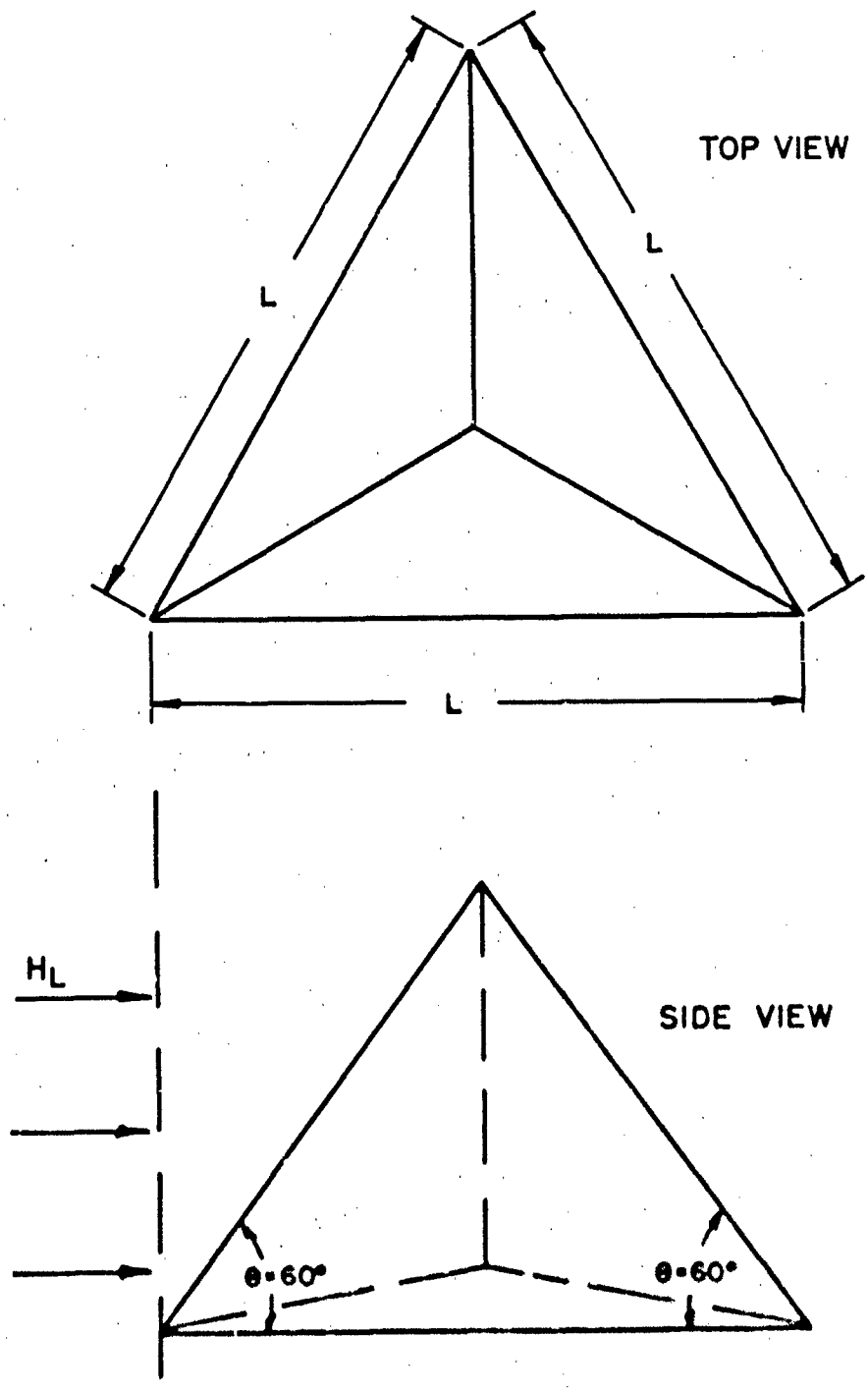

PYRAMID TARGET GEOMETRY

FIGURE 50

(This page is Confidential)

4.4 Interrelation of Variables

The signal return voltage is determined by several system parameters. The derivations given in the previous sections produced a set of equations from which the output voltage of the receiver, for each range and target combination, was computed. Over the ranges tested, the atmospheric absorption at both the laser and phosphor wavelengths was assumed negligible. The coefficient, $(\alpha_1 + \alpha_2)$, was equated to zero in all calculations. Since none of the results showed any significant decrease in system efficiency with range, the assumption was reasonable. Data in the literature indicate that atmospheric scattering and attenuation at both the laser and phosphor wavelengths are quite low, as discussed in Section 3.3.

The relationship between the system parameters given in equation (28) is assumed to be correct. The ratio of the observed voltage to the calculated voltage for each test point has been used to verify the derived range equation. If the ratio is equal to unity and does not vary with range, the range equation is valid. If the ratio is independent of range but not equal to unity, the decrease in return signal with the fourth power of "r" is verified. If the ratio is independent of target area, the predicted influence of target area on range is verified.

4.5 Data Analysis

The primary purpose of the field measurements was to verify the derived range equation and to measure the influence of various natural backgrounds on the system performance. The raw data, taken in the field, consisted of photographs, labeled with the specific test conditions, of the oscilloscope traces of the signal and gating channels of the receiver electronics. Each individual data point corresponds to such a photograph.

An example of a typical data point photograph and description is shown in Figure 28 of Section 3.5.

The data can be divided into two basic sets. The first consists of straightforward measurements of returns from specific targets at known distances. The second set is comprised of measurements of the returns from natural backgrounds of all types and from partially and completely concealed targets. There were no natural targets whose characteristic signal returns could be confused with the phosphor return.

Measurements with concealed targets showed that a phosphor target, with no phosphor directly in the field of view, can be detected. The mechanism consists essentially of reflection of the laser beam from the target surroundings onto the target phosphor. The characteristic target emission was then reflected from the immediate surroundings and detected by the photometer and processing electronics.

Several photographs of semi-obscured targets are shown, in color, in the set of slides provided as part of the data from this program. Black and white photographs of concealed targets are presented in Figures 39 through 46. The laser M & D field measurement test set was able to detect the presence of the marked field jacket concealed partially, or completely, in thick brush and heavily wooded areas. Since the military field jacket blended well with most surroundings and because the phosphor was a neutral color, the concealed, marked jacket was occasionally not detectable by the naked eye, thus proving the ability of the system to aid in the detection of concealed personnel.

The set of data taken with well defined targets at known distances and angles, has proven the range equation and verified the system's basic feasibility.

4.5.1 Data Reduction

The raw data is a set of oscilloscope photographs, one for each datum point. The photo number, test description, signal voltage, range and comments were tabulated for all raw data. Each oscilloscope photograph was then examined carefully. The yield of useful data from the total number of possibly useful points for data reduction is shown in Table 12. For cases where the signal to noise level was high enough to yield a gate but too low to allow for an accurate measurement of signal voltage, only the presence of the gate was used as data. The following sections are step by step descriptions of the various processes used in the handling and evaluation of the data.

4.5.2 Target Definition and Restrictions

The targets, numbered one through twelve, were distinguished by their size, shape, substrate and phosphor coating (both type and density). All useful data were taken at ranges at which the target area was completely within the laser illuminated area. Thus, only the first part of equation (27) applied to the data analysis. The targets are defined in Table 13.

TABLE 12 - YIELD OF USEFUL DATA

SET I - GROUND DATA

Date	No. of Relevent Photos	Yield	Rejected Photos	
			Photo No.	Reason
4/30	11	11/11	--	--
5/1	3	2/3	6	Signal level @ 300' Unintelligible
5/3	3	1/3	23, 24	Saturated Signal
5/4	4	0/4	1-3	190' Range deleted Used data from 200'
			4	180' Range deleted Used data from 200'
5/5	None (all background)	--	--	--
5/6	3	3/3	--	--
5/7	28	26/28	1, 2	System realigned after
5/8	59	57/59	1, 2	System realigned after
5/10	69	59/69	80	550' Too small an increment
			15, 16, 38, 39, 40, 48, 49, 50	Saturated Signal
			66, 67	Signal level unintelligible

TABLE 12 - YIELD OF USEFUL DATA

SET II - TOWER DATA

Date	No. of Relevent Photos	Yield	Rejected Photos	
			Photo No.	Reason
5/11	None	--	--	--
5/12	40	0/40	All	Various targets at 1 range, not same conditions as 5/18
5/13	None	--	--	--
5/14	None	--	All	Generator problems
5/18	90	53/90	16, 24, 33, 43, 51, 55, 64, 104, 105, 111, 113	Signal trace Off scale
			71, 82, 83 86, 87, 88, 95, 96, 100	Saturated Return
			14, 15, 31, 32, 34, 60, 61, 89, 90	Signal level unintelligible
			68, 69, 70 71, 72	Scope scale factor off
			25	Low voltage
			04, 85	Only 1 data pt. for T2, horiz. night

TABLE 13

M & D FIELD TEST TARGETS

Target #	Area (ft^2)	Shape	Substrate	Coating
1.	0.376	Flat, 6-3/8" x 8-1/2"	Smooth masonite	Batch 2 Control card
2.	0.108	Flat square 100 cm^2	Smooth masonite	ZP-7B-2
3.	0.108	Flat square 100 cm^2	*Alzak	ZP-7B-2
4.	0.108	Flat square 100 cm^2	Matte masonite	ZP-7B-2
5.	0.108	Flat square 100 cm^2	White krylon on masonite	ZP-7B-2
6.	0.108	Flat square 100 cm^2	Clear krylon on masonite	ZP-7B-2
7.	0.293	9" diameter sphere	White krylon on plastic ball	ZP-7B-2
8.	2.08	Back of field jacket	Twill material	ZP-7B-2
9.	0.314	Field cap	Twill material	ZP-7B-2
10.	0.144	Equilateral pyramid (Side 1)	Smooth masonite	ZP-7B-2 one thin layer
11.	0.144	Equilateral pyramid (Side 2)	Smooth masonite	ZP-7B-2 two thin layers
12.	0.144	Equilateral pyramid (Side 3)	Smooth masonite	ZP-7B-2 three thin layers

* Electro-polished aluminum

Target numbers 10 through 12 are the three sides of the pyramid. The areas given in Table 13 are computed as the effective areas. For the flat targets the effective surface area is equal to the physical area. For shaped targets, the effective area is determined by equations (36) and (40) above.

4.5.3 Definition of System Constants

The computations made of the theoretically predicted signal returns in volts, were made using the values of system parameters listed in Table 14.

TABLE 14

System Parameters

Peak Power = 965 watts
$R = 4.59 \times 10^5$ volts/watt/ft^2
K = 0.466%, Batch 2 control
K = 0.625%, ZP-7B-2
$\theta_L = 7.63 \times 10^{-3}$ radians (circular beam)
$(\alpha_1 + \alpha_2) = 0$, negligible for ranges tested

Based on these values, (their measurement is described in this report) the signal voltage was computed and compared to the observed return voltage.

4.5.4 Signal Voltage Calculations

The calculated signal voltage for each range and target combination used in the field tests is presented in Table 15. These values were corrected for the angle θ, when used in the tower tests. The angle was determined by measurement of the slant range and the tower height.

4.5.5 Comparison of the Observed to the Calculated Signal Voltage

The experimental field data was broken down by target, range, angle of view, time and location. All data points of common conditions were averaged to form one data value, $\bar{V}_{obs}$, for that test condition. This data is presented in Table 16. The observed voltage, $\bar{V}_{obs}$, was first plotted as a function of calculated voltage, to establish the basic relation between the two

TABLE 15

CALCULATED SIGNAL VOLTAGE

Target	Range (feet)	150	200	250	300	350	400
1		10.7	3.37	1.38	0.664	0.362	0.211
2		4.11	1.30	0.532	0.256	0.139	--
3							
4							
5							
6							
7		11.2	3.53	1.45	0.694	0.378	--
8		--	--	10.3	4.93	2.68	1.56
9		12.0	3.77	1.55	0.744	--	--
10		5.49	1.73	0.71	0.341	--	--
11		1.73	0.71	0.341	--	--	--
12		1.73	0.71	0.341	--	--	--

Target	Range (feet)	450	500	600	685	750	800
8		.973	.641	.312	0.182	0.126	.098

(This page is Confidential)

TABLE 16

AVERAGE AND STANDARD DEVIATION
FROM AVERAGE OF TARGET SIGNAL LEVELS

G - Denotes Ground Tests
T - Denotes Tower Tests

$$\bar{V}_{OBS} \equiv \sum_{i=1}^{n} \frac{V_{obs_i}}{n}$$

$$\sigma_{\bar{V}_{OBS}} \equiv \left(\sum_{i=1}^{n} (V_{obs_i} - \bar{V}_{OBS})^2 / n-1 \right)^{1/2}$$

TARGET NO.	LOCATION	DATE	PHOTO	RANGE	V_{OBS}	$\bar{V}_{OBS}$	$\sigma_{V_{OBS}}$	n
1	G-Day	5/10	1	150 ft.	.850	.850	0	2
		5/10	2	150	.850	-	-	-
		5/3	1	200	.320	.305	.0257	13
		5/1	3	200	.320	-	-	-
		5/1	5	200	.290	-	-	-
		5/6	15	200	.280	-	-	-
		5/6	16	200	.260	-	-	-
		5/6	17	200	.320	-	-	-
		5/7	3	200	.300	-	-	-
		5/7	4	200	.300	-	-	-
		5/7	5	200	.260	-	-	-
		5/7	6	200	.320	-	-	-
		4/30	1	200	.320	-	-	-
		4/30	2	200	.330	-	-	-
		4/30	3	200	.340	-	-	-
		4/30	4	250	.180	.183	.0126	4
		4/30	5	250	.170	-	-	-
		5/8	16	250	.200	-	-	-
		5/8	17	250	.180	-	-	-
		5/8	50	300	.090	.112	.0211	9
		5/8	51	300	.160	-	-	-
		5/8	52	300	.120	-	-	-
		4/30	6	300	.090	-	-	-
		4/30	7	300	.110	-	-	-
		4/30	8	300	.110	-	-	-
		4/30	9	300	.100	-	-	-
		4/30	10	300	.110	-	-	-
		4/30	11	300	.120	-	-	-
1	G-Night	5/10	32	150	.900	.975	.106	2
		5/10	33	150	1.150	-	-	-
		5/10	44	200	.500	.500	0	2
		5/10	45	200	.500	-	-	-

TABLE 16
(Con't.)

TARGET NO.	LOCATION	DATE	PHOTO	RANGE	V_{OBS}	$\overline{V}_{OBS}$	σV_{OBS}	n
1	G-Night	5/10	53	250 ft.	.240	.210	.0425	2
		5/10	54	250	.180	-	-	-
		5/10	60	300	.150	.165	.031	4
		5/10	61	300	.210	-	-	-
		5/10	62	300	.140	-	-	-
		5/10	63	300	.160	-	-	-
2	G-Day	5/10	30	150	.460	.470	.014	2
		5/10	31	150	.480	-	-	-
		5/7	9	200	.160	.180	.0283	5
		5/7	10	200	.140	-	-	-
		5/7	11	200	.200	-	-	-
		5/7	12	200	.200	-	-	-
		5/7	13	200	.200	-	-	-
		5/8	24	250	.110	.105	.0071	2
		5/8	25	250	.100	-	-	-
2	G-Night	5/10	36	150	.600	.600	0	2
		5/10	37	150	.600	-	-	-
		5/10	41	200	.300	.300	0	3
		5/10	42	200	.300	-	-	-
		5/10	43	200	.300	-	-	-
		5/10	55	250	.140	.147	.0116	3
		5/10	56	250	.140	-	-	-
		5/10	57	250	.160	-	-	-
3	G-Day	5/10	5	150	.560	.560	0	2
		5/10	6	150	.560	-	-	-
		5/7	14	200	.280	.270	.0141	2
		5/7	15	200	.260	-	-	-
		5/8	26	250	.180	.157	.0322	3
		5/8	27	250	.170	-	-	-
		5/8	28	250	.120	-	-	-
		5/8	55	300	.140	.145	.0071	2
		5/8	56	300	.150	-	-	-
4	G-Day	5/10	7	150 ft.	.480	.480	0	2
		5/10	8	150	.480	-	-	-
		5/7	16	200	.180	.192	.0179	5
		5/7	17	200	.180	-	-	-
		5/7	18	200	.200	-	-	-
		5/7	19	200	.180	-	-	-
		5/7	20	200	.220	-	-	-
		5/8	29	250	.120	.127	.0116	3

TABLE 16
(Con't.)

TARGET NO.	LOCATION	DATE	PHOTO	RANGE	V_{OBS}	$\overline{V}_{OBS}$	$\sigma_{V_{OBS}}$	n
4	G-Day	5/8	31	250 ft.	.120	-	-	-
5	G-Day	5/10	9	150	.560	.570	.0141	2
		5/10	10	150	.580	-	-	-
		5/7	21	200	.240	.240	0	2
		5/7	22	200	.240	-	-	-
		5/8	32	250	.180	.170	.010	3
		5/8	33	250	.160	-	-	-
		5/8	34	250	.170	-	-	-
		5/8	57	300	.100	.100	0	2
		5/8	58	300	.100	-	-	-
6	G-Day	5/10	11	150	.380	.380	0	2
		5/10	12	150	.380	-	-	-
		5/7	23	200	.190	.173	.0163	4
		5/7	24	200	.160	-	-	-
		5/7	25	200	.180	-	-	-
		5/7	26	200	.160	-	-	-
		5/8	35	250	.100	.108	.0077	3
		5/8	36	250	.110	-	-	-
		5/8	37	250	.115	-	-	-
7	G-Day	5/10	13	150	.675	.688	.0177	2
		5/10	14	150	.700	-	-	-
		5/7	27	200	.240	.250	.0141	2
		5/7	28	200	.260	-	-	-
		5/8	38	250	.130	.153	.0318	2
		5/8	39	250	.175	-	-	-
8	G-Day	5/7	29	200	1.400	1.425	.0354	2
		5/7	30	200	1.450	-	-	-
		5/8	40	250	1.075	1.088	.0318	2
		5/8	41	250	1.100	-	-	-
		5/8	59	300	.520	.505	.0212	2
		5/8	60	300	.490	-	-	-
		5/8	61	350	.400	.395	.0212	2
		5/8	62	350	.390	-	-	-
		5/8	63	400	.380	.333	.0416	3
		5/8	64	400	.300	-	-	-
		5/8	65	400	.320	-	-	-
		5/8	66	450	.240	.226	.0134	5

TABLE 16
(Con't.)

TARGET NO.	LOCATION	DATE	PHOTO	RANGE	V_{OBS}	$\overline{V}_{OBS}$	σV_{OBS}	n
8	G-Day	5/8	67	450 ft.	.240	-	-	-
		5/8	68	450	.210	-	-	-
		5/8	69	450	.220	-	-	-
		5/8	70	450	.220	-	-	-
8	G-Night	5/10	58	250	1.050	1.025	.0354	2
		5/10	59	250	1.000	-	-	-
		5/10	68	300	.750	.730	.0283	2
		5/10	69	300	.710	-	-	-
		5/10	70	400	.260	.245	.0212	2
		5/10	71	400	.230	-	-	-
		5/10	72	450	.220	.220	.0082	4
		5/10	73	450	.220	-	-	-
		5/10	74	450	.210	-	-	-
		5/10	75	450	.230	-	-	-
		5/10	76	500	.120	.130	.0082	4
		5/10	77	500	.140	-	-	-
		5/10	78	500	.130	-	-	-
		5/10	79	500	.130	-	-	-
		5/10	81	600	.100	.120	.0245	4
		5/10	82	600	.130	-	-	-
		5/10	83	600	.150	-	-	-
		5/10	84	600	.100	-	-	-
9	G-Day	5/10	17	150	.630	.715	.120	2
		5/10	18	150	.800	-	-	-
		5/8	3	200	.290	.265	.0354	2
		5/8	4	200	.240	-	-	-
		5/8	42	250	.160	.155	.0071	2
		5/8	43	250	.150	-	-	-
10 Side 1	G-Day	5/10	19	150	.310	.315	.0071	2
		5/10	20	150	.320	-	-	-
		5/8	5	200	.120	.130	.0141	2
		5/8	6	200	.140	-	-	-
		5/8	44	250	.100	.090	.0141	2
		5/8	45	250	.080	-	-	-
Side 2	G-Day	5/10	21	150	.500	.490	.0141	2
		5/10	22	150	.480	-	-	-
		5/8	7	200	.200	.180	.0173	3

TABLE 16
(Con't.)

TARGET NO.	LOCATION	DATE	PHOTO	RANGE	V_{OBS}	$\overline{V}_{OBS}$	σV_{OBS}	n
10 Side 2	G-Day	5/8	8	200 ft.	.170	-	-	-
		5/8	9	200	.170	-	-	-
		5/8	46	250	.120	.120	0	2
		5/8	47	250	.120	-	-	-
Side 3	G-Day	5/10	23	150	.670	.665	.0071	2
		5/10	24	150	.660	-	-	-
		5/8	10	200	.220	.237	.0153	3
		5/8	11	200	.250	-	-	-
		5/8	12	200	.240	-	-	-
		5/8	48	250	.170	.160	.0141	2
		5/8	49	250	.150	-	-	-
1	T-Day	5/18	73	150	*.450	.450	.050	3
		5/18	74	.50	*.500	-	-	-
		5/18	75	150	*.400	-	-	-
		5/18	59	200	*.310	.310	-	1
		5/18	41	200	1.075	1.088	.0177	2
		5/18	42	200	1.100	-	-	-
		5/18	10	250	.925	.900	.0354	2
		5/18	11	250	.875	-	-	-
		5/18	20	300	.440	.470	.0424	2
		5/18	21	300	.500	-	-	-
		5/18	35	350	.350	.387	.0473	3
		5/18	36	350	.370	-	-	-
		5/18	37	350	.440	-	-	-
1	T-Night	5/18	101	200	1.625	1.625	-	1
		5/18	102	300	.400	.390	.0141	2
		5/18	103	300	.380	-	-	-
2	T-Day	5/18	76	150	*.280	.195	.0684	4
		5/18	77	150	*.140	-	-	-
		5/18	78	150	*.140	-	-	-
		5/18	79	150	*.220	-	-	-
		5/18	65	150	1.980	1.767	.153	3
		5/18	66	150	1.600	-	-	-
		5/18	67	150	1.800	-	-	-
		5/18	39	200	1.000	1.000	0	2
		5/18	40	200	1.000	-	-	-

* Target Horizontal

TABLE 16
(Con't.)

TARGET NO.	LOCATION	DATE	PHOTO	RANGE	V_{OBS}	$\overline{V}_{OBS}$	$\sigma_{V_{OBS}}$	n
2	T-Day	5/18	56	200	*.140	.167	.0462	3
		5/18	57	200	*.220	-	-	-
		5/18	58	200	*.140	-	-	-
		5/18	17	250	.440	.470	.0424	2
		5/18	18	250	.500	-	-	-
		5/18	22	300	.380	.380	0	2
		5/18	23	300	.380	-	-	-
4	T-Night	5/18	98	200	.780	.780	0	2
		5/18	99	200	.780	-	-	-
		5/18	97	250	.350	.350	-	1
9	T-Day	5/18	44	200	1.400	1.375	.0354	2
		5/18	45	200	1.350	-	-	-
		5/18	12	250	.800	.750	.0707	2
		5/18	13	250	.700	-	-	-
		5/18	26	300	.480	.480	-	1
8	T-Day	5/18	48	500	.360	.350	.0375	3
		5/18	49	500	.320	-	-	-
		5/18	50	500	.370	-	-	-
		5/18	53	685	.360	.300	.060	2
		5/18	54	685	.240	-	-	-
8	T-Night	5/18	110	750	.160	.155	.0771	2
		5/18	112	750	.150	-	-	-
		5/18	115	800	.200	.140	.049	4
		5/18	116	800	.160	-	-	-
		5/18	117	800	.100	-	-	-
		5/18	118	800	.100	-	-	-
		5/18	114	850	.120	.120	-	1

* Target Horizontal

values. Figure 51 is the graph of all valid data points for the set encompassing all daytime, ground targets. Similar plots were obtained for the other data sets. The best fit curve through these data, when compared to Figure 27, is nearly identical to the linear curve of V_{out} vs V_{in} for the photometer preamplifier. If preamplifier saturation is taken into account, the observed return is directly proportional to the values calculated. Each point on Figure 51 represents an average value for one target, at one range. Since the laser output was appreciably different in the tower tests, only pretower data are presented in this Figure. It is important to note that there is a bias at $V_{calc} = 0$, for the best fit curve.

Individual plots of $\bar{V}_{obs}$ vs V_{calc} are given in Figures 52 through 58. The values of the intercept of each line for each target was determined to be due to a bulk effect caused by small nonfiltered reflections and electrical pickup. It is to be noted that this influence was only significant for the small values of $\bar{V}_{obs}$.

4.5.6 Comparison of Observed to Calculated Signal as a Function of Range

The ratio of the observed to the calculated voltage should be independent of range and target area for all targets having identical phosphor coatings. If the calculations were exact in predicting the returns, the ratio of the voltages would always equal unity. It was known that the laser output was several times stronger during the tower tests. Since P_L was measured in the tower, the voltage ratio for pre-tower tests would be lower than the expected value of unity.

The observed voltages were decreased by the bias values, observed in Figures 52 through 58. The corrected voltages divided by the calculated values are plotted as a function of range in Figures 59 through 65.

Comparison of the bulk data to the predicted lines of zero slope shows that the observed data did indeed follow the predicted range equations. The values of the intercepts of the $\bar{V}_{obs}/V_{calc}$ axes did differ between targets and between day and night. These differences are discussed below.

4.5.7 Variation in Signal Return with Target Material

The returns from all targets were compared on the basis

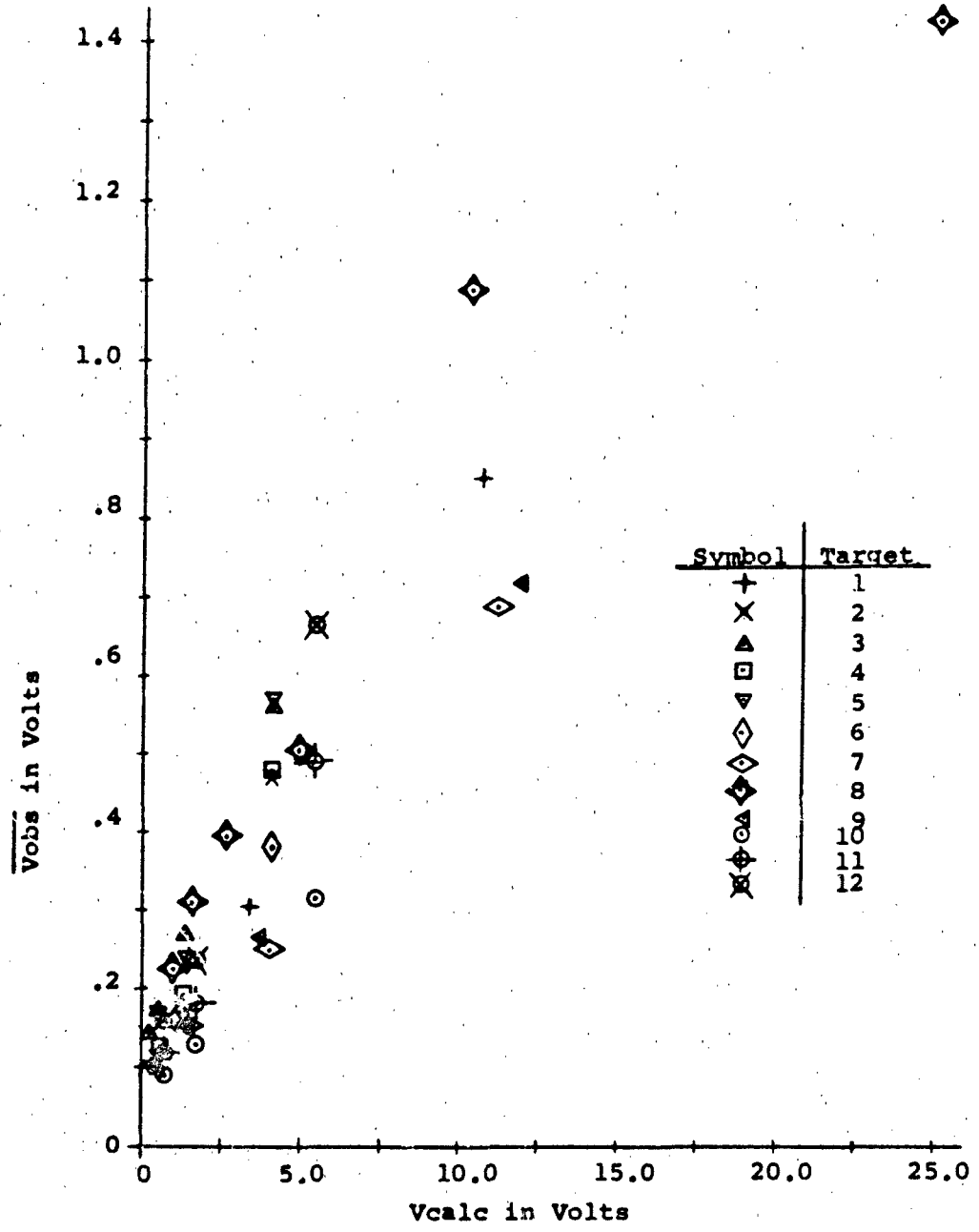

Figure 51. $\overline{\text{Vobs}}$ versus Vcalc for Daytime, Ground Targets.

(This page is Confidential)

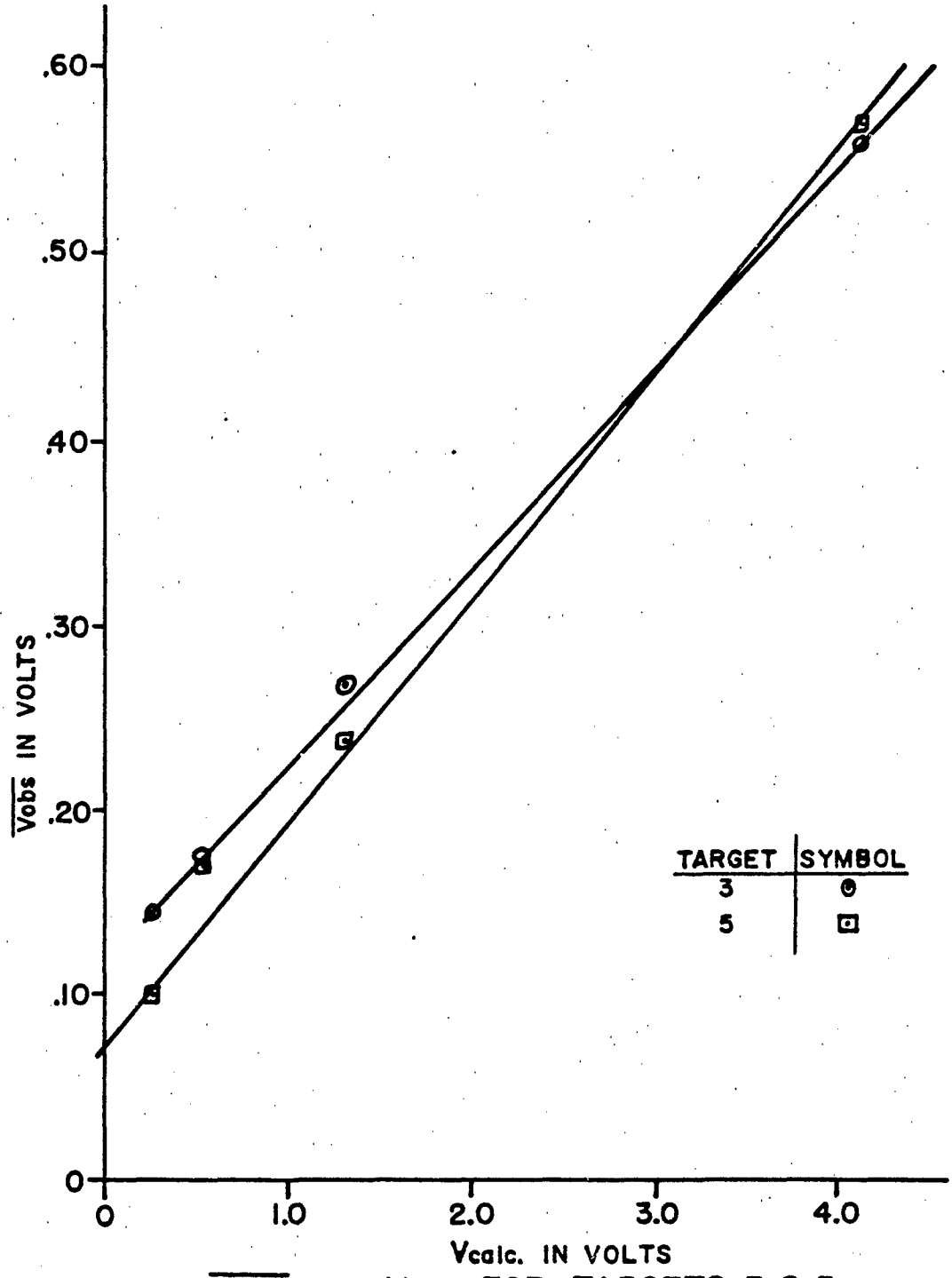

$\overline{V_{obs}}$ vs V_{calc} FOR TARGETS 3 & 5

FIGURE 52

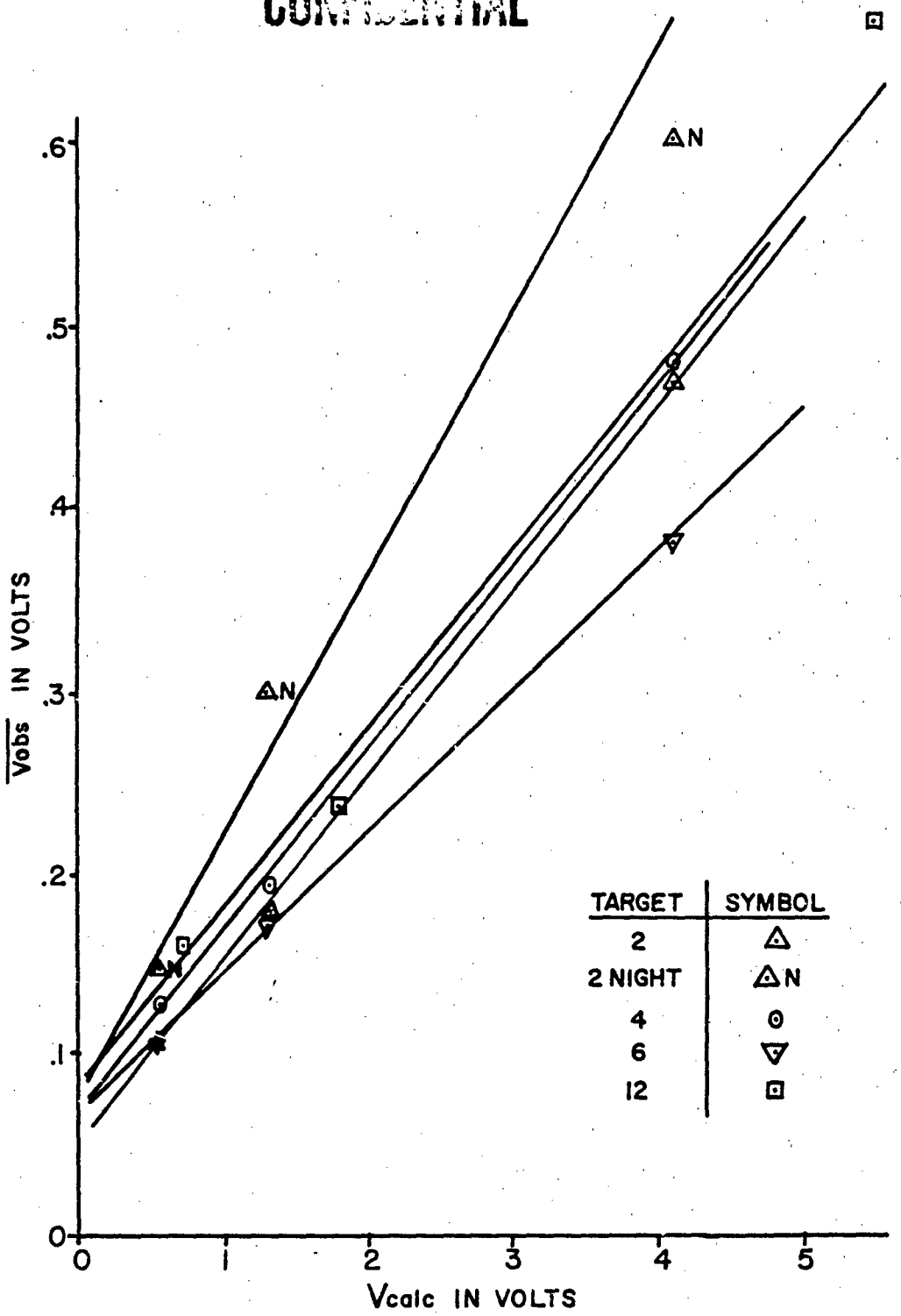

$\overline{V_{obc}}$ vs Vcalc FOR TARGETS 2,4,6,& 12

FIGURE 53

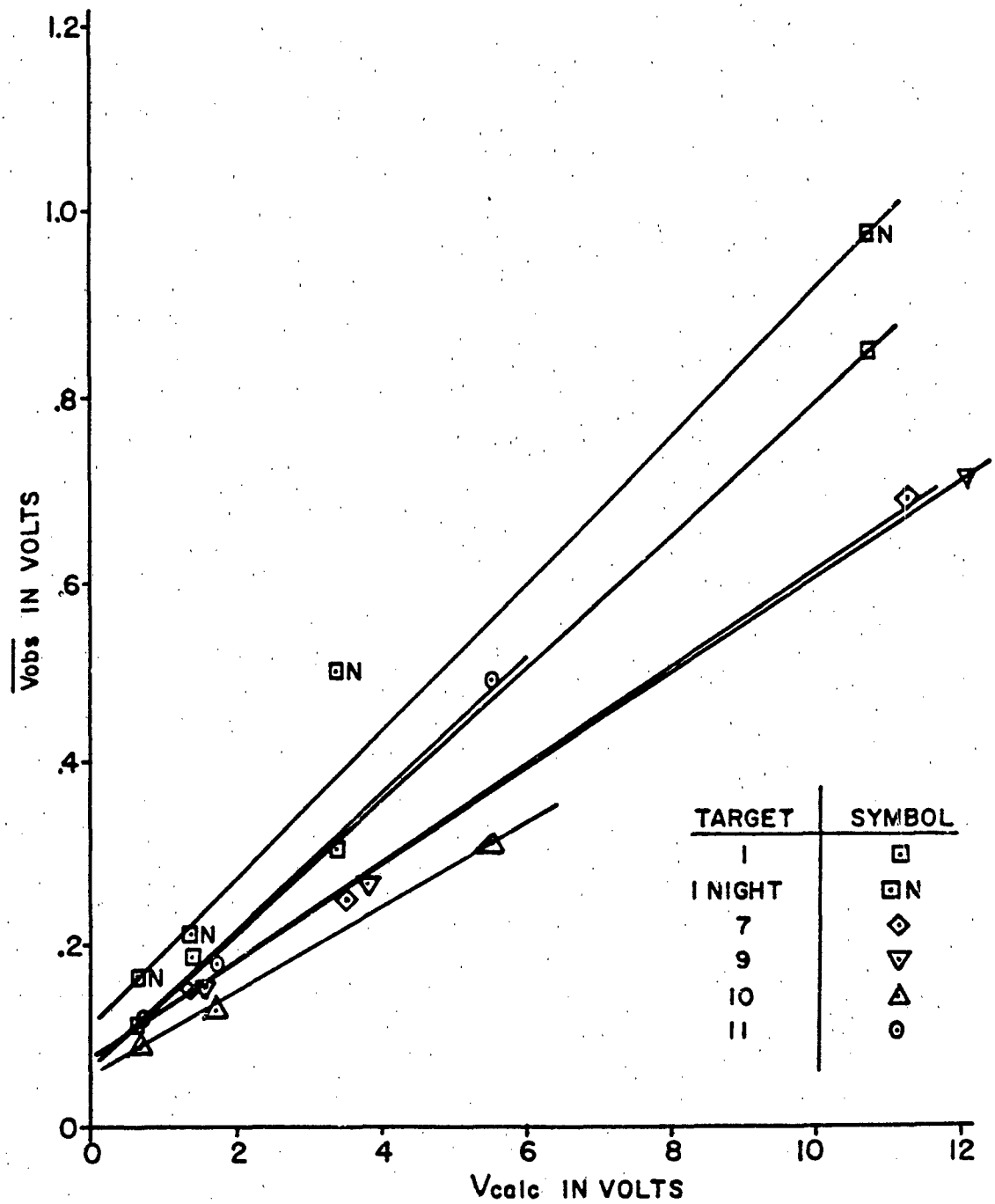

$\overline{V_{obs}}$ vs V_{calc} FOR TARGETS 1, 7, 9, 10, & 11

FIGURE 54

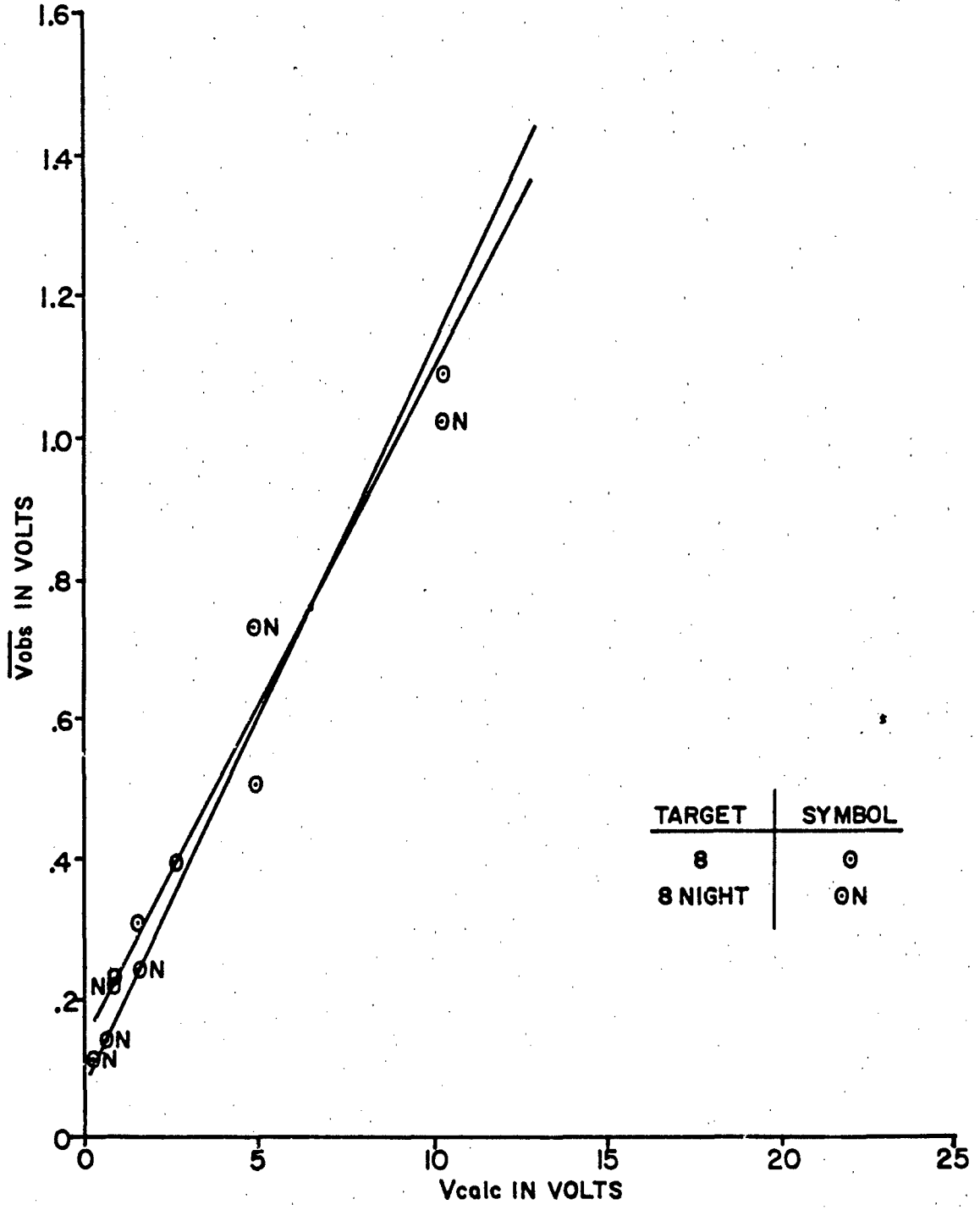

$\overline{V_{obs}}$ vs Vcalc FOR TARGET 8

FIGURE 55

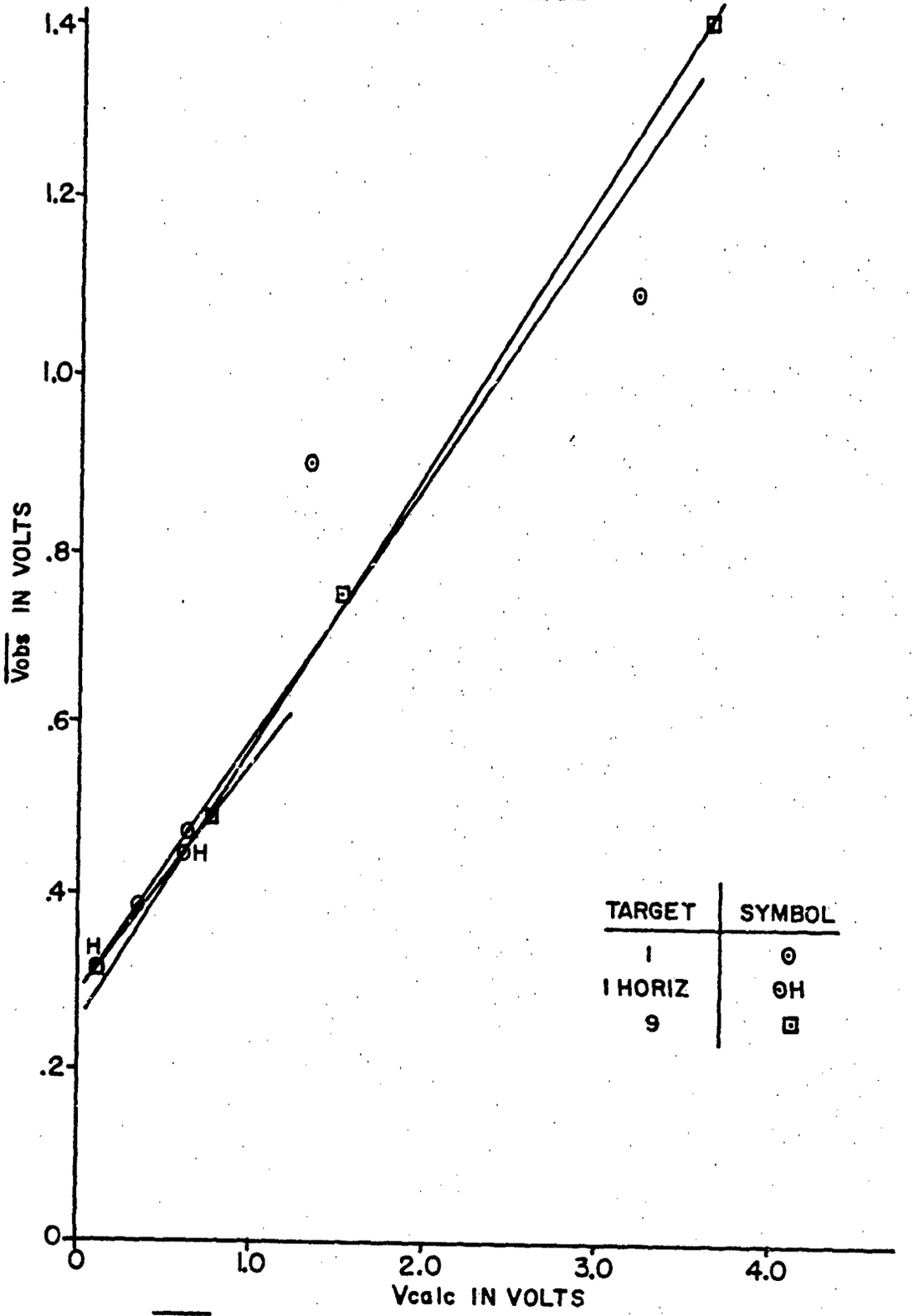

$\overline{V_{obs}}$ vs Vcalc FOR TOWER TARGETS 1 & 9

FIGURE 56

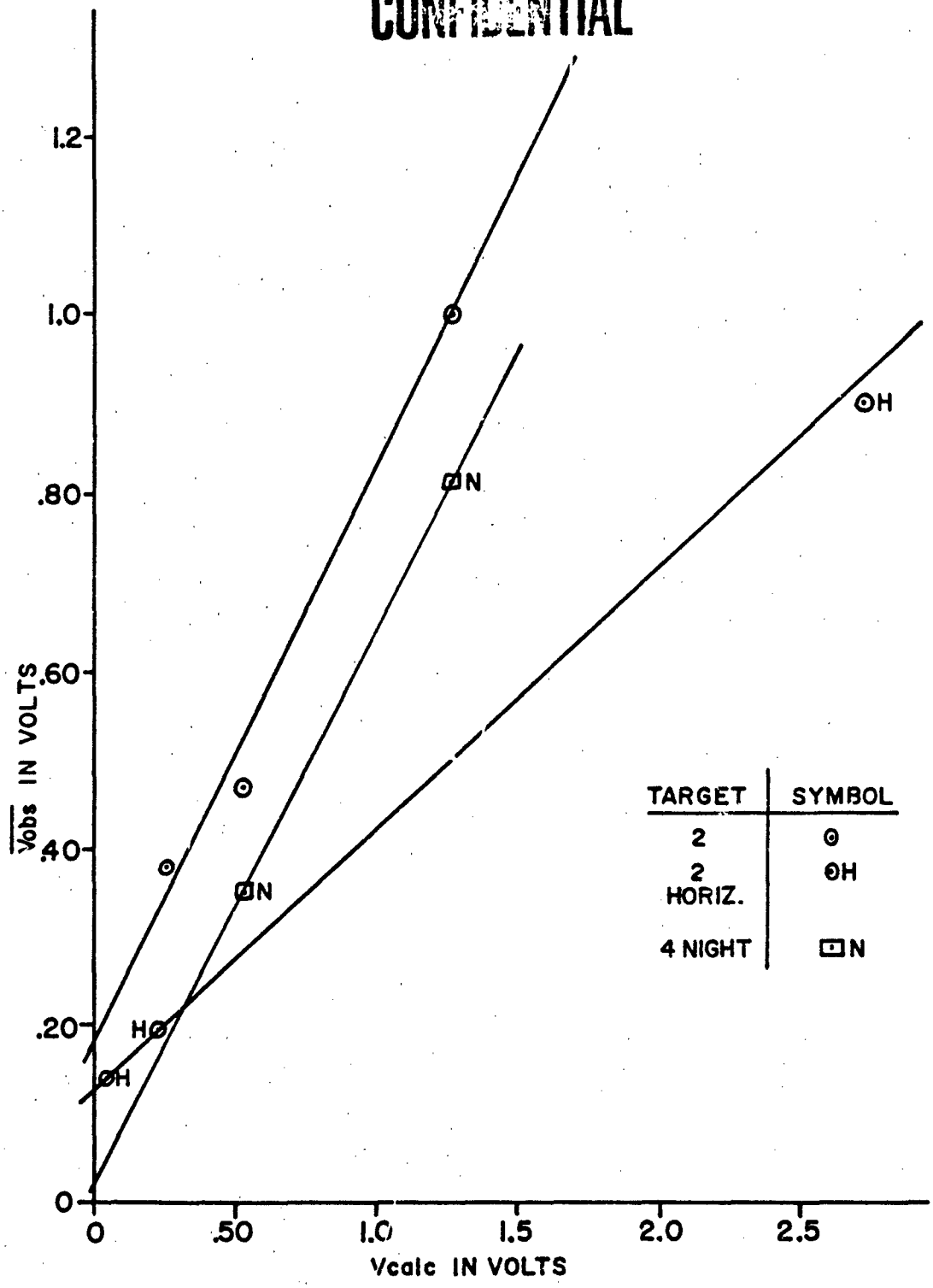

$\overline{V_{obs}}$ VS V_{calc} FOR TOWER TARGETS 2 & 4

FIGURE 57

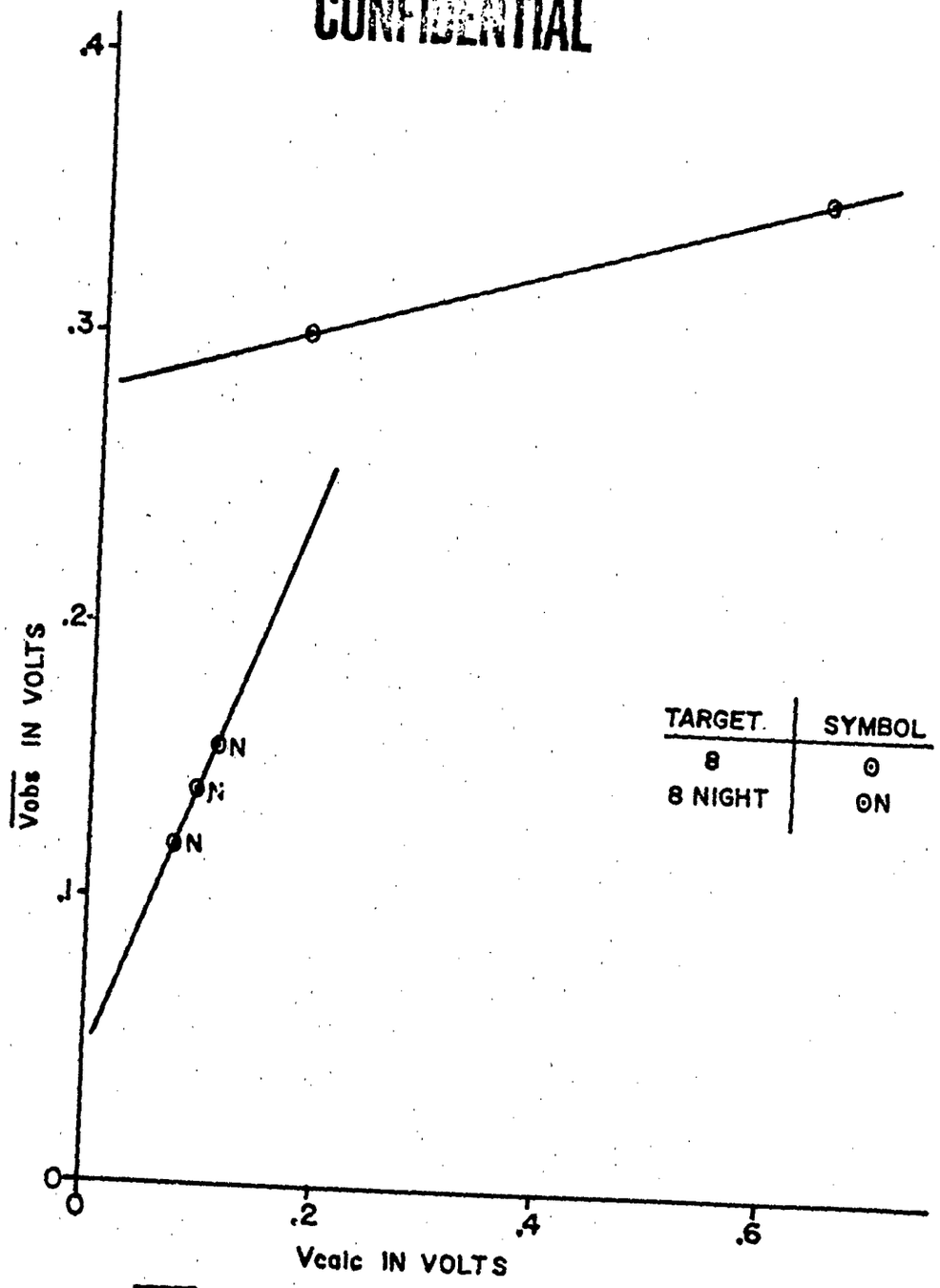

$\overline{Vobs}$ VS Vcalc FOR TOWER TARGET 8

FIGURE 58

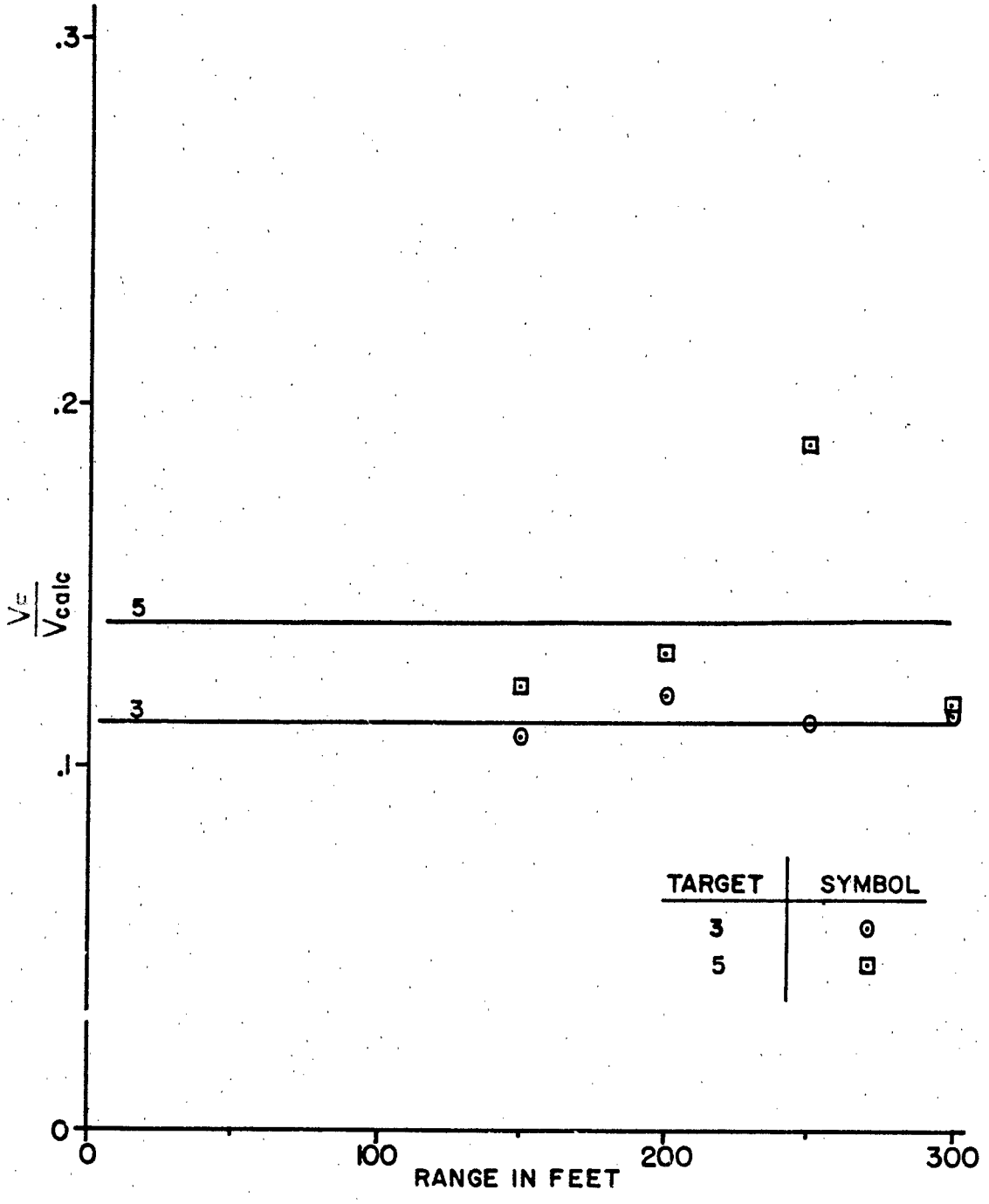

V_F/V_{calc} vs RANGE FOR TARGETS 3&5

FIGURE 59

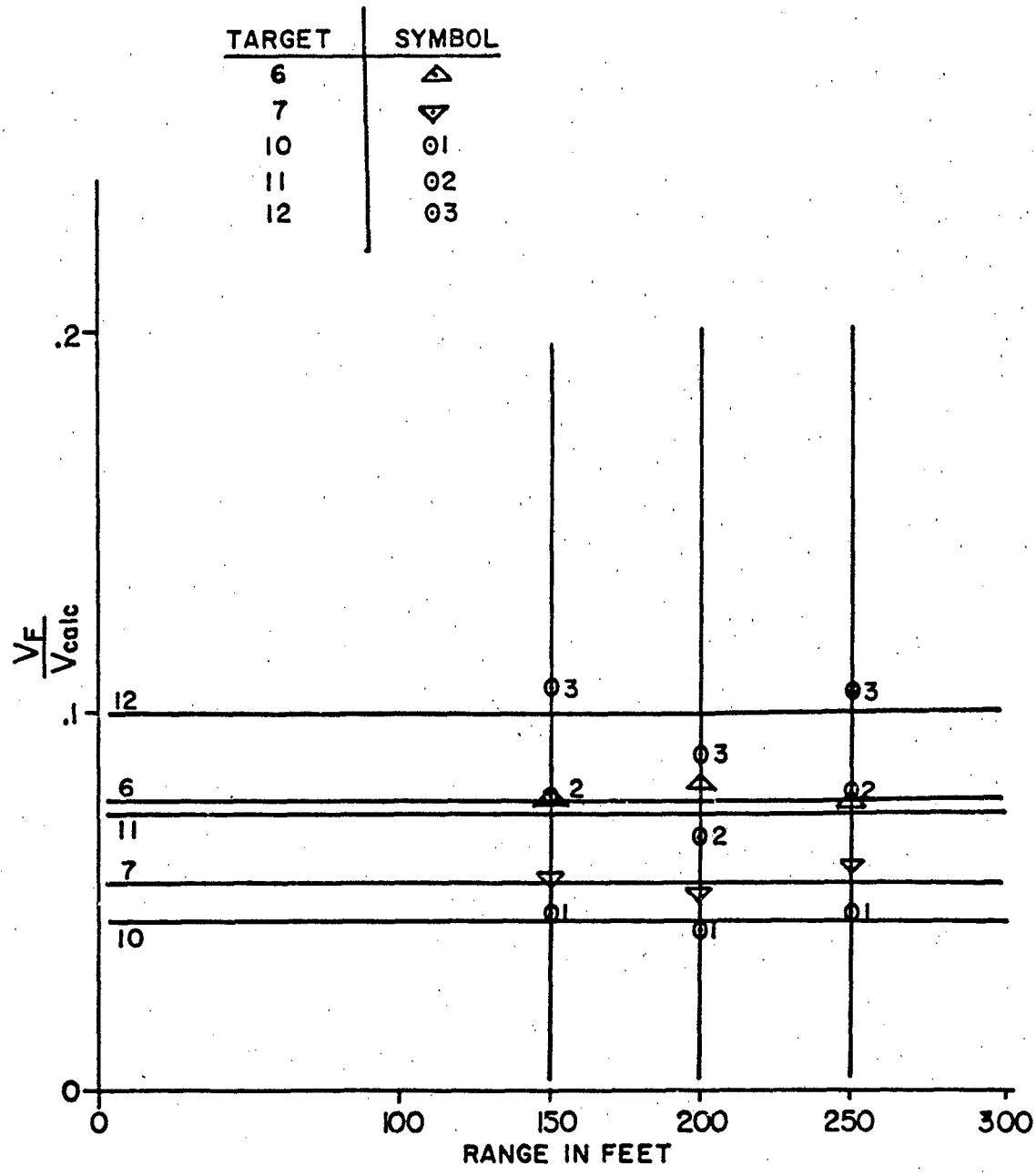

V_F/V_{calc} vs RANGE FOR TARGETS 6, 7, 10, 11, & 12

FIGURE 60

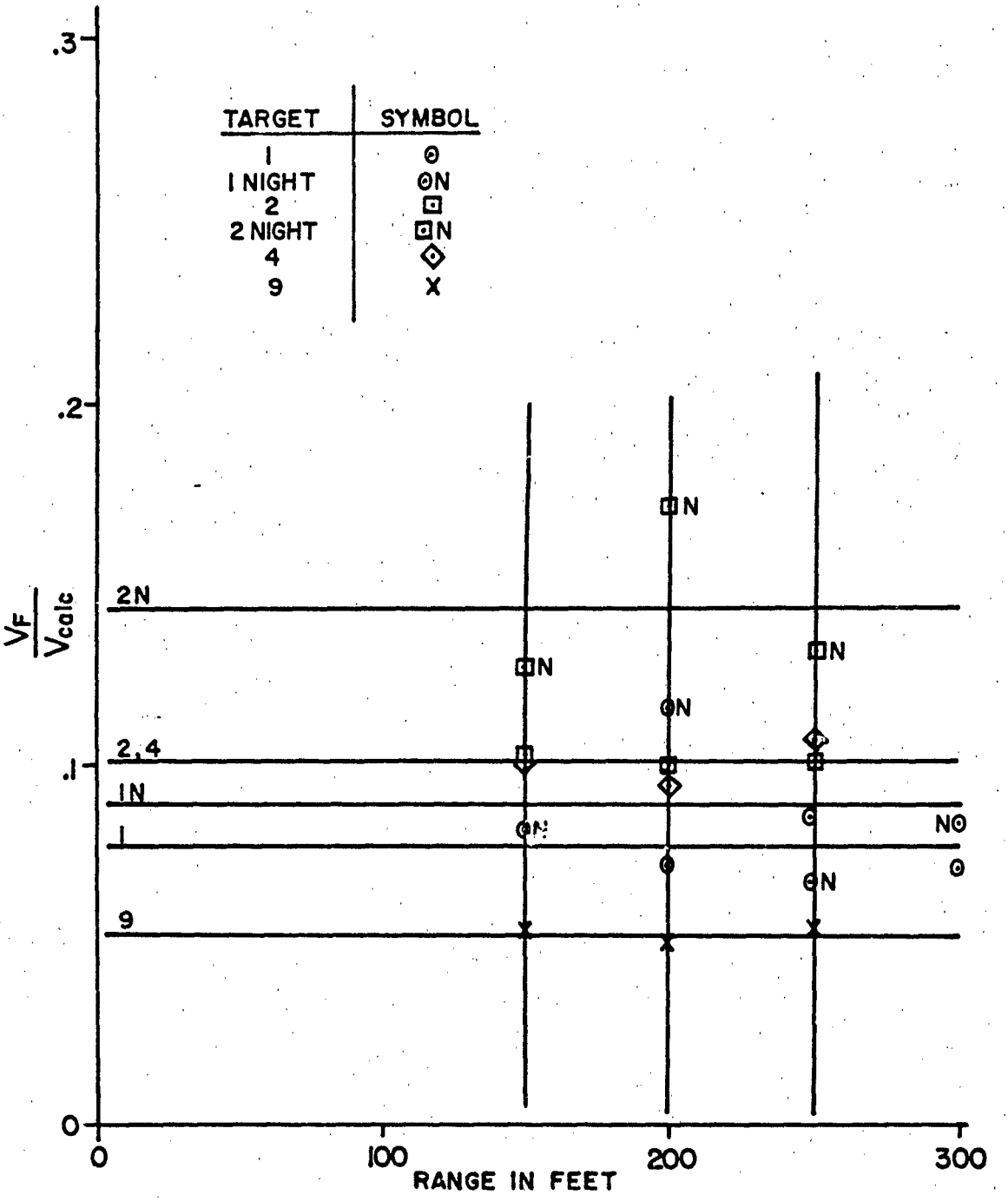

V_F/V_{calc} vs RANGE FOR TARGETS 1,2,4, & 9

FIGURE 61

TARGET	SYMBOL
8	⊙
8 NIGHT	⊙N

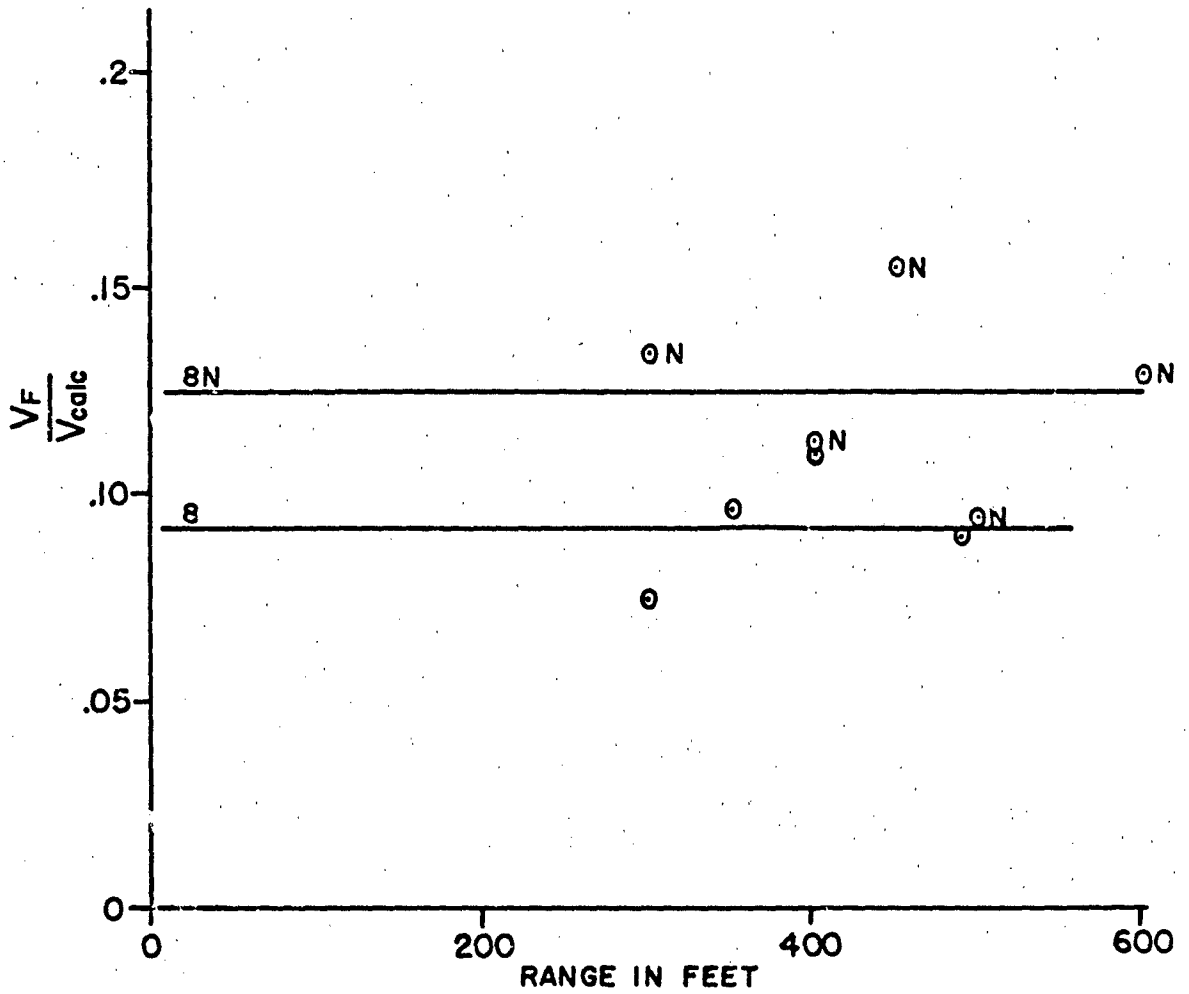

V_F/V_{calc} vs RANGE FOR TARGET 8

FIGURE 62

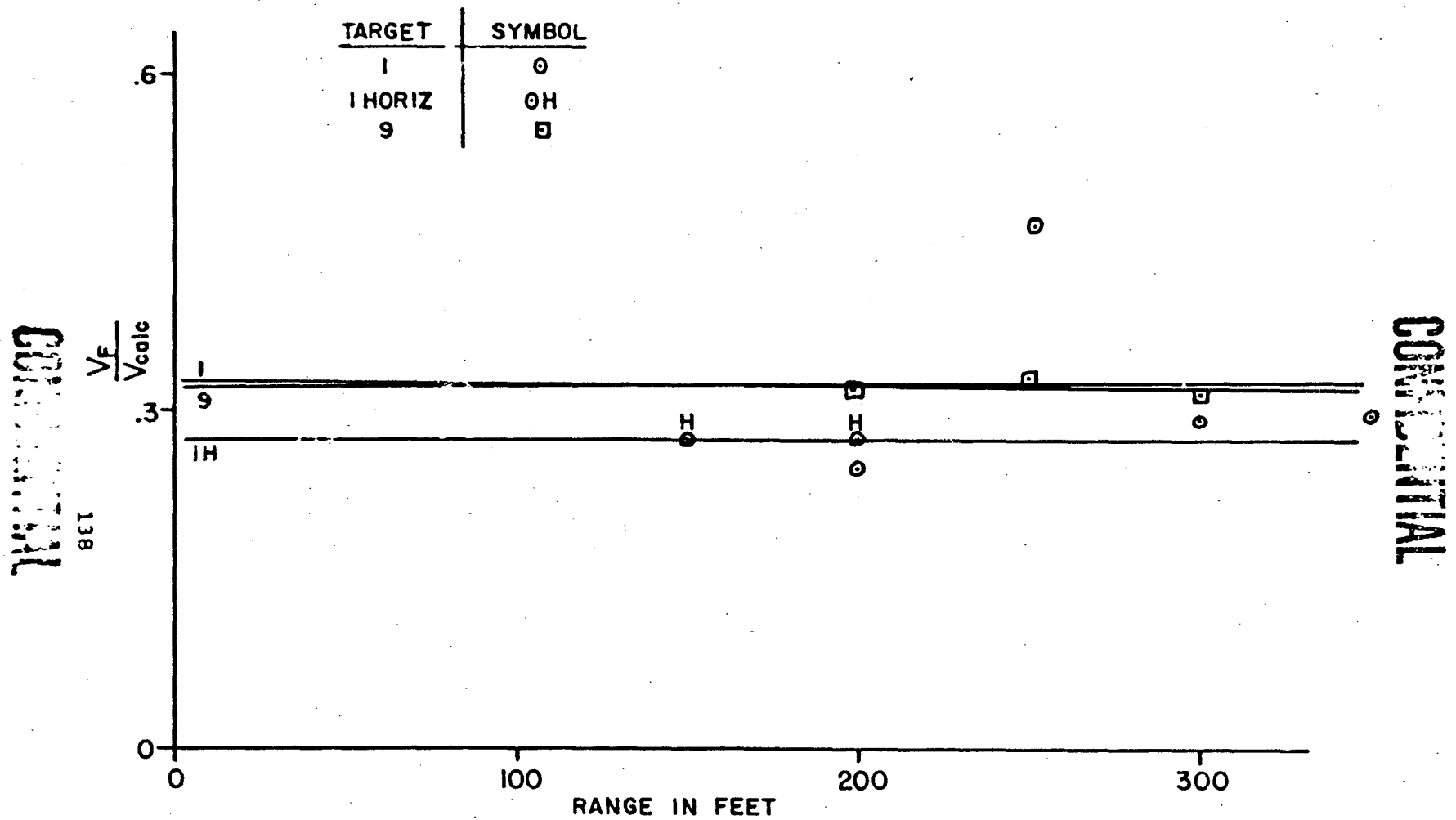

V_F/V_{calc} vs RANGE FOR TOWER TARGET 1 & 9

FIGURE 63

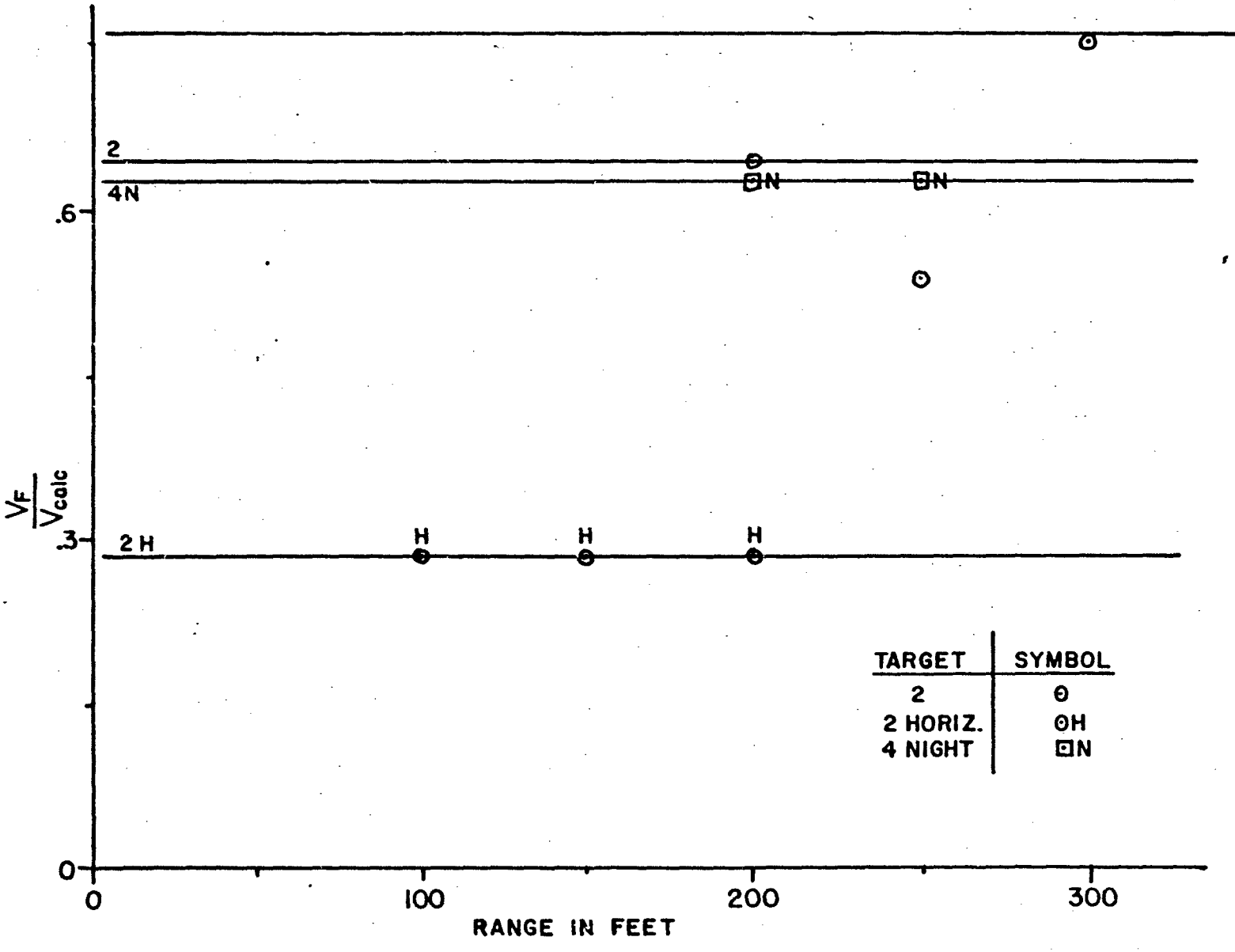

V_F/V_{calc} vs RANGE FOR TOWER TARGET 2&4

FIGURE 64

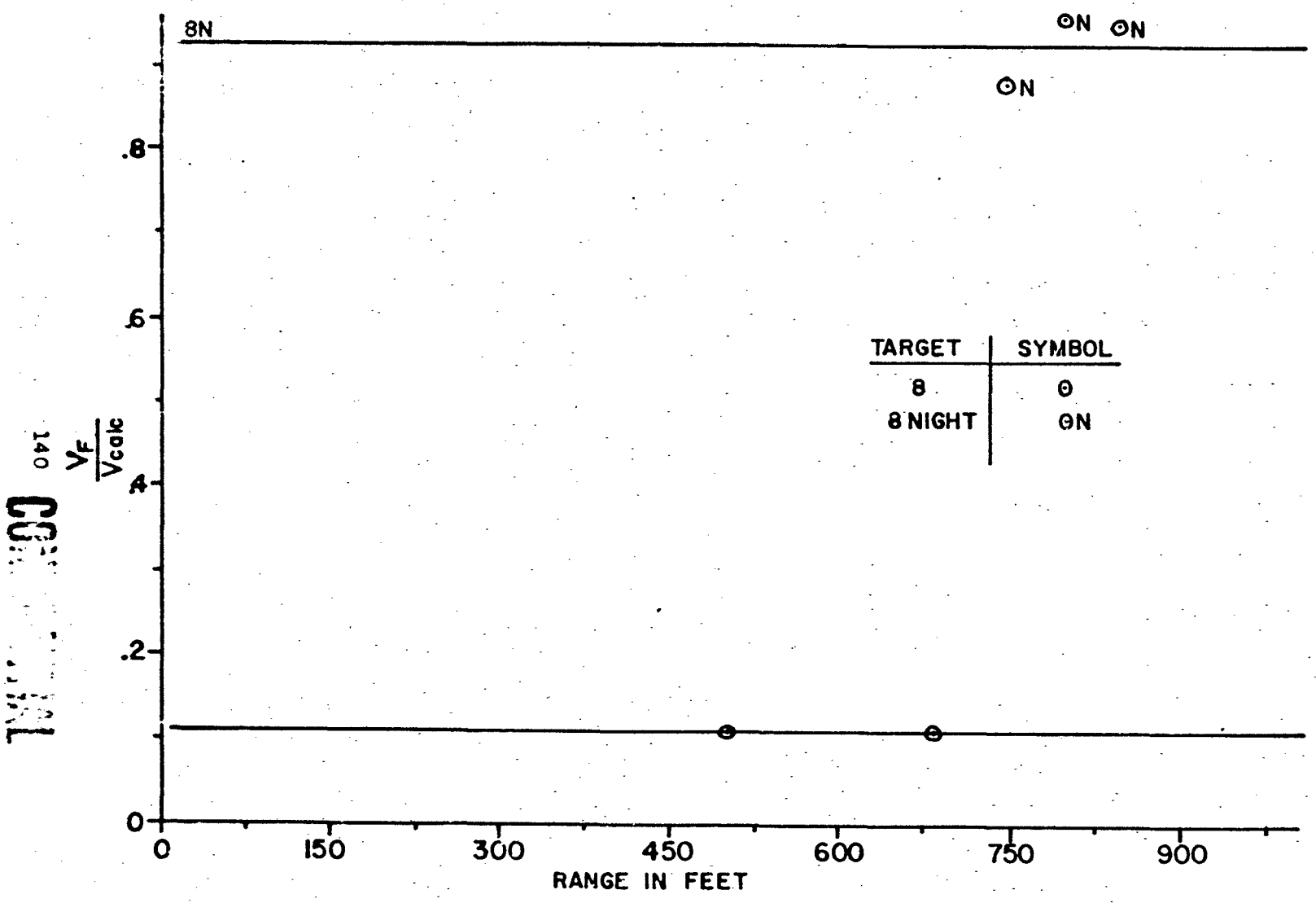

V_F/V_{calc} vs RANGE FOR TOWER TARGET 8

FIGURE 65

of the data plotted as a function of range in Figures 59 through 65. Their relative signal amplitudes are tabulated in Table 17 relative to target five which gave the strongest return.

TABLE 17

Relative Efficiency Per Unit Target Area

Target	Relative Return
1	0.55
2	0.72
3	0.81
4	0.72
5	1.00
6	0.55
7	0.39
8	0.66
9	0.37
10	0.32
11	0.53
12	0.72

The strongest return was obtained from the white Krylon backed Target 5. The higher return from Target 3 and from Target 5 was expected and is primarily due to the fact that any radiation, at λ_L or λ_P, which was scattered back through the paint, was reflected by the substrate. Laser energy, reflected from the substrate, had a second pass at being absorbed by the phosphor. Phosphor radiation, reflected from the substrate, added to the return. A black substrate would have absorbed all energy transmitted back by the phosphor layer and thus prevent its useful return at the phosphor wavelength.

The next pair of relatively strong targets consisted of Targets 2 and 4. The smooth masonite reflects more of the laser power giving a slightly stronger return.

Targets 8 and 9, the field jacket and cap, respectively, produced good signal levels, showing the ability of the coatings to work on cloth as well as solid, hard backings.

The sphere, Target 7, did not quite meet its anticipated return amplitude. One explanation for the lower return is the fact that the reflection coefficient of many painted surfaces increases with the angle from a normal to the surface. Also,

the control of the paint layer thickness was less for the ball than for the flat plates. The net result is that the amplitude error due to an apparent overall gain difference is not surprising.

The pyramid consisted of three coated sides, designated as Targets 10, 11 and 12. Target 10 was given a single thin layer coating, 11 two thin layers and 12 three thin layers of the phosphor paint. The relative returns are in direct relation to the phosphor density.

4.5.8 Variation Between Day and Night Data

Initially the difference in day and night data was attributed to phosphor saturation, although previous laboratory measurements had shown a linear relation between illumination intensity and phosphor output. This measurement was performed again at the higher laser illumination levels experienced during field measurements, with and without a strong background. The presence of background did appear to effect the linearity. The question was resolved by testing the detector alone with a white card, with and without background. The detector output signal was found to be approximately 2.5 times larger without background illumination. This was the same amount by which the phosphor signal deviated from linearity. The factor of 2.5 observed agrees quite well with the differences in response observed in the bulk of day and night data. The same factor accounts for the increase in range observed during measurements made at night, and is due to the variation of detector linearity with the degree of background intensity as described in Section 3.4.5.2.

5. RESULTS AND CONCLUSIONS

The work performed under this contract has further established the feasibility of the Isomet Laser Concept for Marking and Detection. The ability of the system to function properly in a field environment has been demonstrated during field tests at Eglin Air Proving Ground.

Our results and conclusions are as follows:

1. The experimental studies have verified the derived range equation.

2. Large batches of non-toxic phosphors were made which exhibited four times the radiant efficiency of previous compositions. The decay time, radiant efficiency, and emission and excitation spectra of these phosphors were determined.

3. Consultations between Isomet's phosphor chemists and university consultants in the phosphor field resulted in the conclusion that further improvements in decay time and radiant efficiency were definitely possible.

4. The surface brightness was found to increase with increased phosphor layer thickness for the range of coating thicknesses used.

5. Experiments performed with and without high level background illumination and laser beam intensities up to 2.5 watts/cm^2 showed no evidence of phosphor saturation.

6. The power radiant efficiency was affected by variations in input laser pulse duration.

7. The energy radiant efficiency was, as expected, relatively independent of laser pulse width.

8. A suitable test set was designed, fabricated, delivered, and used for performance of field measurements. The test set consisted of a laser transmitter with power supply, beam widening optics and a photometer with a matched field of view.

9. Measurements made in the laboratory and in the field, of the backgrounds and characteristics during day and night operation showed no interference with system performance.

These measurements included scattering and emission from vegetation, solar radiance, terrain, back scattering of fundamental laser excitation from particulate matter in the atmosphere or from terrain and target, and Raman scattering from the terrain.

10. The effective surface brightness of non-flat objects was measured in the field and found to be proportional to the projected area of the phosphor layer, as anticipated.

11. No radiation or glow from the laser aperture or the phosphor coated targets was observed at night. All light wavelengths in the visible region were well below the threshold of the human eye. This proves that the system can covertly detect marked targets during the day and at night.

12. The ability of the system to detect marked targets obscured by appreciable vegetation was demonstrated.

13. The ability of the laser M & D concept to detect the presence and location of marked targets was verified experimentally.

14. The total elapsed time between interrogation of the marked target and a return signal was less than 250 microseconds in the field tests. This time can be reduced if required through the use of faster phosphors, provided they can be found.

6. RECOMMENDATIONS

The studies and measurements made in the laboratory and in the field with the ground based system have demonstrated the basic feasibility of the Isomet laser M & D concept. No experimental or theoretical data have been uncovered which would be considered as basic system limitations. We, therefore, recommend that further development of the system be carried out in three concurrent phases. Such a program would not only involve testing of a flying system based on present technology, but would also advance the state of the art of critical subsystems and components so that more advanced prototypes would have greater capabilities. It is also recommended that an air delivered marking agent and ground reconnaissance system be tested to determine how well it can meet present tactical requirements.

6.1 Flyable Engineering Prototype

It is recommended that a flyable engineering prototype be designed and built based on the present state of the art of flyable subsystems and components. The design and testing of such a prototype permit complete characterization of an operational flying M & D system. The program would consist of the following:

A. Complete evaluation of all parameters, parameter interrelation, and latest techniques.

B. Design and selection of the components which would produce the best overall system.

C. Construction of the prototype.

D. Flight testing with marked targets.

6.2 Air Delivered-Ground Reconnaissance System

Sufficient technology now exists to test a system in which an agent would be delivered from the air and reconnaissance would be conducted from the ground. Such a system could help to determine those individuals who have engaged in actions against us but who appear to be neutral or friendly. Reconnaissance would be carried out in the villages, roads, and checkpoints. There are psychological as well as immediate advantages of such a system.

In operation, enemy personnel would be marked with

phosphor agents disseminated from an aircraft through the medium of bomblets. Ground based personnel would use the portable system in identifying individuals who had been in a target area. The detection device can be designed for hand-held or vehicle mounted operation.

6.3 Marking Agent Development

The basic goal of this program is the improvement of marking agent effectiveness and the study of dissemination techniques. Areas where improvements can be obtained are as follows:

A. Phosphor time constant; a decrease in time constant will allow shorter duration pump time with resultant increase in peak output power.

B. Phosphor efficiency; increasing phosphor efficiency increases operational range.

C. Materials; study of additional phosphor formulations, fixatives, and means of enhancing effectiveness.

D. Dissemination Techniques; particle shape, and size, encapsulents, delivery vehicles.

APPENDIX I

I. System Description and Operation - Contract AF08(635)-4299

1. The laser consists of 2 3/8" diameter by 3" length calcium tungstate laser rods doped with 0.75% neodymium. The laser is excited by a zenon flash lamp to which a maximum of 600 joules of electrical energy are supplied by the power supply. The duration of the flash lamp and laser light output are approximately 200 μsec. The laser light is directed through a telescope (5.75 magnification) in order to reduce the beam divergence (approximately 55 milliradians - reduced to 10 milliradians) and thereby increase the effective range of the device. The laser output wavelength is 1.06 microns.

2. The photometer utilizes a gold doped germanium detector and transistorized amplifier with associated optics which provide a two inch clear aperture. Filters are provided to reject the 1.06 micron exciting wavelength and pass the phosphor emission which extends from 1.5 to 2.1 microns.

3. Signal processing electronics - The processing electronics are designed to identify phosphor signals obtained from the target at a time when both the flash lamp and laser pulse are over. This is possible because the phosphor does not reach its peak output until approximately 70 microseconds before the laser turns off and continues to emit after excitation is completed. In the present set-up, the phosphor return is monitored about 10 to 20 microseconds after the laser turns off. At this point the phosphor output is only reduced to 80-90% of the peak output.

4. Phosphor - The phosphor is zinc sulfide doped with silver and vanadium (2×10^{-4} molar). The peak of the excitation spectrum is 1 micron. The decay time of the fluorescent emission is between 170 and 180 μsec.

SET UP PROCEDURES FOR ELECTPONICS PACKAGES
Figure I-1

II. Connectors

All system interconnections must be made before the power leads are plugged into the 60 cycle 115 volt lines.

1. Laser Power Supply - A total of three connectors are used between the Laser Power Supply and the Laser Head. Connect the two HN type connectors marked "Positive-Shield" and "Negative-Shield" to the corresponding connectors on the Laser Head. The WK-5 unit is then mated to the connector located below the HN units on the Laser Head.

Connect the other ends of the three cables to the Laser Power Supply. Observe the polarity marking on the HN connectors. Check to insure that the HN connectors are tightly screwed down.

2. Processing Electronics - With one exception all connections between the Laser Head and the Processing Electronics are made with polarized connectors. Cable connections are as follows:

A. WK-S5
B. WK-5
C. 31-224 (small size, two pin)
D. UG 102/U (large size, two pin)
E. The cable for providing cooler power has been left out since detector cooling is not advisable.

The UG 102/U connectors are not mechanically polarized. Therefore, the mating connections have been painted with a red dye to provide polarity information. Be sure that the pin surrounded by red painted material is inserted in the socket similarly painted.

3. Signal Monitoring Connections - The phosphor return signal and the gating signal are obtained from the Processing Electronics plug-in boards. Suitable cables with banana plugs on one end and oscilloscope connectors on the other have been provided. A dual beam oscilloscope must be used (Tektronix 555 or 656).

The gating signal is usually displayed on the upper trace and the phosphor return on the lower trace of the oscilloscope.

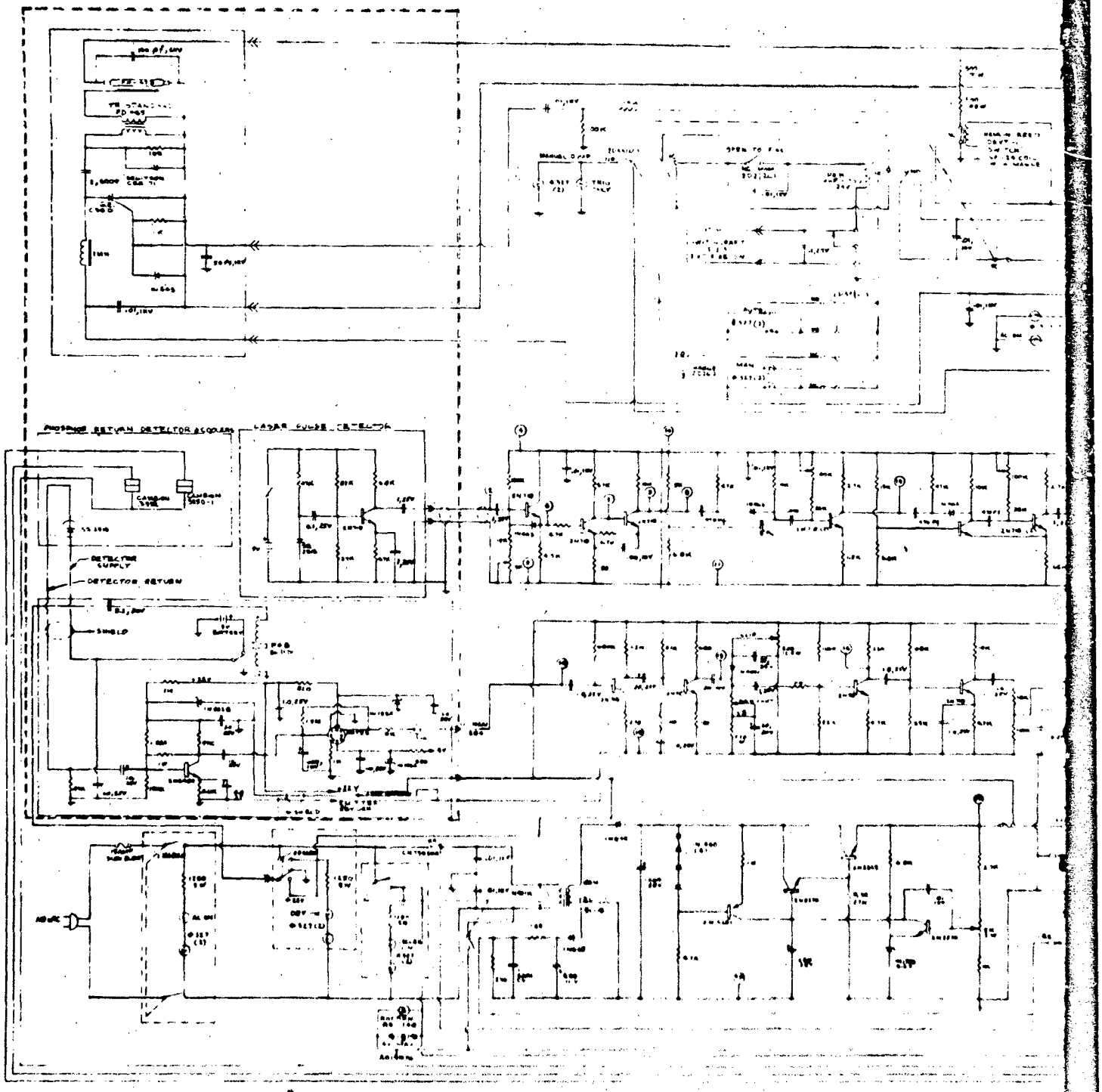

1

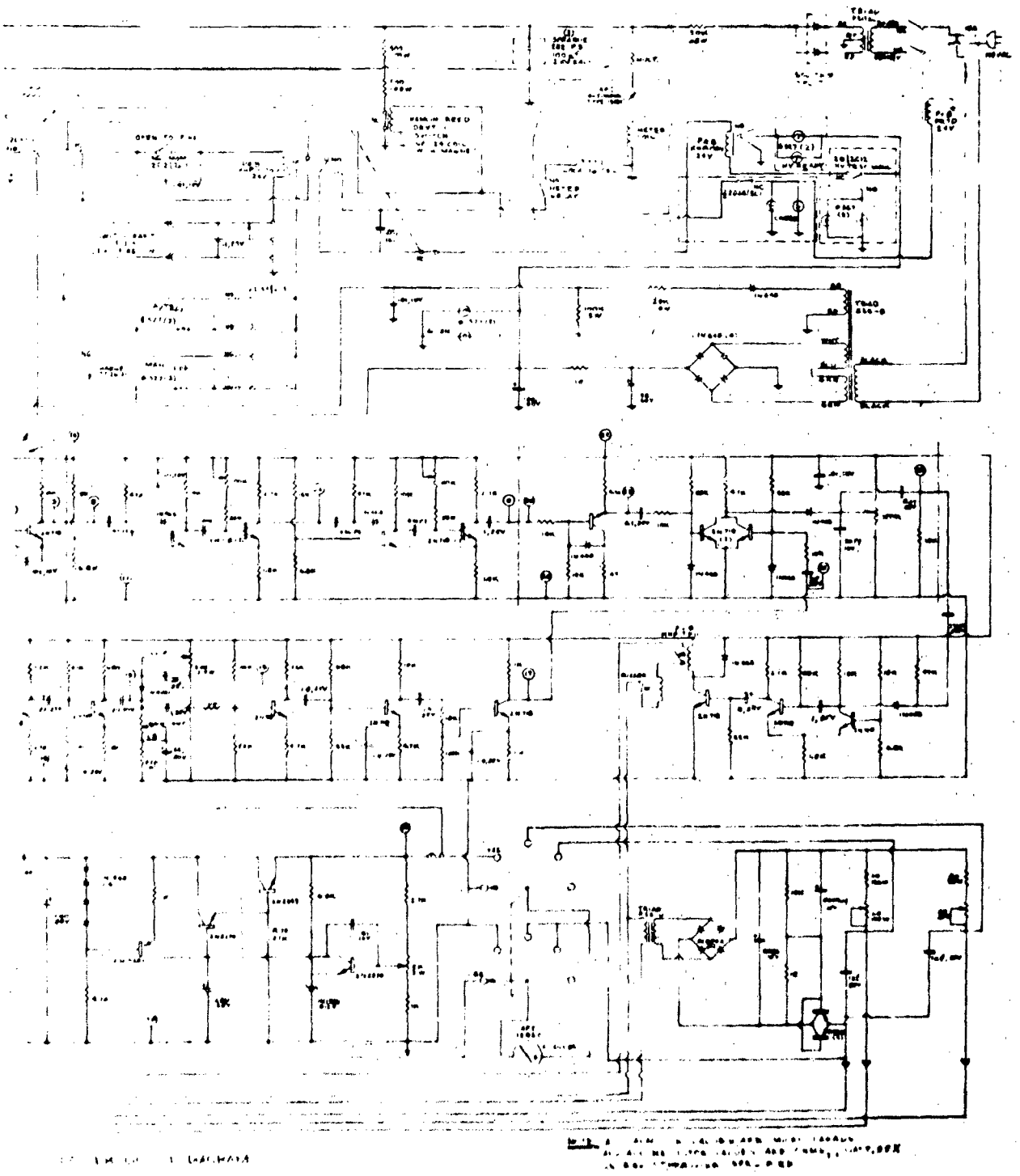

2

For the gating channel, connect a cable to the scope upper trace input; at the other end of the cable, the red banana plug is pushed into jack no. 24, the black plug into jack no. 25.

For the phosphor return signal, connect another cable to the scope lower trace input. Insert the red banana plug into jack no. 14 and the black plug into jack no. 18.

III. Turn On Procedure

1. Laser Power Supply - When the 60 cycle, 115 volt plug is connected to the supply, the "AC ON" light will be energized. The "Manual Dump" Switch should be depressed to make the light in the switch turn on. When the light is on, the high voltage portion of the supply is inactive. In this condition, the flash lamp trigger circuit may be used for synchronizing the oscilloscope. By depressing the "Fire" button, a high voltage pulse is applied to the flash lamp. It is this pulse that synchronizes the scope.

To charge the storage capacitors, the high voltage circuits must be activated. This is done by first pressing the "Manual Dump" switch so that its light goes off. Observe the "Automatic-Manual" switch. If the Automatic portion of the switch is lighted the supply will be charging and the voltage can be read directly on the 0 to 2000 volt meter. If the "Manual" section of the switch is lighted, the "Charge" button must be pushed to initiate the cycle. When the preset voltage is reached, the meter-relay contacts will close and the "HV Ready" light will go on. If any appreciable time elapses between the "HV Ready" light going on and firing the laser, the "HV Test" button should be pressed to recharge the capacitor back to the proper voltage.

After firing, if the supply is in the "Automatic" mode, the capacitors will be recharged automatically. If the "Manual" section of the switch is lighted, the "Charge" button must be depressed to initiate each charge cycle.

When turning the supply off, depress the "Manual Dump" switch until its light goes on. Then remove the 60 cycle line plug.

2. Processing Electronics - Connect the 60 cycle, 115 volt plug to the socket. There are two on-off switches in this unit. The toggle switch located in the upper left corner should be left in the ON position at all times. Actual application of power is controlled by depressing the red "AC ON" switch so that its lights go on.

Since the coolers are not in use, the cooled switch should not be touched. Its lights should be off.

The "Detector ON" switch should not be depressed until the volt meter indicates 22 volts. This switch controls a relay in the photometer assembly which supplies power from a battery to the detector. If the system is properly connected, when the "Detector ON" button is pushed, the phosphor return alarm buzzer will sound. This should not occur when the switch is pushed to the off position.

The detector should be turned off between firings to minimize noise. When the equipment is to be shut down, make sure the detector is turned off by first turning it on, then off. This must be done before the "AC ON" button is pushed to the off position.

3. Lamp Pickup Circuit and Detector - This circuit is powered by a battery contained within the can holding the circuit and detector. It is important that the unit be turned off at the end of each series of tests. The switch is located in an opening in the front panel of the laser head where the front of the telescope is located. The off position of the toggle is to the left when the switch is observed from the front of the laser head.

APPENDIX II

II.1 Physiological Effects of Laser Radiation

The eye is the organ most susceptible to laser injury. For Laser M & D System, the anticipated laser parameters are many orders of magnitude below the levels required for damaging human skin. The only source of potential danger to distant personnel will be the possibility of formation of extremely small lesions in the eye.

A lesion, which can be caused by a distant laser, is normally an extremely small, permanent burn spot on the retina. Typical dimensions of small laser lesions within the eye are between 4.6×10^{-7} sq. cm.[1] and 2×10^{-6} sq. cm.[2]. In the final application of the system, personnel on the ground, both enemy and friend, could receive one lesion each time they look at the laser while it is pulsed on.

Looking at a laser while it is on will not always cause a lesion. Damage can occur only when the energy level entering the eye is high enough to burn retinal tissue. Since the energy density for a given system decreases with distance, there is a threshold range beyond which permanent damage will not occur. Also, since the laser emits a beam of sharply restricted angular dimensions, looking at a laser from an an angle not in the output beam is not necessarily dangerous. For a flying laser system, the hazard only exists for persons in the illuminated area and closer than the threshold range.

The average laser energy density, L, at any range is given by,

$$L = \frac{4 E_o}{\pi \phi_L^2 R^2}$$

where E_o = total energy emitted in one laser pulse (joules)

ϕ_L = laser beam divergence (radians)

r = range (cm)

The laser energy, E_e, which enters an eye of iris diameter D_e is:

1. C.H. Swope and C.J. Koester, Appl. Opt. 4,523 (1965)
2. H.W. Straub, "Protection of the Human Eye from Laser Radiation," AD #436705

[redacted]

$$E_e = \frac{L\,\pi D_e^2}{4} = E\left(\frac{D_e}{\phi_L\ r}\right)^2$$

The ratio $\left(\frac{D_e}{\phi_L\ r}\right)^2$ is equal to the F described in reference 1. The damage under consideration here is due only to the energy absorbed per unit area on the retina. The ratio, (TA), of input to absorbed energy for the eye is plotted as a function of wavelength in reference 1. The area of absorption on the retina for a distant laser source is given above as typical dimensions of a laser focal spot in the eye. Representing the area of the retinal image by A_R, the energy density on the retinal surface, I, can be computed from the equation:

$$I = \frac{(TA)E_o}{A_R}\left(\frac{D_e}{\phi_L\ r}\right)^2$$

The value of I at which a threshold lesion occurs is an average physical constant for the eye, I_t. For a system with fixed beam size and energy, the threshold range, R_t, can be computed from the relationship,

$$R_t = \frac{[(TA)E_o]^{1/2}}{(A_R\ I_t)^{1/2}}\qquad\frac{D_e}{\phi_L}$$

For the laser M & D field measurement test set, ϕ_L = 7.6 and E = 0.1. At ranges greater than seventy five feet, the retinal image size does not decrease significantly with range, since the resolution limit is reached at about this distance. Substituting the value for TA of 0.2, as given in reference 1, and the values of A_R and I_t given in references 1 and 2, the threshold range can be computed. The diameter of the iris, D_e, is assumed to be the maximum for a fully dilated pupil, D_e = 8 mm. Using the values in reference 1, the threshold range is approximately 1100 feet. Using reference 2, the threshold range is approximately five hundred feet. Personnel working with the laser measurement test set should wear safety glasses whenever they are in the field of laser illumination.

The reflections from diffuse scatterers such as a white card, fine sand, etc., offer little potential danger to the eye.

[redacted]

[redacted]

[redacted]

High energy (100 joule) ruby laser beams [redacted]ected as a small circle from a white card, can be safely viewed by the naked eye at close proximity (ten feet). The primary cause of the eye damage to ground based personnel by an airborne system will be direct illumination. If the personnel do not look up at the aircraft at exactly the time they are illuminated, no eye damage will result. The only exception is when an individual's eye is illuminated by a reflected glint of the laser beam from a specular reflector. The probability of this occurring is so low as to be negligible.

Consideration will have to be given to possible eye damage in any final system. Protective goggles can be used, but are inconvenient. Retinal damage in the form of lesions is normally unnoticed unless large numbers of burns caused by many laser pulses are inflicted. It is common to find large numbers of retinal lesions caused by the sun, arc welding, and exposure to bright lamps. In a reconnaissance mission, exposure to more than a few pulses by any one individual will be improbable.

[redacted]

[redacted]

Security Classification

DOCUMENT CONTROL DATA - R&D

(Security classification of title, body of abstract and indexing annotation must be entered when the overall report is classified)

1 ORIGINATING ACTIVITY (Corporate author) Isomet Corporation 433 Commercial Avenue Palisades Park, N. J.	2a. REPORT SECURITY CLASSIFICATION [redacted] 2b GROUP 4

3 REPORT TITLE

MARKING AND DETECTION (LASER TECHNIQUE)

4 DESCRIPTIVE NOTES (Type of report and inclusive dates)

Final Report - May 26, 1964 to March 31, 1966

5 AUTHOR(S) (Last name, first name, initial)

R. Goldstein, B. Hammond, J. Richman, Richard Vesper

6. REPORT DATE	7a. TOTAL NO. OF PAGES	7b. NO. OF REFS
July 1966	164	8

8a CONTRACT OR GRANT NO. AF08(635)-4299 b. PROJECT NO. c. d.	9a. ORIGINATOR'S REPORT NUMBER(S) AFATL-TR-66-64 9b. OTHER REPORT NO(S) (Any other numbers that may be assigned this report)

10. AVAILABILITY/LIMITATION NOTICES In addition to security requirements which must be met, this document is subject to special export controls and each transmittal to foreign governments or foreign nationals may be made only with prior approval of the Air Force Armament Laboratory (ATCB), Eglin Air Force Base, Florida.

11. SUPPLEMENTARY NOTES Available in DDC	12. SPONSORING MILITARY ACTIVITY Air Force Armament Laboratory Eglin Air Force Base, Florida

13. ABSTRACT

Further experimental studies and field measurements confirmed the feasibility of the Isomet laser concept for marking and detection of individuals. In this concept a phosphor agent is disseminated from an aircraft on military targets, which are later interrogated by a laser transmitter. The phosphor return, as well as the laser pulse, are in the infrared spectrum and hence are completely covert.

No basic system limitations were uncovered by the tests or studies. A ground based test set was designed, built and used in field measurements at Eglin Air Force Base. Background radiation from sunlight, terrain and foliage did not materially degrade the system performance. System operation was demonstrated in the field over an unobstructed path as well as through foliage. Phosphors with improved characteristics were developed.

DD FORM 1 JAN 64 1473

[redacted]

Security Classification

[redacted]

Security Classification

14. KEY WORDS	LINK A		LINK B		LINK C	
	ROLE	WT	ROLE	WT	ROLE	WT
Marking and detection [redacted] IR Phosphors IR Lasers Detectors Photometers						

INSTRUCTIONS

1. ORIGINATING ACTIVITY: Enter the name and address of the contractor, subcontractor, grantee, Department of Defense activity or other organization *(corporate author)* issuing the report.

2a. REPORT SECURITY CLASSIFICATION: Enter the overall security classification of the report. Indicate whether "Restricted Data" is included. Marking is to be in accordance with appropriate security regulations.

2b. GROUP: Automatic downgrading is specified in DoD Directive 5200.10 and Armed Forces Industrial Manual. Enter the group number. Also, when applicable, show that optional markings have been used for Group 3 and Group 4 as authorized.

3. REPORT TITLE: Enter the complete report title in all capital letters. Titles in all cases should be unclassified. If a meaningful title cannot be selected without classification, show title classification in all capitals in parenthesis immediately following the title.

4. DESCRIPTIVE NOTES: If appropriate, enter the type of report, e.g., interim, progress, summary, annual, or final. Give the inclusive dates when a specific reporting period is covered.

5. AUTHOR(S): Enter the name(s) of author(s) as shown on or in the report. Enter last name, first name, middle initial. If military, show rank and branch of service. The name of the principal author is an absolute minimum requirement.

6. REPORT DATE: Enter the date of the report as day, month, year, or month, year. If more than one date appears on the report, use date of publication.

7a. TOTAL NUMBER OF PAGES: The total page count should follow normal pagination procedures, i.e., enter the number of pages containing information.

7b. NUMBER OF REFERENCES: Enter the total number of references cited in the report.

8a. CONTRACT OR GRANT NUMBER: If appropriate, enter the applicable number of the contract or grant under which the report was written.

8b, 8c, & 8d. PROJECT NUMBER: Enter the appropriate military department identification, such as project number, subproject number, system numbers, task number, etc.

9a. ORIGINATOR'S REPORT NUMBER(S): Enter the official report number by which the document will be identified and controlled by the originating activity. This number must be unique to this report.

9b. OTHER REPORT NUMBER(S): If the report has been assigned any other report numbers *(either by the originator or by the sponsor)*, also enter this number(s).

10. AVAILABILITY/LIMITATION NOTICES: Enter any limitations on further dissemination of the report, other than those imposed by security classification, using standard statements such as:

(1) "Qualified requesters may obtain copies of this report from D C."

(2) "Foreign announcement and dissemination of this report by DDC is not authorized."

(3) "U. S. Government agencies may obtain copies of this report directly from DDC. Other qualified DDC users shall request through

_____."

(4) "U. S. military agencies may obtain copies of this report directly from DDC. Other qualified users shall request through

_____."

(5) "All distribution of this report is controlled. Qualified DDC users shall request through

_____."

If the report has been furnished to the Office of Technical Services, Department of Commerce, for sale to the public, indicate this fact and enter the price, if known.

11. SUPPLEMENTARY NOTES: Use for additional explanatory notes.

12. SPONSORING MILITARY ACTIVITY: Enter the name of the departmental project office or laboratory sponsoring *(paying for)* the research and development. Include address.

13. ABSTRACT: Enter an abstract giving a brief and factual summary of the document indicative of the report, even though it may also appear elsewhere in the body of the technical report. If additional space is required, a continuation sheet shall be attached.

It is highly desirable that the abstract of classified reports be unclassified. Each paragraph of the abstract shall end with an indication of the military security classification of the information in the paragraph, represented as *(TS)*, *(S)*, *(C)*, or *(U)*.

There is no limitation on the length of the abstract. However, the suggested length is from 150 to 225 words.

14. KEY WORDS: Key words are technically meaningful terms or short phrases that characterize a report and may be used as index entries for cataloging the report. Key words must be selected so that no security classification is required. Identifiers, such as equipment model designation, trade name, military project code name, geographic location, may be used as key words but will be followed by an indication of technical context. The assignment of links, rules, and weights is optional.

[redacted]

Security Classification